

**PROTON CONDUCTION AND WATER DIFFUSION IN  
SILICATE GLASSES AND MELTS**

Von der Naturwissenschaftlichen Fakultät der  
Gottfried Wilhelm Leibniz Universität Hannover  
zur Erlangung des Grades

**Doktor der Naturwissenschaften**

**- Dr. rer. nat. -**

genehmigte Dissertation  
von

**Dott.ssa Sara Fanara**

geboren am 30.08.1978 in Rom, Italien

2009

Referent: Prof. Dr. Harald Behrens

Korreferent: Prof. Dr. Claus Henning Rüscher

Tag der Promotion: 24.06.2009

## ACKNOWLEDGEMENTS

I am extremely thankful to Professor Dr. Harald Behrens, Institute of Mineralogy, Leibniz University of Hannover, Germany, who has introduced me into the experimental petrology world. His continuous supervision, providing new ideas for explaining new findings, have brought this thesis to its present form.

My heartfelt thanks to Professor Dr. Youxue Zhang, Department of Geology, University of Michigan, USA, for giving me the opportunity to work in his laboratory and to provide jewels suggestions .

Thanks to Wanja Dziony and Tapas Debnath for all your help and encouragements in my thesis work as in the day life time.

Thanks to Oliver Beermann, Jan Stelling, Elke Schlechter, Marcus Oelze and Renat Almeev to provide helps and suggestions in the lab. work. A special thank to Annette in correcting this thesis in good English.

Thanks to Willy, Bettina, Ulrich and all the other guys working in the workshop. A special thank to Otto for the huge amount of samples and thin section prepared for me.

I thank all of my colleagues in the institute, specially Renat Almeev, Roman Botcharnikov, Sara Cichy, Lydéric France, Tanja Höfs, Marieke van Lichtervelde, Elzbieta Mielcarek, Aftab A. Shaikh, Tatiana Shishkina, Guglielmo Torresi who always make my life joyful.

Vorrei anche ringraziare tutti i ragazzi italiani che mi hanno fatto compagnia qui ad Hannover per periodi più o meno lunghi: Marcella Davì, Maria Luisa e Giorgia.

A special thanks to all the people I want to thanks but I forget righth now. I apologize for that!

Grazie ai miei genitori che mi hanno aiutato per questi quattro anni e che sono qui con me anche mentre scrivo le ultime pagine di questa tesi. Grazie!

At the end, I would like to thanks Dr. Sascha Beutel that helps me correcting this thesis and supporting me in many ways. You know you are not at the last place in my thoughts.

Finally, I would like to thank the Ministry of Science and Culture, Land Niedersachsen for providing me “Georg-Christoph-Lichtenberg-Stipendium”, which has made possible my studies in Germany.

# Content

## Acknowledgments

Zusammenfassung ..... I

Abstract ..... IV

I. Introduction ..... 1

II. Glasses and Melts ..... 5

II.1 – Glass components and network hypotheses ..... 6

II.2 – The time-dependent glass transformation behavior ..... 7

II.3 – Relaxation time and Maxwell equation ..... 9

III. Structure of Glasses ..... 11

III.1 – Coordination of the network cations ..... 11

III.2 – Network connectivity ..... 11

III.3 – Overview on Oxide Glasses ..... 12

*III.3.1 – Single – Component Glasses* ..... 12

*III.3.2 – Influence of  $X_2O$*  ..... 13

*III.3.3 – Influence of  $XO$*  ..... 13

IV. Transport Properties ..... 14

IV.1 – Different diffusion types ..... 15

*IV.1.1 – Vacancy diffusion* ..... 16

*IV.1.2 – Interstitial diffusion* ..... 17

IV.2 – Diffusion Laws ..... 17

IV.3 – Nernst-Einstein equation ..... 18

IV.4 – Temperature dependence.....	19
IV.5 – Solution to diffusion equation.....	21
<i>IV.5.1 – Initial and boundary conditions.....</i>	21
<i>IV.5.2 – Experimental technique and solution methods.....</i>	21
<i>IV.5.3 – Concentration-dependent D and Boltzmann analysis.....</i>	22

## V. Electrical Properties..... 24

V.1 – Relation between conductivity and diffusion.....	24
V.2 – Dependence on composition.....	25
<i>V.2.1 – Mixed alkali effect.....</i>	27
<i>V.2.2 – Effect of water on ionic transport in glasses.....</i>	28
V.3 – Dependence of $\sigma$ on temperature.....	29

## Chapter 1 – Proton conduction in glasses of the join $\text{CaMgSi}_2\text{O}_6$

### (Di) – $\text{CaAl}_2\text{Si}_2\text{O}_8$ (An)

1.1 – Abstract.....	31
1.2 – Introduction.....	33
1.3 – Starting materials.....	35
1.4 – Experimental and analytical methods.....	37
<i>1.4.1 – Hydrous glasses.....</i>	37
<i>1.4.2 – Density and Karl-Fischer titration.....</i>	38
<i>1.4.3 – IR spectroscopy.....</i>	39
<i>1.4.4 – Impedance spectroscopy.....</i>	40
<i>1.4.4.1- Sample preparation.....</i>	40
<i>1.4.4.2- Conductivity measurements.....</i>	41
1.5 – Results.....	43
<i>1.5.1 – IR spectroscopy.....</i>	43
<i>1.5.1.1- Procedure for baseline correction of the combination bands...46</i>	

1.5.1.2- Determination of molar absorption coefficients.....	47
1.5.2 – Impedance spectroscopy.....	52
1.5.2.1- Cell constant.....	52
1.5.2.2- Ionic conductivity.....	53
1.5.2.3- Stability of samples during impedance measurements.....	68
1.5.3 – Temperature dependence of $\sigma_{dc}$ .....	69
1.6 – Discussion.....	71
1.6.1 – Water diffusion.....	71
1.6.2 – Mechanism of proton conduction .....	74
1.6.3 – Comparison to literature .....	78

## Chapter 2 – Diffusion of water in Phonolite and Trachyte melts

2.1 – Abstract.....	80
2.2 – Introduction .....	82
2.3 – Precedent studies.....	83
2.4 – Starting materials.....	88
2.5 – Experimental procedures.....	90
2.5.1 – Hydrous glasses.....	90
2.5.2 – Diffusion couple experiments.....	91
2.5.2.1- Piston Cylinder Apparatus.....	91
2.5.2.2- Internal Heated Gas Pressure Vessel.....	93
2.6 – Analytical procedures.....	97
2.6.1 – Karl-Fischer Titration.....	97
2.6.2 – Colorimetric determination of ferrous iron.....	97
2.6.3 – Infrared analyses.....	98
2.7 – Results.....	100
2.7.1 – IR spectroscopy.....	100
2.7.1.1- Band assignment and peak position.....	100

2.7.1.2- Procedure for baseline correction of the combination bands	101
2.7.1.3- Determination of molar absorption coefficients.....	102
2.7.2 – Evaluation of diffusion profiles.....	106
2.7.3 – Results from colorimetric determination of ferrous iron.....	111
2.7.4 – Major oxide concentration profile.....	112
2.8 – Discussion.....	114
2.8.1 – The effect of redox state on water transport.....	114
2.8.2 – Modelling H <sub>2</sub> O diffusion.....	115
2.8.2.1- Error function fit.....	116
2.8.2.2- Modified Boltzmann-Matano method.....	116
2.8.2.3- Numerical fitting.....	119
2.8.3 – P-T-C <sub>H<sub>2</sub>O</sub> dependence on bulk water diffusivity.....	120
2.8.3.1- Modelling of Phonolite.....	120
2.8.3.2- Trachyte.....	122
2.8.4 – Water diffusion in Natural Melts.....	125
2.8.5 – Moving species.....	127
<b>Conclusion.....</b>	<b>129</b>
<b>References.....</b>	<b>132</b>
<b>Appendix.....</b>	<b>145</b>

## Zusammenfassung

Die Diffusion von Wasser in Gläsern bei niedriger Temperatur spielt eine wichtige Rolle in verschiedenen Prozessen, wie z.B. Glaskorrosion und Entgasen industrieller Schmelzen oder natürlicher Magmen. Weiterhin ist die Entwicklung von Gläsern als schnelle Protonenleiter für die Gewinnung sauberer Energie von Interesse, z.B. für den Einsatz in Brennstoffzellen oder in Wasserstoff-Sensoren. Erkenntnisse über die Diffusion von Wasser bei hohen Temperaturen in Kieselsäure-haltigen Schmelzen sind für die Modellierung von Entgasungsprozessen und Fragmentierung von Magmen während vulkanischer Eruptionen, sowie der Blasenbildung wichtig. Die Diffusion von Wasser dürfte auch einen Einfluss auf pre-eruptive Prozesse haben, welche in der Magmakammer ablaufen. Hier seien beispielsweise die Wechselwirkungen zwischen Fluiden und Schmelze oder Magma mixing / -mingling genannt. Ziel dieser Arbeit ist es, neue Erkenntnisse über die Transportmechanismen von Wasser in silikatischen Gläsern und Schmelzen zu gewinnen.

Der erste Teil dieser Arbeit beschäftigt sich mit der Diffusion von Wasser in wasserhaltigen, silikatischen Gläsern mit Zusammensetzungen entsprechend Diopsid (Di,  $\text{CaMgSi}_2\text{O}_6$ ) bis Anorthit (An,  $\text{CaAl}_2\text{Si}_2\text{O}_8$ ), mit Wassergehalten bis zu 3 Gew.-%  $\text{H}_2\text{O}$ . Die untersuchten Gläser wurden in Platin-Kapseln bei Temperaturen zwischen 1523 und 1723 K und einem Druck von 2 kbar in einer intern beheizten Gasdruck-Apparatur (IHPV) synthetisiert. Die Proben konnten mittels „rapid quench“, mit einer Abkühlrate von etwa 150 K/s, in den meisten Fällen zu reinem Glas abgeschreckt werden. Der Wassergehalt wurde durch Karl Fischer-Titration bestimmt. Die homogene Verteilung des Wassers sowie die Konzentration von Hydroxyl-Gruppen (OH) und Wassermolekülen ( $\text{H}_2\text{O}$ ) vor- und nach den Leitfähigkeits-Messungen wurden mittels Infrarot-Mikrospektroskopie kontrolliert. Die elektrische Leitfähigkeit wurde durch Impedanz-Spektroskopie bei Temperaturen bis 685 K ermittelt, ohne dass signifikante Veränderungen der Proben durch Rekristallisation und Wasserverlust auftraten. Es zeigte sich, dass die elektrische

Leitfähigkeit für Gleichstrom in den wasserhaltigen Gläsern der Zusammensetzungen  $\text{Di}_{100}$ ,  $\text{An}_{100}$ , und  $\text{An}_{50}\text{Di}_{50}$  um mindestens eine Größenordnung höher ist als in den wasserfreien Gläsern analoger Zusammensetzung. Die messbare Leitfähigkeit der trockenen Gläser wird der Anwesenheit geringer Mengen von  $\text{Na}_2\text{O}$  (von 0,15 Gew.-% in  $\text{An}_{100}$  bis 0,05 Gew.-% in  $\text{Di}_{100}$ ) zugeschrieben. Es ist bekannt, dass gelöstes Wasser die Mobilität von Alkalimetall-Ionen in Gläsern herabsetzt. Daraus wird gefolgert, dass die el. Leitfähigkeit für Gleichstrom, die in den wasserhaltigen Gläsern beobachtet wurde, hauptsächlich auf die Erzeugung von Ladungsträgern bei der Hydratisierung der Gläser zurückzuführen ist. Entsprechend der Beobachtungen anderer Autoren wird vorgeschlagen, dass entweder Protonen oder  $\text{OH}^-$ -Gruppen, die nicht an tetraedrisch koordinierte Kationen gebunden sind, für den Ladungstransport verantwortlich sind. Aus der protonen-bedingten elektrischen Leitfähigkeit wurden mit der Nernst-Einstein Gleichung Diffusions Koeffizienten für geladene H-spezies berechnet. Die so erhaltenen Diffusionskoeffizienten variieren von  $10^{-17} \text{ m}^2/\text{s}$  (für  $\text{An}_{50}\text{Di}_{50}$  mit 1,50 Gew.-%  $\text{H}_2\text{O}_t$  bei 596 K) bis  $10^{-12} \text{ m}^2/\text{s}$  (für  $\text{An}_{50}\text{Di}_{50}$  mit 2,77 Gew.-%  $\text{H}_2\text{O}_t$  bei 685 K).

Der zweite Teil dieser Arbeit beschäftigt sich mit der Diffusion von Wasser in phonolitischen- und trachytischen Schmelzen. Die Diffusionspaar-Experimente wurden in einer „Piston Cylinder“ Apparatur (PCA) und in einer IHPV Anlage bei Temperaturen von 1373 K bis 1673 K und Drücken von 2 bis 25 kbar durchgeführt. Hierbei wurden Paare von trockenen und wasserhaltigen Gläsern mit zwischen 1 und 6 Gew.-% gelöstem  $\text{H}_2\text{O}_t$  über einen Zeitraum von 108 bis 1186 Sekunden erhitzt. Die Konzentrationsverläufe der verschiedenen Wasser-Spezies ( $\text{OH}$  Gruppen und  $\text{H}_2\text{O}$  Moleküle) entlang der Diffusionslinie wurden mittels IR Mikrospektroskopie gemessen. Daraus wurde der Gesamt-Wasser Gehalt ( $C_{\text{H}_2\text{O}_t} = C_{\text{OH}} + C_{\text{H}_2\text{O}_m}$ ) berechnet, der mittels einer modifizierten Boltzmann-Matano Methode sowie – unter der Annahme einer funktionellen Abhängigkeit von  $D_{\text{H}_2\text{O}_t}$  und  $C_{\text{H}_2\text{O}_t}$  voneinander – Konzentrations abhängige Diffusions Koeffizienten abgeleitet. Für Wasser in phonolitischen Schmelzen ergibt sich, dass sich der Diffusionskoeffizient bis 4 Gew.-%  $\text{H}_2\text{O}_t$  proportional zum Gesamt-Wassergehalt

verhält. Die nachfolgende Formel wurde zur Abschätzung von  $D_{\text{H}_2\text{O}_t}$  ( $\text{m}^2/\text{s}$ ) als Funktion von  $T(\text{K})$  für 1 Gew.-%  $\text{H}_2\text{O}_t$  abgeleitet:

$$\log D_{\text{H}_2\text{O}_t} = -7,11 - 2,07 \log C_{\text{H}_2\text{O}_t} - \frac{(4827 - 4620 \log C_{\text{H}_2\text{O}_t})}{T}$$

Die experimentell erhaltenen Daten können mit dieser Beziehung mit einem Standardfehler von 0,07 log Einheiten beschrieben werden. Für die Proben mit trachytischer Zusammensetzung konnte aufgrund experimenteller Probleme wie z.B. Kristallbildung keine verlässliche Diffusionsgleichung aufgestellt werden, da hierdurch zuwenige Proben zur Verfügung standen. Eine Druckabhängigkeit des Diffusionskoeffizienten konnte für die Proben mit phonolitischer Zusammensetzung im Bereich 2 bis 25 kbar nicht ermittelt werden, jedoch wurde bei den Proben mit trachytischer Zusammensetzung eine leichte Abnahme der Diffusion mit zunehmendem Druck beobachtet.

Schlüsselwörter: Diffusion, Impedanz-Spektroskopie, Phonolit, Trachyt, Silikatische Schmelzen

## Abstract

Diffusion mechanisms of hydrous species in glasses at low temperature play an important role in several processes such as corrosion of glass and degassing of industrial melts or natural magmas. Furthermore, developing of fast proton conducting glasses is of high interest in clean energy field, such as hydrogen gas sensors and hydrogen fuel cells. Knowledge on water diffusion behaviour at high temperature is especially needed for silica rich melts to model magma degassing and fragmentation during volcanic eruptions and bubble growth. Diffusion of water may also affect pre-eruptive processes in the magma chamber such as fluid-melt interaction and magma mingling and mixing.

The aim of this study is to provide new information on the mechanisms of transport of hydrous species in silicate glasses and melts.

The first chapter of this thesis focuses on water diffusion in hydrous silicate glasses with compositions along the join diopside ( $\text{Di}$ ,  $\text{CaMgSi}_2\text{O}_6$ ) - anorthite ( $\text{An}$ ,  $\text{CaAl}_2\text{Si}_2\text{O}_8$ ), containing up to 3 wt%  $\text{H}_2\text{O}$ . The studied glasses were synthesized in platinum capsules at temperatures between 1523 and 1723 K and pressures of 2 kbar in an internally heated gas pressure vessel (IHPV). Using a rapid-quench device (cooling rate  $\approx 150$  K/s), melts could be quenched to glasses in most cases. The water content of the glasses was analyzed by Karl-Fischer titration (KFT). Using infrared microspectroscopy (IR), the homogeneity of water distribution in the samples was checked and concentrations of OH groups and  $\text{H}_2\text{O}$  molecules were determined before and after conductivity measurements. The electrical conductivity was measured by impedance spectroscopy at temperature up to 685 K without significant alteration of the samples, such as crystallization and water loss. It was shown that the dc conductivity in hydrous glasses with compositions  $\text{Di}_{100}$ ,  $\text{An}_{100}$  and  $\text{An}_{50}\text{Di}_{50}$  (in mol%) is higher by at least one order of magnitude than in dry glasses with analogue compositions. The measurable conductivity shown by the dry glasses was attributed to the presence of a minor amount of  $\text{Na}_2\text{O}$  (from 0.15 wt% in  $\text{An}_{100}$  to 0.05 wt% in

Di<sub>100</sub>). It is known that dissolved water reduces the mobility of alkali cations in glasses and, hence, it is inferred that the dc conductivity observed in the hydrous samples is mainly due to the charge carriers produced by hydration of the glasses. Consistent with findings in literature it is suggested that the mobile charge carriers are either protons or OH<sup>-</sup> groups, which are not bound to tetrahedral cations. Conductivity data were evaluated in terms of proton diffusivity by the Nernst-Einstein equation. The obtained diffusion coefficients range from 10<sup>-17</sup> m<sup>2</sup>/s for An<sub>50</sub>Di<sub>50</sub> with 1.50 wt% of H<sub>2</sub>O<sub>t</sub> at 596 K to 10<sup>-12</sup> m<sup>2</sup>/s for An<sub>50</sub>Di<sub>50</sub> with 2.77 wt% of H<sub>2</sub>O<sub>t</sub> at 685 K.

The second chapter of this thesis focuses on water diffusion in phonolitic and trachytic melts. Experiments were performed in a Piston Cylinder Apparatus (PCA) and in an Internally Heated Gas Pressure Vessel (IHPV) at temperatures of 1373 - 1673 K and pressure between 2 - 25 kbar, using the diffusion couple technique. Pairs of nominally dry glasses and hydrous glasses containing between 1 - 6 wt% of dissolved H<sub>2</sub>O<sub>t</sub> were heated for 108 - 1186 s. Concentration profiles of hydrous species (OH groups and H<sub>2</sub>O molecules) and total water ( $C_{H_2O_t}$  as sum of OH and H<sub>2</sub>O<sub>m</sub>) were measured along the cylindrical axis of the diffusion sample using IR microspectroscopy. Bulk water diffusivity ( $D_{H_2O_t}$ ) was derived from profiles of total water using a modified Boltzmann-Matano method as well as using fittings assuming a functional relationship between  $D_{H_2O_t}$  and  $C_{H_2O_t}$ . In case of phonolitic melts, fitting of the profiles indicate that the water diffusivity is proportional to the total water content up to 4 wt% H<sub>2</sub>O<sub>t</sub>.

The following formulation was derived to estimate  $D_{H_2O_t}$  (m<sup>2</sup>/s) at 1 wt% H<sub>2</sub>O<sub>t</sub> in melts with phonolitic composition, as a function of T (K):

$$\log D_{H_2O_t} = -7.11 - 2.07 \log C_{H_2O_t} - \frac{(4827 - 4620 \log C_{H_2O_t})}{T}$$

The experimental data are reproduced by this relationship with a standard error of 0.07 log units. Due to experimental problems (i.e. partial crystallization) only few experiments were successful for trachytic melts, insufficient to derive a reliable diffusion law. A pressure effect on water diffusivity could not be resolved for

phonolitic melts in the range 2 - 25 kbar, while for trachyte composition smaller diffusivities at higher pressures were registered, indicating a negative pressure effect.

Keywords: Water diffusion, Impedance spectroscopy, Diffusion couple, Phonolite, Trachyte, Silicate melts.

## I - Introduction

The physical transport of mass plays a crucial role in many kinetic processes. Wherever there are heterogeneities and sufficient mobility, there is transport. In general, convection and fluid flow are the dominant ways of transport in gases and liquids, but diffusion is the only way of mass transfer in the solid-state reaction. Therefore, magma erupts by fluid flow, while a crystal becomes homogeneous by diffusion. Anyway, diffusion and convection may be superimposed in magmas, depending on viscosity, temperature gradients or pressure gradients.

Diffusion plays a significant to dominant role in extremely various geological processes such as fluid-rock interaction, magma mixing, crystal dissolution and growth from a liquid or gas or solid phase, homogenization of zoned crystals and of decay products of radioactive elements in a mineral. Studying diffusion helps not only to improve the understanding of the physical processes, but also provides a way to infer the geological and thermal history of rocks.

Many theoretical or empirical relations have been proposed between diffusivity and other parameters, such as conductivity, viscosity and particle size. In particular, diffusivity and ionic conductivity are related. Diffusion is caused by random motion of particles under a concentration gradient, while conduction is due to motion of ions in an electric field.

Water diffusion plays a crucial role in explosive volcanic eruptions, in fact it was inferred that the exsolution of water drives explosive volcanic eruptions (Wilson et al., 1980; Woods, 1995; Zhang, 1996; Zhang et al., 1997). The dissolution of water in melts has an important effect on melt and glass properties, such as strength of glasses and crystallization sequence of melts. Therefore, the diffusion of water in silicate glasses and melts has been extensively investigated. Water may exist in silicate melt as at least two species: molecular water ( $\text{H}_2\text{O}_m$ ) and hydroxyl ions ( $\text{OH}^-$ ), as indicated by infrared and NMR spectroscopy (Scholze, 1960; Bartholomew et al., 1980; Stolper, 1982). Therefore, the diffusion of water in silicate melt is a multi-species diffusion.

It has been inferred that the total diffusivity of water ( $D_{H_2O_t}$ ) is a complicated function of the total water content ( $H_2O_t$ ). In 1969, Doremus discovered, in a study on fused silica, that the  $D_{H_2O_t}$  is roughly proportional to the  $H_2O_t$ , for  $H_2O_t < 0.1$  wt%. In this case, the  $H_2O_m$  was considered as diffusing species, even for extremely low  $H_2O_m$  concentrations. With the successive studies of Shaw, in 1974, and Delaney and Karsten, in 1981, the  $D_{H_2O_t}$  was found dependent on  $H_2O_t$  in a complicated way. Then, the microanalytical method for determination of species concentrations was introduced into Geosciences by Stolper, in 1982. Subsequently, Zhang was able to calculate the  $D_{OH}$  and  $D_{H_2O_t}$ , for  $H_2O_t < 1.7$  wt%, considering that the two diffusivities are independent from  $H_2O_t$  concentration (Zhang et al., 1991). The  $D_{OH}$  was found negligible compared to  $D_{H_2O_m}$ . Nowak and Behrens, in 1997, discovered that the  $D_{H_2O_m}$  was not constant for higher  $H_2O_t$ . In the last decade, Zhang and Behrens (2000) evidenced that  $D_{H_2O_m}$  is an exponential function of  $H_2O_t$ . In particular, the  $D_{H_2O_m}$  is roughly constant and  $D_{H_2O_t}$  increases roughly proportionally to  $H_2O_t$ , for  $H_2O_t < 2$  wt%; instead  $D_{H_2O_t}$  increases exponentially with  $H_2O_t$ , for  $H_2O_t > 2$  wt%.

It was inferred that diffusion of  $H_2O_m$  in polymerized silicate glasses and melts is controlled by two different mechanisms. The mechanism controlling the movement is determined by the temperature. At temperature below the glass transition temperature, the silicate network is rigid and it was suggested by several authors that the  $H_2O_m$  migrates through the structure by direct jumps from one cavity to another.  $H_2O_m$  is then immobilized in the new position by reaction with oxygen of the silicate network (Doremus, 1969; Wasserburg, 1988; Zhang et al., 1991; Doremus, 1995). Above the glass transition temperature, the structural relaxation is fast enough to allow the migration of pairs of transient OH groups, formed by reaction between  $H_2O$  molecules and network oxygen (Roberts et al., 1966; Tomozawa, 1985; Behrens and Nowak, 1997).

In the depolymerized glasses a high concentration of single bonded oxygens is present, which can react with protons to form OH groups. Therefore, it has been suggested that a coupled motion of  $H^+$  and  $OH^-$  is the predominant mechanism for diffusion of water under these conditions (Haider and Roberts., 1970).

In this work, diffusion of hydrous species in silicate glasses and melts was studied at low and high temperatures, respectively by impedance measurements and diffusion couple experiments.

In chapter 1, hydrous silicate glasses with composition along the join Diopside ( $\text{CaMgSi}_2\text{O}_6$ ) – Anorthite ( $\text{CaAl}_2\text{Si}_2\text{O}_8$ ) containing up to 3 wt% of  $\text{H}_2\text{O}_t$ , were investigated by impedance spectroscopy up to a temperature of 685 K. The aim of this work is to improve the understanding of diffusion mechanisms of hydrous species in glasses, which play a crucial role in many natural and industrial processes such as degassing of magmas, corrosion of glass and fining of manufactured glasses. Using infrared microspectroscopy (IR) the homogeneity of water distribution in the samples was checked and concentration of OH group and  $\text{H}_2\text{O}_m$  were determined before and after conductivity measurements. The dc conductivity was found to be higher by at least one order of magnitude in hydrous glasses than in dry ones. Consistent with findings in literature, it was suggested that the mobile charge carriers are either protons or  $\text{OH}^-$  groups which are not bound to tetrahedral cations.

In order to study volcanological and magmatic processes such as bubble growth, magma degassing during volcanic eruptions, magma fragmentation and mixing,  $\text{H}_2\text{O}$  diffusion data for melts of various compositions are required. The diffusion of  $\text{H}_2\text{O}$  in dacitic, andesitic, rhyolitic and basaltic magmas has been extensively studied and well understood (Shaw, 1974; Zhang and Stolper, 1991; Nowak and Behrens, 1997; Zhang and Behrens, 2000; Behrens et al., 2004; Liu et al., 2004; Okumura & Nakashima, 2004 – 2006; Ni & Zhang, 2008), but knowledge on water diffusion behavior are particularly important and still incomplete for silica rich melts to model volcanic eruptions. Therefore, in chapter 2, water diffusion in trachytic and phonolitic melts was investigated. As starting materials we have used synthetic analogues of potassium-rich trachyte from the Phlegrean Fields, Italy, and potassium-rich phonolite from the Laacher See, Germany. Diffusion couple experiments were performed in a piston cylinder apparatus (PCA) at pressure from 5 - 25 kbar, at 1573 K and for durations of 0 - 5 min. Additional experiments were carried out in an internally heated high pressure vessel

(IHPV) at pressure from 2 - 4 kbar, with temperature ranging from 1373 - 1673 K, for duration of 1-8 min.

In a successive step, diffusion couple and dehydration experiments were carried out at low temperature, ranging from 773 - 863 K, at 2 kbar in a cold seal pressure vessel (CSPV) for duration of 48 h - 96 h.

Water concentration profiles were measured by Fourier transform infrared microspectroscopy using the peak heights of combination bands of OH and H<sub>2</sub>O in the near-infrared. Water diffusion coefficients were calculated from the total water profiles by the Boltzmann-Matano analysis and/or numerical fitting. In case of phonolite melts, an empirical formulation was derived to estimate  $D_{\text{H}_2\text{O}_t}$  at 1 wt% H<sub>2</sub>O<sub>t</sub> in melts. By combining our new data with previous results, we attempt to discuss the mechanism of water diffusion and to estimate his dependence from temperature and pressure.

## II – Glasses and Melts

Glasses were historically defined as inorganic products of fusion, cooled to a rigid condition without crystallizing (Scholze, 1991). This definition is not completely satisfactory because it restricts the term glass to products that are cooled from a molten state, while nowadays glasses are produced also by vapour deposition or by sol-gel processing of solutions. Besides, most glasses are inorganic, but we currently use a large number of organic glasses, too. A structural definition calls glass a non-crystalline solid, but a non-crystalline solid is not necessarily a glass as for the case of some organic resins. Thus, it is difficult to give a definition of glass, but we can say that all glasses share two common characteristics: they are lacking in long range, periodic atomic structure and exhibit time-dependent glass transformation behaviour. This behaviour occurs over a temperature range called glass transformation region and will be described in paragraph II.2.

In nature glasses are not very common and form prevalently when molten volcanic lavas reach the earth's surface and cool down rapidly such as basalts (pillow lavas). Obsidians are the most famous natural glasses, they were used to make knives and arrowheads since the Stone Age and present a composition close to that of the modern industrial glasses. Obsidians are black or grey and show a typical brittle fracture called conchoidal due to the high cooling rates during quench. They contain less than 3 wt% of H<sub>2</sub>O and may present microscopic bubbles or crystalline inclusions such as feldspars, micas or pyroxenes. Pitchstones are natural volcanic glasses, too. They resemble obsidians in many ways such as dull, resinous luster and conchoidal fracture, but they differ from the latter in having a higher water content of up to 7 wt% (Heide et al., 2003). Natural glasses can also be formed by lightning strikes (fulgurites), or meteorite impacts (tektites). In particular the latter are of commercial interest for hazardous waste immobilisation or conversion due to their extremely high durability (Shelby, 2005).

Apart of these natural cases, all glasses are essentially artificial products. The silicate glasses are the most important ones, covering the major part of the industrial glass products.

### II.1 - Glass components and network hypotheses

If liquids have an unordered structure, this must also be true for glasses as frozen-liquids. The beginnings of the network studies go back to Zachariasen (1932) that introduced the so called “Random Network Theory”. He evaluated that the energy differences between glass and crystal of the same composition are rather small and therefore inferred that in the glass the structural units and the bonding states are the same as in the crystal. V.M. Goldschmidt in 1937, searching a rule for the vitrification conditions of simple oxides, thought that the criterion could be the ratio of the ionic radii  $r_A/r_O$  of the cation and oxygen.

Zachariasen defined a series of rules that describe a generic network structure, which are valid for glasses as well as crystals:

- Each oxygen atom is linked to not more than two cations,
- The oxygen coordination number of the network cation is small,
- Oxygen polyhedra share only corners and not edges or faces,
- At least 3 corners of each oxygen polyhedron must be shared in order to form a three-dimensional network.

To apply these rules to explain the glass formation, it has to be assumed that the network

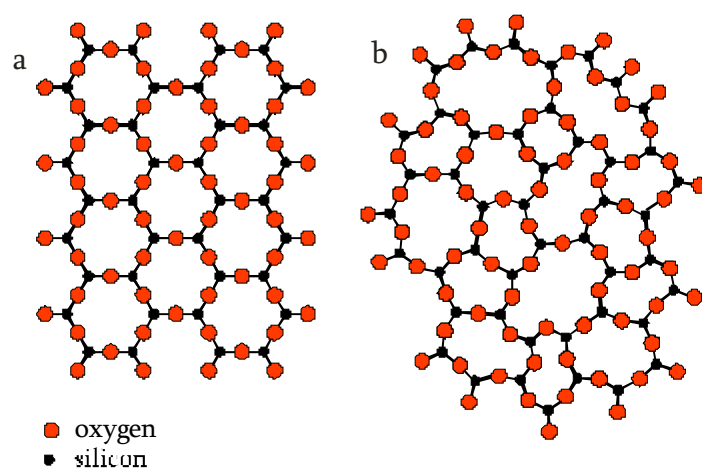


Fig.1 a - b Two dimensional image of an ordered SiO<sub>2</sub> structure two dimensional image of a continuous random SiO<sub>2</sub> network. (Model after Zachariasen and Warren, 1930).

will be distorted in some way so that the long range periodicity is destroyed. The distortion can be due to variations in bond lengths and bond angles and to rotation of structural units around their axes.

Fig. 1 (a-b) shows a comparison of an ordered and an unordered silicate network. The base of a glass formation is the network, in the given example it is just built

by  $\text{SiO}_4$  tetrahedrons, but a vitreous silicate network can be built by several components. The cations able to form this kind of polyhedron are called network formers and are the base of the glass structure. Different elements like Si, B, P and Al can act as network formers and a first classification of the glasses can be done according to the principal glass formers. Different former oxides may influence the properties of the glasses:

- Silica is the most important glass network former, building a disordered three-dimensional structure based on  $\text{SiO}_4$  tetrahedra. It reduces the thermal expansion coefficient and improves mechanical strength.
- $\text{B}_2\text{O}_3$  decreases the viscosity at high temperature and increases it at low temperature. It also improves the resistance to mechanical abrasion.
- $\text{P}_2\text{O}_5$  raises the UV- and reduces the IR-transmission. Furthermore it reduces the chemical resistance of a glass.
- $\text{Al}_2\text{O}_3$  increases the viscosity and the chemical durability of glasses.

A large number of other compounds such as  $\text{GeO}_2$ ,  $\text{Bi}_2\text{O}_3$ ,  $\text{Ga}_2\text{O}_3$  and  $\text{V}_2\text{O}_5$  may act as glass formers together with other oxides under certain conditions. Finally, cations that never act as network formers but are able to depolymerise the structure are called network modifiers. They are largely used in the industry as fluxes to reduce the high melting temperature of pure  $\text{SiO}_2$ . The most used are:

- $\text{Na}_2\text{O}$ , which reduces the viscosity and the chemical resistance while it increases the expansion coefficient and the electrical conductivity.
- $\text{Li}_2\text{O}$  and  $\text{K}_2\text{O}$  increase the devitrification behaviour by reducing viscosity.
- $\text{CaO}$  and  $\text{MgO}$  are the most important among the alkaline-earth oxides. In particular  $\text{CaO}$  improves the chemical resistance of  $\text{SiO}_2$ - $\text{Na}_2\text{O}$  glasses by reducing their solubility in acids.  $\text{MgO}$  improves the chemical durability.

### ***II.2 - The time-dependent glass transformation behaviour***

Glasses respond to a change of temperature in a characteristic way: they do not show a melting point like crystals but they soften with increasing temperature and progressively pass from an elastic solid to a less and less viscous liquid. This is called the glass transformation. The glass transformation behaviour is shown in the enthalpy versus

temperature diagram of Fig.2. Considering a small volume of melt quite above the melting temperature and cooling it down below the melting temperature of the crystal, it will form a long range periodic atomic arrangement and therefore a crystalline state.

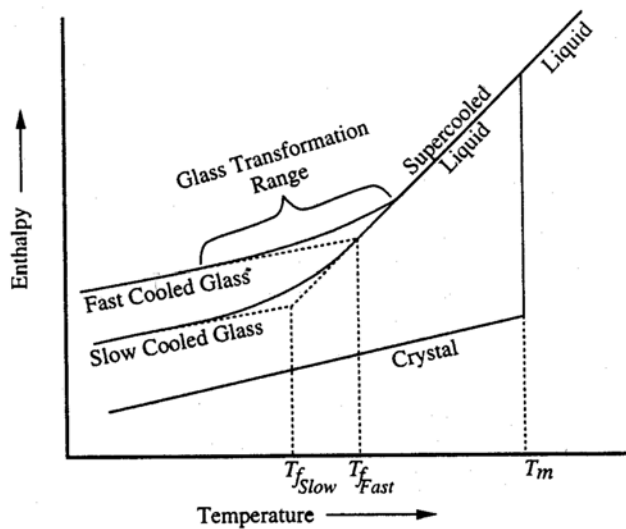


Fig. 2 : (from Shelby, 1997) Schematic diagram of the effect of temperature on the enthalpy of a glass.

In this case the enthalpy will decrease to the appropriate value of the crystal. If the cooling is fast enough, the melt will not form crystals but a supercooled liquid. In this case the enthalpy will not decrease abruptly, due to the kinetically hampered structure rearrangement. Continued cooling of the freezing melt will produce an increase of viscosity until the atoms will be no longer able to

rearrange to the equilibrium liquid structure in a short time. The enthalpy shows a gradually decreasing slope and the viscosity increases, so that the structure of the liquid becomes fixed and no longer temperature-dependent. The temperature zone bordered by the enthalpy of the equilibrium liquid and that of the frozen solid is defined as glass transformation region. Below that region the liquid is a glass.

The temperature at which the enthalpy departs from the equilibrium curve is controlled by several parameters such as the viscosity of the liquid and kinetic factors. The use of a slower cooling rate will allow the enthalpy to follow the equilibrium curve to lower temperature better than the use of a faster cooling rate. Therefore, also the atomic arrangement will be the characteristic one of the equilibrium at a lower temperature rather than that of the faster cooled glass. To characterize the thermal history of glasses, it was introduced the concept of fictive temperature  $T_f$ . It may be defined as the intersection of the extrapolations of the glass and of the supercooled liquid lines.

It is evident that the glass transformation occurs over a range of temperatures but it is commonly referred to just as a single temperature, called the glass transition temperature ( $T_g$ ), as indication of the onset of the glass transformation region during heating of a glass. The  $T_g$  of a glass is defined by standard procedures consisting of sequence of heating and cooling ramps at different rates.  $T_g$  cannot be considered as a true property of a glass; it can be obtained from changes in thermal analysis curves or thermal expansion curves and is strongly dependent on the heating rate used during the experiments. Anyway,  $T_g$  can be used to evaluate the approximate temperature at which the supercooled liquid converts to a solid for cooling or converse for heating. According to a rather conventional definition, the glass transition occurs at a temperature where the viscosity of the supercooled liquid reaches  $10^{12}$  Pa·s (Scholze and Kreidl, 1986). This viscosity has been chosen because at this value the relaxation times for macroscopic properties are about 15 min (at usual laboratory cooling rates), which is similar to the time required to measure these properties (Litovitz, 1960).

### ***II.3 – Relaxation time and Maxwell equation***

Silicate melts show two different mechanical responses to an applied stress:

- *Elastic*: the strain response to an applied stress is time independent and reversible. The slope of the stress-strain ( $\sigma$ - $\varepsilon$ ) curve gives the elastic constant for the material. This is called the elastic modulus E:

$$E = \frac{\sigma}{\varepsilon} \quad [1]$$

- *Viscous*: the strain response to an applied stress is time dependent and non-reversible. The non-elastic relation between the applied stress  $\sigma(t)$  and the deformation  $\varepsilon$  for Newtonian fluids is described by the following expression:

$$\sigma(t) = \eta \frac{d\varepsilon}{dt} \quad [2]$$

where  $\eta$  is the Newtonian viscosity of the material.

The intermediate region between the elastic and the viscous behaviour is called visco-elastic region. The structural relaxation time  $\tau$  is a convenient approximation of the

timescale of deformation over which transition from a purely elastic to a purely viscous behaviour occurs, and it is expressed by:

$$\tau = \frac{\eta}{E} \quad [3]$$

Recent studies have shown that the transition between liquid-like to a solid-like mechanical response can play a crucial role in volcanic eruptions (Dingwell and Webb, 1990; Sato et al., 1992; Dingwell et al., 1996; Papale; 1999). In particular, the intersection of this kinetic boundary during an eruptive event may have catastrophic consequences, because the mechanical response of the magma or lava to an applied stress at this brittle/ductile transition governs the eruptive behaviour (Sato et al., 1992).

The melt viscosity and the relaxation time are related by the Maxwell (1867) relationship (Dingwell and Webb, 1990):

$$\tau = \frac{\eta_N}{G_\infty}, \quad [4]$$

where  $G_\infty$  is the shear modulus with a value of  $\log_{10}(\text{Pa}) = 10 \pm 0.5$  (Webb and Dingwell, 1990) and  $\eta_N$  is the Newtonian shear viscosity. Due to the thermal activation processes of structural relaxation, Newtonian viscosity in the glass transition range depends on the cooling history. For cooling rates on the order of several K/min, viscosities of approximately  $10^{12}$  Pa·s (Scholze and Kreidl, 1986) give relaxation times on the order of 100 s (Scherer, 1984; Stevenson et al., 1995).

## III – Structure of Silicate Glasses

### *III.1 – Coordination of the network cations*

The glass network constitutes of structural units such as tetrahedra, octahedra or triangles which provide a short range order at a level of several associated atoms or ions. Therefore, the most basic element to define a glass structure is the coordination number of all the constituent cations. At the beginning it was calculated using the cation's radius ratio or observing the cation's coordination states in other materials, such as crystals with well defined structures. Nowadays many modern spectroscopic methods, such as the magic angle spinning nuclear magnetic resonance (MAS-NMR) and the X-ray absorption spectroscopy (XAS), can directly determine the coordination state. In this way it was found that silicon at ambient pressure presents mostly a tetrahedral coordination, while boron can exist in 3- and 4-fold coordination (Fleet & Muthupari, 1999) and aluminium and germanium show either a 4- or 6-fold coordination in oxide glasses (Ildefonse et al., 1998; Henderson & Wang, 2002). At high pressure, silicon can show also a 5- or 6-fold coordination (Williams & Jeanloz, 1988).

### *III.2 – Network connectivity*

Four kinds of bonds are generally of interest:

- Covalent or atomic bonds, in which two bonding electrons are shared by two partners; this is a direct bond.
- Heteropolar or ionic bonding, in which the cation gives a valence electron and the anion receives it.
- Metallic bond, where electrons are easily mobile in the network.
- Secondary valence bond, a relatively weak one, where atoms or molecules are attracted by their permanent or induced electric dipoles. Of great importance is the so called hydrogen bond, in which an H atom is partially bound to an adjacent O atom by the so called “Van der Waals” interactive force.

In a glass network the number and the arrangement of bridging and non-bridging bonds in the structure is of fundamental importance. That determines the links between the structure units and is called network connectivity. In particular, the distribution and concentration of non-bridging oxygens (NBO), those which do not connect polyhedra, is important. The parameter NBO/T, non-bridging oxygens per tetrahedron (Mysen et al, 1985), is frequently used as a structural parameter to indicate the degree of polymerisation of a silicate melt. If NBO/T=0, the melt is fully polymerised. According to Mysen et al. (1985) the NBO/T can be calculated using:

$$\frac{NBO}{T} = \frac{1}{T} \sum_{i=1}^i nM_i^{n+} \quad [5]$$

where T is the total atomic abundance of tetrahedrally coordinated cations,  $M_i^{n+}$  is the proportion of network modifying cations, “i”, with electrical charge  $n+$  after subtraction of the portion required for charge-balancing trivalent cations on tetravalent sites (Mysen,1988). The use of this equation is controversial and non-univocal because it is not easy to define “*a priori*” the cation coordination that is in fact dependent on the composition.

### ***III.3 – Overview on Oxide Glasses***

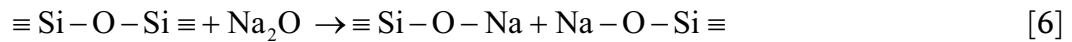
The major number of glasses contains oxygen as an anion, which occurs during linking as bridging oxygen.

#### ***III.3.1 – Single-Component Glasses***

Among the single-component glasses, the silicate ones (SiO<sub>2</sub>) are the most famous and used for the virtue of their composition and the consequent technical applications. In the two-dimensional representation shown in fig. 1-b, the network shows rings of different dimensions that surround empty spaces. The resulting reticulate is rather broad and, e. g., allows some gases like He, Ne and Ar to diffuse through.

***III.3.2 – Influence of X<sub>2</sub>O***

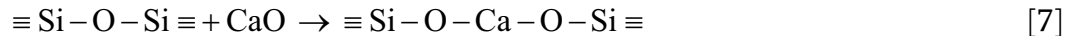
In the single-component glasses all O<sup>2-</sup> occur as bridging oxygens, while in the alkali silicate glasses non-bridging oxygens occur adjacent to the alkali ions by the reaction:



The introduction of Na<sub>2</sub>O causes an opening of closed connections. Each Na<sup>+</sup> ion that is introduced produces a non-bridging oxygen. This formation of non-bridging oxygens represents the most important influence of the alkali oxides. In that way, they destabilise the glass structure, whereas it is strengthened by the formation of Si-O-Si bridging oxygens.

***III.3.3 – Influence of XO***

Several glasses contain both alkali and alkaline earth elements. Ca is the most common constituent of alkaline-earth oxides and its incorporation in the silicate network can be described in a similar way to the introduction of an alkali atom:



The Ca-O bond is clearly stronger than that of Na-O, so that the two non-bridging oxygens that are formed maintain a bond with the Ca<sup>2+</sup> ion.

## IV – Transport properties

Historically, the properties of glasses were summarized in two principle types (Shelby, 1997):

- On the one hand those related to the structure and to impurities are transport properties such as electrical and thermal conductivity and the various “losses” like dielectric and viscoelastic.
- On the other hand those related to the composition of the glass, which are basically dependent on the nature of the atoms and on interactions between them, such as density, elastic constant, specific heat, dielectricity and permittivity.

This distinction is not straight forward, since structure and composition are inter-related. Therefore, diffusion could be also described as a function of composition.

Two fundamental mass transport types exist:

- First convection, in which matter is transported by the large-scale motion of fluxes in the fluid. In convective processes, the flux is generated mostly by differences in density or by pressure gradients. Convection is mainly described by Darcy’s law, which models the flow of a liquid through a permeable medium:

$$v = \frac{\kappa}{\eta} (-\rho g + \nabla P) \quad [8]$$

where  $v$  is the velocity,  $\kappa$  the permeability,  $\eta$  the viscosity,  $\rho$  the density,  $g$  the gravity and  $\nabla P$  the pressure gradient.

- Second diffusion, in which the matter transport is determined by thermal motion of particles that move more or less independently and on an atomic scale. In diffusion processes the underlying basic of the migration is thermal motion of particles. The presence of chemical potential gradients imposes a preferred direction for the motion. The random motion is excited by thermal energy. In the case of pure diffusion, there is no bulk flow. If there is no gradient in chemical or electric potential, random motion still occurs but it does not lead to detectable changes. Usually diffusion is driven

by a chemical potential gradient. In the case of a stable phase, chemical potential and concentration of a component are positively correlated and the diffusion would homogenize the phase. Instead, if the phase is metastable, diffusion will lead to a separation into two phases and will help to homogenize each of them.

In liquid and gas, flow or convection are the dominant ways of mass transfer. However, diffusion plays an important role in many geological processes, such as solid-state reactions in crystal growth or dissolution, fluid-rock interaction, magma mixing, exsolution etc.. The study of diffusion is crucial for the determination of rock ages, for thermochronology, and geospeedometry researches.

A large number of glass properties are related to diffusion, or transport of atoms and ions through the vitreous network. In the case of oxide glasses, the electrical conductivity is often controlled by the diffusion of the monovalent ions under the influence of an external electric or magnetic field. Dielectric and mechanical losses are often due to the movement of mobile ions under the influence of a reversing electric or stress field. Chemical dissolution, often used to increase the mechanical strength of a glass, is also a diffusion phenomenon occurring at the glass surface and involving alkali ions from the glass and protons from the surrounding fluid. The permeation of gases (e.g. noble gases) through glasses is controlled by the mobility of ions or molecules or atoms through the glass network and is important in industrial processes for the elimination of gas bubbles in the process of glass fining (Doremus, 1960; Shelby, 1997).

In the following chapter, the explained concepts apply to crystals and not to glasses or melts.

#### *IV.1 – Different diffusion types*

If a component is not homogeneously distributed in a phase in that way that its concentration in one part is higher than in another, there is net atom-by-atom migration, called diffusion, of the component following the concentration gradient. This diffusion will lead eventually to homogeneous distribution.

In a system, two or more distinguishable components could be present such as different isotopes or chemical species. For simplicity, a binary system, that is a system with two components, is considered here. If the two species are two different isotopes of the same elements, such as  $^{18}\text{O}$  and  $^{16}\text{O}$ , the diffusion is called “*self diffusion*”. If marked particles present in very low concentration, such as stable or radioactive isotopes of a minor or major component of the material, move through a homogeneous medium, the diffusion is called “*tracer diffusion*”. If diffusion in a system involve three or more components, such as Ca, Fe and Mg diffusion in garnet, is called “*multicomponent diffusion*”. If a diffusion component may be present as two or more different species, as  $\text{H}_2\text{O}$  or  $\text{CO}_2$ , the diffusion of the component is referred as “*multi-species diffusion*”.

An atom in a network can have a position in the lattice itself or can occupy an interstitial position. Defects, that are a local perturbation of the periodicity in a lattice structure, play an important role in diffusion, in particular in crystalline phases. If defects are due to impurity content, they are called extrinsic defects. Otherwise they are called intrinsic defects. With the production of defects, there are different ways to maintain charge neutrality for intrinsic defects. If stoichiometric proportions of vacancies are produced in cation and anion sites, then it is called Schottky defect. If equal numbers of vacancies and interstitials of one ion are produced, then it is called Frenkel defect (Zhang, 2008).

Based on the lattice or interstitial positions, two fundamental diffusion mechanisms can occur: vacancy diffusion and interstitial diffusion.

#### *IV.1.1 – Vacancy diffusion*

Vacancy diffusion is conducted by the movement of atoms from one atomic site to

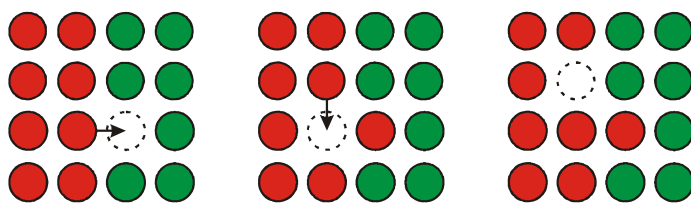


Fig. 3: Vacancy diffusion occurs primarily when the diffusing atoms are of similar size or substitutional atoms by exchange of atoms with vacancies. The rate of diffusion depends on the number of vacancies and on the activation energy for the exchange.

another (Fig. 3). Crystalline solids present a very regular atomic structure in which the local positions of atoms with respect to each other are repeated at the atomic scale, but

may present some defects due to the presence of impurities or free sites. In the first case, a simple substitution occurs in which one atom or ion occupies the net position of another one. In the second case a vacancy in the lattice is present and one of the adjacent atoms can move into the vacancy, creating another vacancy on its former site.

The diffusion of an atom is therefore dependent on the concentration of defects on an adjacent site, on the frequency and on the distance at which one ion can move into another position.

#### *IV.1.2 – Interstitial diffusion*

Interstitial diffusion occurs when the diffusing atom is on an interstice and not on a lattice site (Fig. 4). In this case, the diffusing species is free to move from one interstice to another. Here the fraction of atoms on interstitial sites and their mobility is determining the diffusion. Examples are Ag diffusion and Na diffusion in feldspars (Behrens et al.,

1990). Interstitial diffusion is more rapid than

vacancy diffusion.

The dependence on the presence of vacancies makes vacancy diffusion slower than interstitial diffusion.

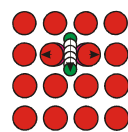
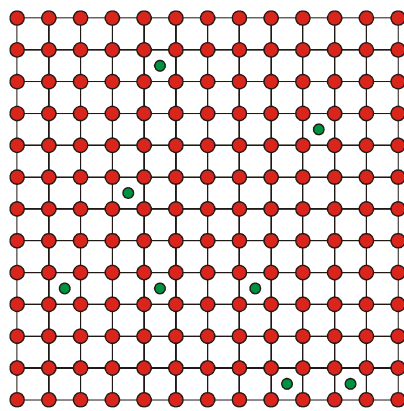


Fig. 4: interstitial diffusion applies to interstitial impurities and to main constituents with Frenkel defects.

#### *IV.2 – Diffusion Laws*

Considering a glass with an internal concentration gradient of the element  $i$  and a temperature  $T$  high enough, diffusion will occur. Measuring the distribution of the element  $i$  at successive time  $t_1$ ,  $t_2$ ,  $t_3$ , a progressively smoother concentration profile will be obtained, eventually leading to an uniform distribution of  $i$ . The flux  $J$  can be expressed as the amount of the component  $i$  that migrate through a unit area per second. The Fick's First Equation shows that the flux  $J$  is in first order proportional to the

concentration gradient. The following expression is Fick's first law for one-dimensional diffusion:

$$J = -D \frac{\partial c}{\partial x} \quad [9]$$

where  $D$  is the diffusivity,  $\frac{\partial c}{\partial x}$  is the concentration gradient and the negative sign indicates that the direction of diffusive flux is in the direction of the lower concentration. The second Fick's law deals with a non-uniform concentration gradient describing diffusion into a sample by the rate of change of concentration with time at a given distance:

$$\frac{\partial c}{\partial t} = D \frac{\partial^2 c}{\partial x^2} \quad [10]$$

where  $D$  is the constant diffusivity, independent from the concentration, and  $t$  is the time. This equation shows that the concentration will change quickly if the concentration gradients and the diffusivity are high.

### ***IV.3 – Nernst-Einstein equation***

Einstein recognised that the main driving force of diffusion was the chemical potential  $\mu$ , describing the flux with the relation:

$$J = -M \frac{\partial \mu}{\partial x} \quad [11]$$

where  $M$  is the mobility. The velocity  $v_i$  of the ion  $i$  under a defined chemical potential gradient is expressed by:

$$v_i = -B \frac{1}{N} \frac{\partial \mu_i}{\partial x} \quad [12]$$

where  $B$  is the absolute mobility,  $N$  is the Avogadro's number and  $\mu_i$  is the chemical potential of  $i$  species. In this way, the flux of the species  $i$  with concentration  $C_i$  can be defined by:

$$J_i = C_i v_i \quad [13]$$

by substitution, considering the activity coefficient equal to one, it is obtained:

$$J_i = -\frac{RT}{N} \frac{\partial c}{\partial x} B_i \quad [14]$$

Comparing this result with Fick's equation, the diffusion coefficient  $D_i$  for the species  $i$  is:

$$D_i = kT_i B_i \quad [15]$$

This is the Nernst-Einstein relation and will be used in the next chapter (V.1) for the electrical conductivity.

#### IV.4 – Temperature dependence

Practical experiments determined that often thermally activated process shows an Arrhenius type temperature dependence:

$$D = D_0 e^{\frac{-E_a}{RT}} \quad [16]$$

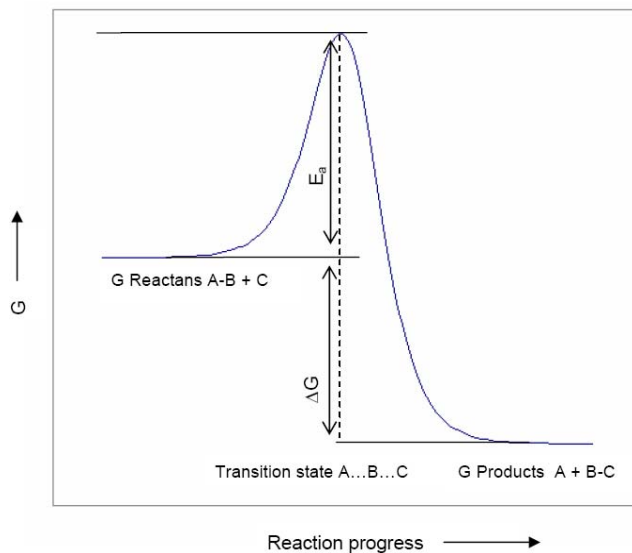
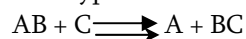


Fig. 5: Energetics of a hypothetical reaction:



The y axis shows the free energy  $G$  of the system.  $E_a$  is the activation energy, which is released again at the end of the molecular reaction (from Binnewies et al., 2004).

where  $E_a$  is the apparent activation energy for diffusion,  $D_0$  is the frequency factor,  $T$  is the temperature and  $R$  is the gas constant. For physical and chemical processes often an energy barrier exist, which impedes progress from an initial high-energy state to a lower-energy configuration in which the system would be more stable, as shown in Fig. 5.

The barrier arises because the reactants have to pass through a higher energy transition state to lead to the products. For a reaction

involving the breaking of one bond and the formation of a new one, the process involves the formation of a less stable intermediate molecular species, called the activated complex. The activation energy  $E_a$  in the Arrhenius relation may be visualized as the height of the barrier relative to the initial reactant assemblage. The proportion of

molecular encounters involving kinetic energies greater than the critical value  $E_x$  is given by:

$$n \propto e^{\frac{-E_a}{RT}} \quad [17]$$

where the right term is called Boltzmann factor. It is a measure of the proportion of the reactant molecule collision that possesses sufficient energy at the temperature  $T$  to reach the transition state and therefore to complete the reaction. It is evident that by increasing the temperature the energy distribution will shift towards higher energies, while by decreasing the temperature the reaction will be inhibited. In other words, the activation energy indicates how sensitive the rate of a reaction will be to changes in temperature. Transforming both sides of the Arrhenius equation into natural logarithms, it is obtained:

$$\log D = \log D_0 - \frac{E_a}{R} \frac{1}{T} \quad [18]$$

Thus a linear relationship between  $\log D$  and  $1/T$  is expected in case of an Arrhenian behavior with the slope corresponding to  $-E_a/R$ . However, the activation energy may include contributions of defect formation as well.

The diffusivity increases with increasing temperature and may decrease or increase with increasing pressure:

$$D = A \exp \left[ - \frac{(E_a + P\Delta V)}{RT} \right] \quad [19]$$

where  $A$  is a pre-exponential factor,  $E_a$  is the activation energy that is always positive, and  $\Delta V$  is the volume difference between the activated complex and the diffusing species that can be positive or negative. Arrhenius behaviour is generally valid only in a limited temperature range, structural changes of the diffusion medium as well as a change in the diffusion mechanism can lead to non-arrhenian diffusion behaviour.

In general, diffusivity decreases with pressure, due to the expanded size during movement of atoms from one stable site to another one (activation volume  $\Delta V$ ). An increase with pressure is observed only if defects are formed upon pressurization. This could be either weakened or disrupted bonds or fluid-induced defects (e.g. dissolved  $H_2O$  may react with the host materials imposed by water fugacity).

### *IV.5 – Solution to diffusion equations*

Studies of diffusion require the solving of a diffusion equation, which is often in the form of a partial differential equation. It is necessary to specify the initial and the boundary conditions to calculate the solution for the specific equation.

#### *IV.5.1 – Initial and boundary conditions*

The initial condition is in general  $C_{t=0} = f(x)$ . In the most simple case, the concentration at  $t=0$  is constant.

The boundary conditions may be more complicated and three cases are identified (Zhang, 2008):

- For one-dimensional diffusion, there are two ends. In the case that both ends participate in diffusion, the diffusion medium is called a finite medium with two boundaries.
- For one-dimensional diffusion, if diffusion starts somewhere in the inner part and has not yet reached either of the two ends, the diffusion medium is called an infinite medium (as in the case of diffusion couple considered in Chapter 2). In that case there are no boundaries and the  $C_{x=-\infty}$  or the  $C_{x=+\infty}$  must be finite and equals to the respective initial concentration.
- If diffusion starts from one end (surface) and has not reached yet the other end in one dimensional diffusion, the diffusion medium is called a semi-infinite medium (as in the case of the dehydration illustrated in Chapter 2).

#### *IV.5.2 – Experimental technique and solution methods*

Several methods to solve a partial differential equation were elaborated, such as Boltzmann transformation, principles of superposition, Laplace transform, etc. (Crank, 1975). To describe these methods, as to consider the various sorts of diffusion, would be outside the scope of this work. Therefore, in this section, just a few cases will be taken into account.

The most common experimental technique in diffusion studies is the diffusion couple. It consists of a coupling of two halves of media, each of these initially homogeneous, with two different compositions or concentration gradients. During the experiment, a diffusive flux moves across the interface trying to homogenize the couple. The duration of the experiment should be short enough to have at both ends still the initial concentrations. Under such conditions, the diffusion medium can still be treated as infinite and the diffusion problem can be solved using the Boltzmann transformation method.

### *IV.5.3 – Concentration-dependent $D$ and Boltzmann analysis*

Considering that the concentration at the two ends are unaffected by diffusion, it is possible to define the interface between the two halves as  $x = 0$ , the initial concentration for  $x < 0$  as  $C_1$ , and the initial concentration for  $x > 0$  as  $C_2$ . When diffusivity varies with concentration, for one-dimensional diffusion depending on concentration, the following equation must be used :

$$\frac{\partial C}{\partial t} = \frac{\partial}{\partial x} \left( D(C) \frac{\partial C}{\partial x} \right) \quad [20]$$

Even if this equation is non linear, as long as initial and boundary conditions allow, the Boltzmann transformation can be applied to obtain concentration-dependent diffusivity from experimental diffusion profiles. In particular, if  $D$  depends on concentration, but the functional dependence is not known,  $D$  could be obtained at every concentration along the diffusion profile by the equation (Zhang, 2008):

$$D = \frac{\int_{C(x_0)}^{C(\infty)} x dC}{2t \left( \frac{dC}{dx} \right) \Big|_{x=x_0}} \quad [21]$$

for a diffusion couple or a semi-infinite diffusion medium with uniform initial concentration, with  $C_{x>0} = C(\infty)$ , then  $\partial C / \partial x = 0$  for  $x = \infty$  (Zhang, 2008). In order to use this equation, the position of the interface  $x = 0$  needs to be accurately determined. For a semi-infinite diffusion medium this is easy, being  $x = 0$  for the surface. In contradiction, for the diffusion couple, it could be very difficult to find the interface.

A modified method that makes this step unnecessary was proposed by Sauer and Freise in 1962 as follow:

$$D = \frac{1}{2t \left( \frac{dy}{dx} \right)_{x=x_0}} \left[ (1-y)|_x \int_x^{+\infty} y dx + y|_x \int_{-\infty}^x (1-y) dx \right] \quad [22]$$

where  $y = \frac{(C - C_{\min})}{(C_{\max} - C_{\min})}$  and considering the curve plotted with  $y = 1$  at  $x = -\infty$  and  $y = 0$

at  $x = \infty$ . The smoother the empirically fit of the data, the more accurate will be the evaluation of the diffusivity D.

## V – Electrical Properties

Among the electrical properties of glasses, conduction and dielectric properties play the major roles. In the glass structure the network modifier cations, such as alkali, are ionically bounded to the other network neighbours. These ions have certain mobility and give a glass electrical conductivity.

The conductivity  $\sigma$  is defined by the relation:

$$\vec{j} = \sigma \vec{E} \quad [23]$$

where  $\vec{j}$  is the current density and  $\vec{E}$  is the applied electric field. The reciprocal value of  $\sigma$  is the electric resistance  $\rho$ . The conductivity of a glass is strictly related to its composition and to the temperature at which the measurement is performed. Conductivity rises with temperature and an insulator material progressively transforms into a conductor.

In a general form, the conductivity  $\sigma_i$  associated with a carrier  $i$ , can be described by:

$$\sigma_i = C_i z_i \mu_i \quad [24]$$

where  $C_i$  is the concentration or the number of carriers with the charge  $z_i$  per volume unit, showing the mobility  $\mu_i$ . The mobility of the charge  $i$  can also be related to the absolute mobility  $B_i$  by:

$$\mu_i = z_i B_i \quad [25]$$

The total conductivity  $\sigma_T$  is the sum of the partial conductivities  $\sigma_i$ . The transport number of the species  $i$  is defined by:

$$t_i = \frac{\sigma_i}{\sigma_T} \quad [26]$$

Conductivity is mostly measured by alternating current methods because, in this way, polarization phenomena can be prevented (Zarzycki, 1990; Shelby, 1997).

### *V.1 – Relation between conductivity and diffusion*

Assuming electrical and diffusion mechanisms are the same, the mobility  $\mu_i$  of the  $i$  ion is related to the self-diffusion coefficient  $D_i$  by the Einstein equation:

$$\mu_i = z_i B_i = \frac{z_i D_i}{kT} \quad [27]$$

where by replacing  $\mu_i$  by  $\frac{\sigma_i}{C_i z_i}$  and introducing the transport number  $t_i$ , it is obtained:

$$(D_i)_\sigma = \frac{\sigma_i t_i}{C_i z_i^2} kT \quad [28]$$

which is called the Nernst-Einstein equation. (It was already derived in case of diffusion in paragraph IV.3)

This equation was investigated by several authors but only in few cases the measured conductivity corresponded to the calculated one. In particular for soda-lime silica glasses it was found that the measured coefficient  $D_i$  was always smaller than the calculated  $(D_i)_\sigma$  one (Zarzycki, 1990). Therefore, a correlation factor  $f$ , resulting with  $0 < f \leq 1$ , has been introduced in:

$$D_i = f(D_i)_\sigma \quad [29]$$

The corrected Nernst-Einstein relation can then be written as:

$$(D_i)_\sigma = f \frac{\sigma_i t_i}{C_i z_i^2} kT \quad [30]$$

## V.2 – Dependence on composition

Conductivity is related to the glass composition in a complex way because many parameters enter into the process. If it is considered an ion in a potential state separated by a potential barrier of height  $E_a$  from another potential state at a distance  $a$ , then for the jump probabilities in an electrical field  $E$  the following relation for the specific electrical conductivity is obtained:

$$\sigma = \frac{a^2 z^2 e^2 \nu N}{2kT} e^{-\frac{E_a + E/2}{kT}} \quad [31]$$

where  $z$  is the charge of the ion,  $e$  is the elementary charge,  $\nu$  is the oscillation frequency of the ion,  $N$  is the quantity of ions able to migrate per  $\text{cm}^3$  and  $k$  is the Boltzmann's constant (Scholze, 1991).

If the charge carriers move independently, the electrical conductivity is directly proportional to the number of charge carriers as well as to their mobility. Otherwise,

cooperative processes may be present which act in reducing the conductivity. Not only the valence and the size of the charge carriers are important but also the structure of the network, which also changes with the concentration of the mobile species. Ravaine, in 1980, has shown that the smaller the difference of electronegativities of the network former and the anion is, the larger will be the electrical conductivity. These factors influence also the activation energy, considering a  $\text{SiO}_2 - \text{X}_2\text{O}$  (with  $\text{X} = \text{Li}, \text{Na}, \text{or K}$ ) glass. At low concentration of the component X, the activation energy will increase following the increasing ionic radius, while at higher concentrations it will increase with the order of ionic forces. In the first case the apparent activation energy will be higher for a  $\text{K}^+$  ion that has the biggest atomic radius, whereas in the second case the  $\text{Li}^+$  ion has the highest ionic field. Concentration and conductivity are not related by a simple proportionality; rather, the increase of conductivity is sharper than that of concentration. The Nernst-Einstein equation is useful to understand the electrical conductivity since many data on self diffusion are available, especially for silicate glasses (Frischat, 1975). Using diffusion data it has been shown that the alkali cations have in the most cases the highest diffusion rates, determining the electrical conductivity of a glass through forming non-bridging oxygens atoms. Therefore, if a glass contains no network modifiers, it should possess no non-bridging oxygens and consequently very slight conductivity. Instead, many conductivity measurements done on vitreous silica show deviations by several orders of magnitude compared to the expected ones. This phenomenon is referred to the presence of a very low amount of impurities, such as Na, in the analysed glasses. In particular, it was shown that a content of only 0.04 ppm of Na in a vitreous silica at 573 K gives a resistance of about  $10^{13} \Omega\text{cm}$ , while increasing the amount of Na to 20 ppm the resistance decreases to about  $5 \cdot 10^9 \Omega\text{cm}$  (Owen and Douglas, 1959; Scholze, 1991). Taking into account other alkali cations, two parameters have to be considered: the bond-strength of ions in a network and the size of the atoms.  $\text{K}^+$  ions are bonded more weakly than  $\text{Li}^+$  and  $\text{Na}^+$ , but their larger radius strongly increases the resistance to diffusion. Therefore, for alkali silicate glasses, the resistance increases along the sequence  $\text{Li}^+ - \text{Na}^+ - \text{K}^+$ .

Considering the substitution of  $\text{SiO}_2$  by other oxides (as measured by Fulda in 1927 for a  $\text{Na}_2\text{O}$ - $\text{SiO}_2$  glass with  $\text{SiO}_2$  replaced proportionately by weight by  $\text{CaO}$ ,  $\text{MgO}$ ,  $\text{PbO}$ ,  $\text{ZnO}$ ,  $\text{B}_2\text{O}_3$ ,  $\text{Al}_2\text{O}_3$  and  $\text{Na}_2\text{O}$ ), it has been shown a consolidation of the network and consequently a large increase of resistivity for  $\text{CaO}$ ,  $\text{BaO}$  and  $\text{B}_2\text{O}_3$ . In this case the mobility of alkali cations is reduced.

### *V.2.1 – Mixed alkali effect*

With glasses containing alkalis, a surprising behaviour has been discovered: with gradual substitution of one alkali ion by another alkali ion, some properties display a non linear behaviour, for example electrical conductivity, but also dielectric loss, internal friction and self-diffusion, thus all properties which are affected by transport mechanisms (Day, 1976). This effect is called the mixed alkali effect, although meanwhile it turns out that the non-alkali oxides can also show such an effect (Isard, 1969; Scholze, 1991; El-Damrawi, 2001). In a mixed alkali glass with two different types of alkali ions, the diffusivities of both increase with increasing the relative concentration. When the concentrations of the dissimilar ions are identical, it is reached a crossover point where the diffusivities are identical, too. On both sides of the diffusivity crossover point, the charge transport, for example for the electrical conductivity, is dominated by the more mobile ionic species. Therefore, the ionic conductivity reaches a minimum at a composition close to the diffusivity crossover composition (Isard, 1969; Day, 1976; Ingram, 1987). This behaviour, compared to that of the single alkali glasses, is attributed to interactions between dissimilar ions (Mazurin, 1965; Hendrickson et al., 1972; Dietzel, 1983; Sato et al., 1992), to phase separations (Cahn et al., 1965) or to cation sites of different size (Lengyel, 1963; Stevels, 1957). In the model of Bunde et al., 1993-1994 the hopping of each occurs via sites of its own type, while additional activation energy is required to enter a site of a different type. When the number density of the ions of one type decreases, also the number of favourable sites decreases. This leads to an increase of the activation energy required for the long-range transport.

### *V.2.2 – Effect of water on ionic transport in glasses*

Water, as hydrogen oxide, can be considered in first approximation as an alkali oxide with a cation with high field strength, due to the small cation-anion distance in the H-O bonding, which is less than the ionic radius of the O<sup>2-</sup> ion.

Various studies have been made on the effect of dissolved water on ionic transport in glasses. Schëffer et al. (1979) reported that increasing OH content in SiO<sub>2</sub> glass reduce the Na mobility. They inferred that this effect was due to an interaction between hydrogen and sodium ions similar to the “mixed alkali effect” in silicate glasses. Milnes and Isard (1962) observed an increase in the conductivity of lead-silicate glass with increasing water content. McVay et al. (1976) demonstrated that the dc conductivity of Na<sub>2</sub>O·3SiO<sub>2</sub> glass decrease by a factor of circa 3 and that the Na<sup>+</sup> diffusion coefficient also decrease by a factor of circa 1,6, with increasing water content from 0,003 to 0,027 wt%. Successively, Takata et al. (1980) reported that the dc conductivity of Na<sub>2</sub>O·3SiO<sub>2</sub> glass containing 4 wt% water was approximately two orders of magnitude lower than that of the same composition without water.

Although it is widely accepted that water depolymerises the structure of silica and alkali-silicate glasses (McMillan & Remmele, 1986; Mysen & Virgo, 1986), it is still highly debated whether alumino-silicate glasses depolymerise upon hydration. Most water solubility models based on vibrational spectroscopy propose the depolymerisation of the network either by rupture of Si-O-Si and/or Si-O-Al bonds and formation of Si-OH and/or Al-OH groups (e.g., Bartholomew & Schreurs, 1980; Stolper, 1982; Mysen, 1980) or by formation of Al-OH and Na-OH complexes and nonbridging oxygen (Mysen and Virgo, 1986). However, based on multinuclear nuclear magnetic resonance (NMR) spectroscopic studies (<sup>1</sup>H, <sup>23</sup>Na, <sup>27</sup>Al, <sup>29</sup>Si, <sup>1</sup>H-<sup>29</sup>Si CP), Kohn (Kohn et al., 1989; Kohn et al., 1992; Kohn et al., 1998) found no evidence for significant depolymerisation of the structure of hydrous albite (NaAlSi<sub>3</sub>O<sub>8</sub>) or nepheline (NaAlSiO<sub>4</sub>) glasses. These authors concluded that water dissolution causes only small changes in the aluminosilicate network (no important formation of Si-OH or Al-OH groups) and that water is associated with sodium. Kohn et al. (1989) proposed a water solubility model that involves the replacement of a charge balancing Na<sup>+</sup> by a proton, thus forming a bridging hydroxyl

group on a Si-O-Al linkage. The exchanged Na<sup>+</sup> forms complexes with OH<sup>-</sup> and/or molecular H<sub>2</sub>O. Xue and Kanzaki (2006) have applied one-dimensional H MAS NMR and high-resolution <sup>3</sup>QMAS/HETCORE NMR techniques to KAlSi<sub>3</sub>O<sub>8</sub> (Orthoclase), NaAlSi<sub>3</sub>O<sub>8</sub> (albite) and NaAlSiO<sub>4</sub> (nepheline) glasses containing 0-2 wt% H<sub>2</sub>O. They demonstrated that depolymerisation and formation of AlOH/SiOH is a general water dissolution mechanism for polymerized aluminosilicate glasses and melts.

### *V.3 – Dependence of $\sigma$ on Temperature*

In the relation describing electrical conductivity and composition [31], the temperature dependence is already contained in the form:

$$\log \sigma = A - \frac{E_a}{R} \frac{1}{T} \quad [32]$$

in which  $A$  represents a physical characteristic of glasses, dependent on the temperature (at least for alkali alumino-silicate glasses - Scholze, 1991), and  $E_a$  is the activation energy of the electrical conductivity. In many cases, plotting  $\ln \sigma$  versus  $1/T$  a straight line is obtained, as already shown for diffusion.

In general, the motion of an anion through a network has been shown due essentially to the free volume. With this approach, Sasek and Meissnerova in 1981 represented the electrical conductivity for solid and molten silicate glasses. Near the glass transition temperature, ion's mobility becomes more and more easy, therefore the electrical conductivity becomes higher and an inflection point occurs in the curve  $\log \sigma - 1/T$  (Scholze, 1991).

As already shown for diffusion, the temperature dependence is mostly determined by the activation energy, which is, for the most silicate glasses considering molecular water as charge carriers, varying from 60 - 120 kJ/mol (Scholze et al., 1959; Zhang and Behrens, 2000; Behrens et al., 2002).

The activation energy is determined by the overcoming of potential barriers, therefore a higher activation energy will be expected for the ions with a larger radius as K<sup>+</sup> than for Na<sup>+</sup>; this anticipations were experimentally confirmed. On the other hand, if the quantities of network modifiers increase, as for example K<sup>+</sup>, to a point that the whole glass

structure becomes expanded, then the  $K^+$  ions can migrate through the enlarged network more freely and thus have lower activation energy. That shows dependence on the mobile ion, but also on the glass composition as whole (Scholze, 1991).

# Chapter I – Proton conduction in glasses of the join $\text{CaMgSi}_2\text{O}_6$ (Di) – $\text{CaAl}_2\text{Si}_2\text{O}_8$ (An)

## 1.1 - Abstract

Hydrous silicate glasses with compositions along the join diopside (Di,  $\text{CaMgSi}_2\text{O}_6$ ) - anorthite (An,  $\text{CaAl}_2\text{Si}_2\text{O}_8$ ) containing up to 3 wt%  $\text{H}_2\text{O}$  were synthesized in platinum capsules by high temperature fusion at pressures of 2 to 4 kbar in an internally heated gas pressure vessel. The water content of the glasses was analyzed by Karl-Fischer titration. Using infrared microspectroscopy (IR) the homogeneity of water distribution for each sample of  $\text{An}_{100}$ ,  $\text{An}_{50}\text{Di}_{50}$  and  $\text{Di}_{100}$  was checked and concentrations of OH groups and  $\text{H}_2\text{O}$  molecules were determined for  $\text{An}_{50}\text{Di}_{50}$  before and after conductivity measurements. The electrical conductivity was measured by impedance spectroscopy at temperature up to 685 K without significant alteration of the samples, such as crystallization and water loss. The dc conductivity is higher by at least one order of magnitude in hydrous glasses than in dry glasses with compositions  $\text{Di}_{100}$ ,  $\text{An}_{100}$  and  $\text{An}_{50}\text{Di}_{50}$  (in mol%). However, also the dry glasses show measurable conductivity which is attributed to minor amounts of dissolved  $\text{Na}_2\text{O}$  (0,15 to 0,05 wt%). It is known that dissolved water reduces the mobility of alkali cations in glasses and, hence, we infer that the dc conductivity observed in the hydrous samples is mainly due to the charge carriers produced by hydration of the glasses. Consistent with findings in literature we suggest that the mobile charge carriers are either protons or  $\text{OH}^-$  groups which are not bond to tetrahedral cations.

At a water concentration of circa 1 wt%, activation energies for dc conductivity of, 136 kJ/mol, 124 kJ/mol and 102 kJ/mol were calculated for  $\text{An}_{100}$ ,  $\text{An}_{50}\text{Di}_{50}$  and  $\text{Di}_{100}$ , respectively. Those values are in good agreement with ones calculated for proton conductivity in hydrous barium silicate glasses (Behrens et al., 2002). Conductivity data were evaluated in terms of proton diffusivity by the Nernst-Einstein equation.

The obtained diffusion coefficients ranges from  $10^{-17}$  m<sup>2</sup>/s, for An<sub>50</sub>Di<sub>50</sub> with 1,50 wt% of H<sub>2</sub>O<sub>t</sub> at 596 K, to  $10^{-12}$  m<sup>2</sup>/s for An<sub>50</sub>Di<sub>50</sub> with 2,77 wt% of H<sub>2</sub>O<sub>t</sub> at 685 K.

## 1.2 - Introduction

Proton conductivity has been extensively studied from rather different points of view by material scientists, chemists and physicists. In particular the developing of fast proton conducting glasses can be of high interest in the clean energy field, e.g. for hydrogen gas sensors and hydrogen fuel cells. In the geological field, the aim of the proton conduction studies is to improve the understanding of diffusion mechanisms of hydrous species in glasses that play an important role in several processes such as corrosion of glass and degassing of industrial melts or natural magmas.

Water dissolves in silicate glasses at least in the form of two water species: OH<sup>-</sup> groups and H<sub>2</sub>O molecules (Bartholomew et al., 1980; Scholze, 1960; Stolper, 1982). Due to the high field strength, protons are always directly bond to oxygens. OH<sup>-</sup> groups are the dominating species at water content below 3wt%, increasing the water content the OH<sup>-</sup> group concentration reaches a nearly constant value while the molecular water becomes the dominating species (Silver et al., 1990; Behrens et al., 1996). In particular, different kind of OH<sup>-</sup> groups are identified on the base of their intrinsic hydrogen bond-forming tendencies (Xue & Kanzaki, 2004). In this way, OH<sup>-</sup> groups bond to the framework (e.g. SiOH) (Xue & Kanzaki, 2001) and OH<sup>-</sup> groups acting as charge compensation of the network (i.e. alkaline earth elements: Na) are distinguished. The last ones, like free oxygens, are only linked to metal cations, but not part of the silicate network. That free hydroxyls are favored by more depolymerized melts and network-modifying cations of higher field strength ( $Z/R^2$ : Z: charge, R: cation-oxygen bond length) in the order Mg > Ca > Na. Their formation is expected to cause an increase in the melt polymerization, contrary to the effect of SiOH formation.

Protons are able to function as electrical charges when they are strongly hydrogen bonded in glasses (Abe et al., 1982; Abe et al., 1988; Abe et al., 1993). Previous studies (Nogami & Abe, 1996 and Nogami et al., 1998) have shown that the proton conduction is associated with proton hopping between SiOH and water molecules, according to:



The dissociated proton from the hydroxyl groups moves between the SiOH and the H<sub>2</sub>O bound with SiOH (Nogami et al., 1998). However, the mobile water-derived species may be H<sub>3</sub>O<sup>+</sup>, or H<sup>+</sup> (Stanton et al. 1990).

Previous studies have shown that molecular H<sub>2</sub>O plays an important role in bulk water diffusion, in particular for polymerised glasses (Zhang et al., 1991; Helmich et al., 1993; Zhang and Behrens, 2000; Behrens et al., 2004), but until now the contribution of protons to the transport of hydrogen species was investigated just for depolymerised silicate glasses by Behrens et al., 2002. In that paper was mentioned that hydrous silica glasses does not show significant electrical conductivity. This could invalidate the hopping mechanism proposed above. It was suggested that non bridging oxygens participate in ionic conductivity. That was leading to two possible mechanisms for water diffusion:



In the present study optical and electrical properties of dry and hydrous silicate glasses were investigated. KFT and IR spectroscopy were used to analyze the water content and to quantify the amount of OH<sup>-</sup> groups and molecular H<sub>2</sub>O (e.g., Stolper, 1982; Behrens et al., 1996; Behrens & Stuke, 2003). As a method for measuring the electrical conductivity of glasses, impedance spectroscopy (IS) was chosen, which specifically measures the migration of charged particles (Macdonald, 1996).

## 1.3 - Starting Materials

A suitable material to study proton migration is a hydrous silicate glass containing large alkali or alkaline-earth cations, which have low mobility and, in particular in the case of large alkali, weak bonding to NBO oxygens. The glass should be free of cations with small radius such as high mobile alkalis ( $\text{Na}^+$ ,  $\text{K}^+$  and  $\text{Li}^+$ ) that can mask the proton conductivity.

In this study, optical and electrical properties of pure anorthite glasses ( $\text{An}_{100}$ ,  $\text{CaAl}_2\text{Si}_2\text{O}_8$ ), pure diopside glasses ( $\text{Di}_{100}$ ,  $\text{MgCaSi}_2\text{O}_6$ ) and the binary composition  $\text{An}_{50}\text{Di}_{50}$  (nominal composition in wt %, corresponding to a real composition of  $\text{An}_{56}\text{Di}_{44}$ ) were investigated (Table 1). Anhydrous glasses, used as starting materials, were synthesized from a mixture of oxides and carbonates and silica glass powder. Each mixture was melted in a platinum crucible for 2 h at 1873 K in a conventional chamber furnace in air, quenched, crushed and melted again for another 2 h at the same temperature. Finally the melt was quenched onto a brass plate. Composition and homogeneity of the glasses were analysed by electron microprobe, Cameca SX100, equipped with five wavelength-dispersive spectrometer using 10 nA beam current, 5  $\mu\text{m}$  beam diameter and 8 s counting time with the exception of Na and K, for which 20 s counting time was used. Usually a shorter counting time is used for alkali to avoid their loss during measurements, especially for hydrous glasses, but in this case a larger time was used to improve the detection limits for the dry glasses. The following standards were used: wollastonite (Si and Ca), corundum (Al), periclase (Mg), orthoclase (K), albite (Na),  $\text{Fe}_2\text{O}_3$  (Fe) and  $\text{MnTiO}_3$  (Mn and Ti). Detection limits were also defined by using of “Peak-sight” software, taking into particular account the limit values for the detection of  $\text{Na}^+$  and  $\text{K}^+$ , the presence of those can affect this study. Results are shown in Table 1.

The calculated ratio of non-bridging oxygens to tetrahedral cations (NBO/T) is 2.03 for the anhydrous diopside glass and decreases to 0.65 for  $\text{An}_{50}\text{Di}_{50}$  and further to 0.009 for the anhydrous anorthite glass.

**Table 1:** Composition of starting materials and detection limits (wt %) by electron microprobe.

<b>Sample</b>	<b>SiO<sub>2</sub></b>	<b>Al<sub>2</sub>O<sub>3</sub></b>	<b>Na<sub>2</sub>O</b>	<b>K<sub>2</sub>O</b>	<b>CaO</b>	<b>TiO<sub>2</sub></b>	<b>FeO</b>	<b>MgO</b>	<b>MnO</b>	<b>Total</b>
<b>An<sub>100</sub></b>	45.43	34.86	0.15	b.d.l	19.40	b.d.l.	b.d.l.	b.d.l.	b.d.l.	99.91
<b>1<math>\sigma</math></b>	0.36	0.33	0.04	b.d.l.	0.49	b.d.l.	b.d.l.	b.d.l.	b.d.l.	
<b>An<sub>50</sub>-Di<sub>50</sub></b>	48.72	20.89	0.07	b.d.l	23.11	b.d.l.	b.d.l.	7.57	b.d.l.	100.41
<b>1<math>\sigma</math></b>	0.34	0.33	0.04	b.d.l.	0.52	b.d.l.	b.d.l.	0.03	b.d.l.	
<b>Di<sub>100</sub></b>	55.60	b.d.l.	0.05	b.d.l	26.33	b.d.l.	b.d.l.	18.85	b.d.l.	100.92
<b>1<math>\sigma</math></b>	0.39	b.d.l.	0.03	b.d.l.	0.58	b.d.l.	b.d.l.	0.03	b.d.l.	
<b>Det.Lim.</b>	0.09	0.08	0.05	0.02	0.10	0.06	0.14	0.04	0.15	

**Notes:** Each listed composition is the average of at least ten electron microprobe analyses made on the dry samples of each composition. The detection limits show roughly the same values for the different compositions. Values below the detection limit are noted as b.d.l.. Values of standard deviations ( $1\sigma$ ) are reported.

## 1.4 - Experimental and Analytical Methods

### 1.4.1 Hydrous glasses

For conductivity measurements, two hydrous glasses for each composition with a nominally water content from 1 to 3 wt % were produced. A part of the dry glasses was directly cut in squared thin sections for conductivity measurements. Another part was crushed in agate mortar and sieved to obtain two fine powder fractions with grain sizes of 200 - 500  $\mu\text{m}$  and  $< 200 \mu\text{m}$ . The two fractions were mixed in weight ratio of 1:1 in order to minimize the pore volume. A small amount of crushed glass was sealed with an appropriate amount of distilled water into platinum capsules of 12 mm length, 4 mm diameter and 0.2 mm wall thickness. In a first step, capsules of 3 cm length and 0.5 cm diameter were used. After few synthesis it was clear that those long capsules were subjected to a thermal gradient during quenching, increasing their accumulated stress. All capsules were externally cooled by water during welding and then stored in an oven at 110°C over night. After drying, each capsule was checked for possible leakage by



**Fig.6:** platinum capsule stick to the brass ramp after an experiment. The capsule is circa 3 cm long and 0.5 cm wide. After few try was clear that those long capsules were subjected to a thermal gradient during quenching, increasing their accumulated stress.

controlling the weight again. Finally, the capsules were squeezed to a flat, rectangular shape of circa 10 per 5 mm with a thickness of 2 or 3 mm to increase the surface area and facilitate rapid cooling. Syntheses were performed at a pressure of 200 MPa and at different temperatures from 1523 to 1723 K for circa 30 m in an internally heated gas pressure vessel (IHPV). The normal quench procedure with an initial cooling rate of 2 K/s was found to be too slow to quench the hydrous melt to a glass. To avoid crystallization we have used a rapid quench device with a cooling rate of circa 150 K/s (Benne & Behrens, 2003). During the run, the capsule was hung on a platinum wire in the hot zone of the furnace. At the end of the experiment, the sample was quenched by falling in the

cold part of the vessel after fusing the platinum wire (Berndt et al., 2002).

It required several try to get stress-free glasses that did not break during opening the capsules or during the preparation of the sections. The reasons were a too high cooling rate and the hardening of Pt capsules during anneal. To reduce the cooling rate, it was proposed to stop the capsule not directly at the bottom of the furnace but 0.5 cm above. Therefore, a brass ramp was placed at the bottom of the oven, but it was not successful due to reaction between the hot capsule and the brass piece Fig. 6. An easier and better solution was to place some mullite wool at the bottom of the oven that had the purpose tool to moderate the temperature at sample position after quench ( $\approx 373 - 573$  K), to reduce the heat transfer from the capsule and to stop softly the capsule after fall.

#### ***1.4.2. Densities and Karl-Fischer titration***

The densities of the glasses must be known for quantification of water species and total water by IR absorption spectroscopy (Stolper, 1982). Densities were determined by weighing glass pieces (10-30 mg) in air and in water. Due to the small size of the hydrous glass samples, the uncertainty of the determination was relatively high (3-6 %).

For anorthite and diopside composition, densities of hydrous glasses were estimated from the density of dry glasses by using the partial molar volume of H<sub>2</sub>O in glass after Richet et al. (2000). The calculated equations were:

$$\rho = -21.6 \cdot c_{water} + 2712 \text{ (anorthite)}, \quad [36]$$

$$\rho = -23.2 \cdot c_{water} + 2773 \text{ (diopside)}. \quad [37]$$

For An<sub>50</sub>Di<sub>50</sub> samples, the density calculated by Benne & Behrens (2003) is taken into account for further measurements. It is expressed by the equation:

$$\rho = -17.9(\pm 14) \cdot c_{water} + 2739(\pm 26) \quad [38]$$

The water content was analyzed by Karl-Fischer titration (Behrens & Stuke, 2003; Behrens et al., 1996). For the measurements 10 or 20 mg of each sample was used and wrapped tightly into a platinum foil to avoid fragments loss after explosive dehydration. Each sample was heated up to 1573 K with the “rapid heat” mode by stepwise within 4-6 min, increasing the power of the HF-generator used for heating the Pt sample holder.

The analytical procedure is described by Behrens et al. (1996). Behrens (1995) has shown that residual water contents in polymerised aluminosilicate glasses after KFT are in the range of  $0.10 \pm 0.05$  wt%. However, for more depolymerised melts of dacitic and andesitic compositions Ohlhorst *et al.* (2001) found that the amount of unextracted water is much smaller ( $0.02 \pm 0.02$  wt% H<sub>2</sub>O). For the polymerised Anorthite-bearing melts and the depolymerised Diopside melts we added 0.10 and 0.02 wt% H<sub>2</sub>O, respectively, to the values obtained from KFT in order to account for unextracted water. The uncertainty of the KFT analysis was calculated on the basis of the uncertainty of the titration rate ( $\pm 0.02$  mg·s<sup>-1</sup>) (Behrens *et al.*, 1996; Benne & Behrens, 2003). Densities and KFT values are listed in Table 2 and 3.

### 1.4.3. IR spectroscopy

IR absorption spectra of doubly polished glass plates were collected with an IR microscope (Bruker IR scope II) connected to an FTIR spectrometer (Bruker IFS88) to analyse the water content and the homogeneity of the water distribution within the glasses. At least three spectra for each sample were measured before and after impedance analysis. The latter measurements were done to check for possible water loss and species interconversion during experiment. To limit the volume of the analyzed samples, a focus area of 100 per 100  $\mu\text{m}$  was chosen. Operation conditions were:

light source:

- W lamp for NIR
- globar light for MIR

beamsplitter:

- CaF<sub>2</sub> for NIR
- KBr for MIR.

An MCT narrow range detector was employed in both spectral ranges. Typically, for NIR 100 scans were accumulated for each spectrum, with a spectral resolution of 4 cm<sup>-1</sup>, and for MIR 50 scans were collected with a resolution of 2 cm<sup>-1</sup>.

### 1.4.4. Impedance spectroscopy

#### 1.4.4.1 – Sample preparation

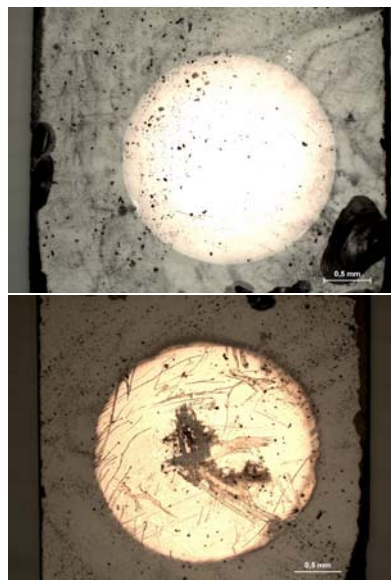


**Fig. 7 a (on top):** electrode gold layer for the sample An<sub>100</sub>-1wt%.

**Fig. 7 b (on bottom):** electrode gold layer for the sample An<sub>100</sub>-2wt% after conductivity measurements.

(Micro-photograph in linear polarized light)

From each glass sample a square piece for impedance measurements was cut with a typical thickness of 0.4 mm and an edge length of 2 - 3 mm. In the most cases, these samples were also used before the impedance analysis for NIR spectroscopic study of hydrous species concentration. For MIR measurements, a new set of glass pieces was polished to smaller thickness of circa 0.1 mm. Both base planes were polished and a delimited circled area of 2 mm diameter was sputtered with gold to produce the electrodes. The used apparatus for sputtering was an Edwards Scancoat Six connected with a pump Edwards RV3. After producing a pressure of 0.1 mbar in the sputtering chamber, the sample was coated at 1.6 kV and 10 mA for 180 s. A hole aperture was used to limit the electrodes area. Sputtering times of 90 and 120 s were not sufficient to produce a homogeneous gold layer thick enough to act as an electrode (Behrens et al., 2002). In order to check the reproducibility of the gold layers, the weight of some samples was measured before and after the sputtering with a precision balance. The obtained differences were in the range of 0.5  $\mu\text{g}$ , far below the detection limit of the balance of circa 5  $\mu\text{g}$ . The electrodes surfaces of each sample were carefully inspected by microscope before and after conductivity measurements to control the presence of damages. In a few cases some scratches and holes in the gold layer were observed after measurements (Fig. 7 a-b). We assume that they were produced by removing the sample from the impedance cell, because it was observed that the samples stick to the electrode contacts in the sample holder during the measurements while the temperature rises.

#### ***1.4.4.2 – Conductivity measurements***

The conductivity experiments were performed in a ceramic cell placed in a horizontal tube furnace. The sample holder has a four-terminal configuration (Fig. 8 a-b). A schematic draw of the cell is given in Fig. 9. Heating was controlled by a Eurotherm 818 programmer-controller. The temperature was measured by a type S thermocouple placed 1 cm beside the sample. Temperature tests to define the “hot zone” of the furnace were run at 473, 573 and 673 K, by millimetric movements of the sample-holder and interval time of 10 min for adjusting temperature. It was found a hot zone of circa 1.50 cm in which the temperature changes are smaller than 1 degree. This zone is considered wide enough to presume temperature uniformity in the sample area. The analyzer was an Alpha-A mainframe equipped with a 4-Wire Impedance Interface ZG4 from Novocontrol. It allows to measure impedance in the range  $0.01 - 10^{14} \Omega$ . Before every session, the impedance analyzer was calibrated with a “Short calibration standard” and a “100  $\Omega$  calibration standard”. The 100  $\Omega$  and the short calibration normals are supplied in two separate boxes with four BNC terminals that have to be connected with the front terminals during the calibration. In the meanwhile the furnace was heated up to 523 K for 1 h to remove traces of water. Then the sample was inserted and 30 min. more were required to reach the temperature (523 K) and to evaporate water absorbed on the sample holder, on the sample surface and on the electrodes. The temperature was subsequently increased in steps of 10 K up to a temperature of 673 - 683 K. Impedance measurements were performed during the dwell. Temperature was strongly increasing within 7 - 10 min. after adjusting to a new set-point, but for a proper stabilization circa 30 min. were required. A waiting time of 30 min. was considered too long for the risk of water lost; therefore impedance spectra were recorded circa 10 min. after setting a new temperature. During one measurement (about 4 min.), the temperature typically increases of 3 - 4 K. The impedance analyser allows measurements in the range from 3  $\mu\text{Hz}$  to 20 MHz, the time required for a complete measurement is nearly 30 min. and was considered too long for the risk of water lost. Furthermore, the analyses in the lower and higher range respectively show a deviation from the ideal trend and an intense scattering

as mentioned in paragraph 1.5.2.2. Therefore, in this study a restricted frequency range was used and data were collected at frequencies ranging from 0.01 Hz to 10 kHz.

To test the reproducibility of measurements, two different slices for the composition  $\text{Di}_{100}$  - 1wt% cut from the same glass body were measured. All parameters were identical and the results of the two conductivity analyses, reported in paragraph 1.5.2.2, were within the error.

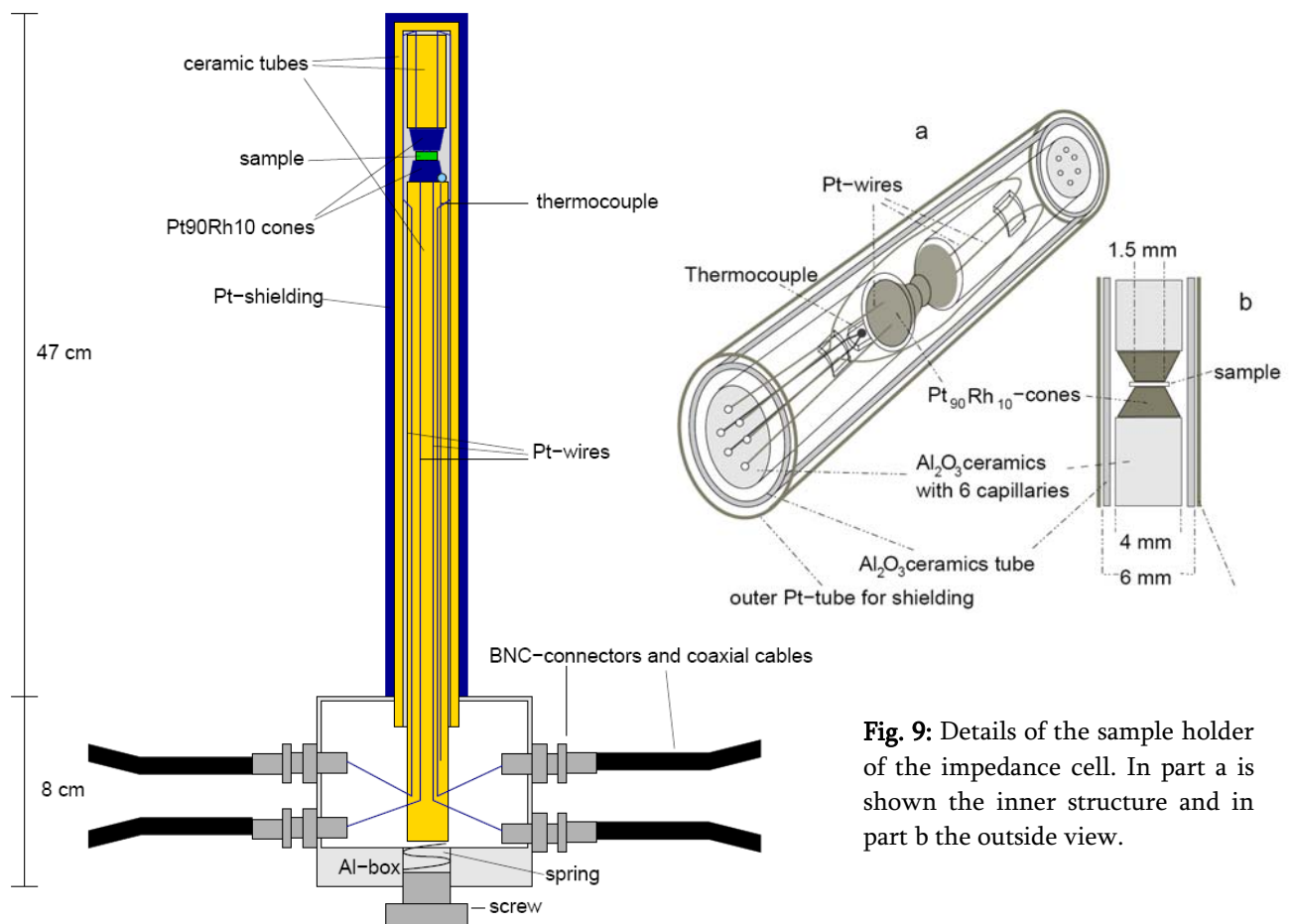


**Fig. 8:** schematic cross section of the impedance cell.

**Fig. 9:** Details of the sample holder of the impedance cell. In part a is shown the inner structure and in part b the outside view.

## 1.5 - Results

### 1.5.1 IR spectroscopy

Figs. 10 – 11 show typical near and middle infrared spectra of An<sub>100</sub>, An<sub>50</sub>Di<sub>50</sub> and Di<sub>100</sub> glasses. Mid-infrared spectra of dry and hydrous glasses are shown in Fig. 10 (a - c) in comparison to the spectra of hydrous barium silicate glass from Behrens et al. (2002). In the MIR range, the spectra of dry glasses show mostly bands below 2000 cm<sup>-1</sup> which are caused by vibrations of the silicate network but it is visible also a weak band at 3550 cm<sup>-1</sup> which is used to estimate the bulk water content. In the spectrum of the hydrous glasses a pronounced asymmetric absorption peak is visible at 3550 cm<sup>-1</sup> which is attributed to OH stretching vibrations of weakly H-bonded hydrous species (Scholze, 1959). This peak could be produced by X-OH groups (i.e. water dissolved as hydroxyl group with) or H-O-H groups (i.e. molecular water) and thus it is not useful to determine the speciation of water in glass (Scholze, 1960). The asymmetry of the peak may reflect a continuum of hydrogen-bond lengths of the hydrogen to non-bridging oxygen (Nakamoto et al., 1955). The band near 2850 cm<sup>-1</sup> is caused by OH stretching of strongly H-bonded hydrous species (Scholze, 1959), but is visible only as a shoulder superimposed to the 3550 cm<sup>-1</sup> band. The weaker band near 2350 cm<sup>-1</sup> indicates also a small fraction of Si-OH groups strongly hydrogen-bonded to non-bridging oxygens (Scholze, 1959). The bands at 2800, 2350 and 1750 cm<sup>-1</sup> belong to the so called ABC triplet characteristic for strong H-bonded species in silicate glasses and minerals (Behrens & Stuke, 2003). In the studied glasses, the ratio  $A_{2350}/A_{3500}$  increases with the Di content of the glasses, indicating an increasing fraction of strongly H-bonded hydrous species. The weak band at 1620 cm<sup>-1</sup> is assigned to the fundamental H<sub>2</sub>O bending vibrations giving evidence for the presence of H<sub>2</sub>O molecules in the glass. The doublet at 1420 and 1490 cm<sup>-1</sup> in the Di<sub>100</sub> and An<sub>50</sub>Di<sub>50</sub> compositions indicates that CO<sub>3</sub><sup>2-</sup> groups were formed during glass synthesis, probably inserted by absorbed CO<sub>2</sub> on the glass powder loaded into the capsule. The spectrum of the barium silicate glass shows a very high intensity of the bands at 2800 and 2350 cm<sup>-1</sup> compared to the band at 3550 cm<sup>-1</sup>. Those bands are also evident in the spectra of hydrous Di<sub>100</sub> composition. This implies that a fraction of hydrous species is strongly H-bonded to non-bridging oxygens. However, its portion is much smaller in Di glass than in Ba<sub>2</sub>S glass. For An<sub>100</sub> compositions only the band at 3550 cm<sup>-1</sup> is evident while for An<sub>50</sub>Di<sub>50</sub> compositions a weak band is visible at 2350 cm<sup>-1</sup> for the high water content spectrum.

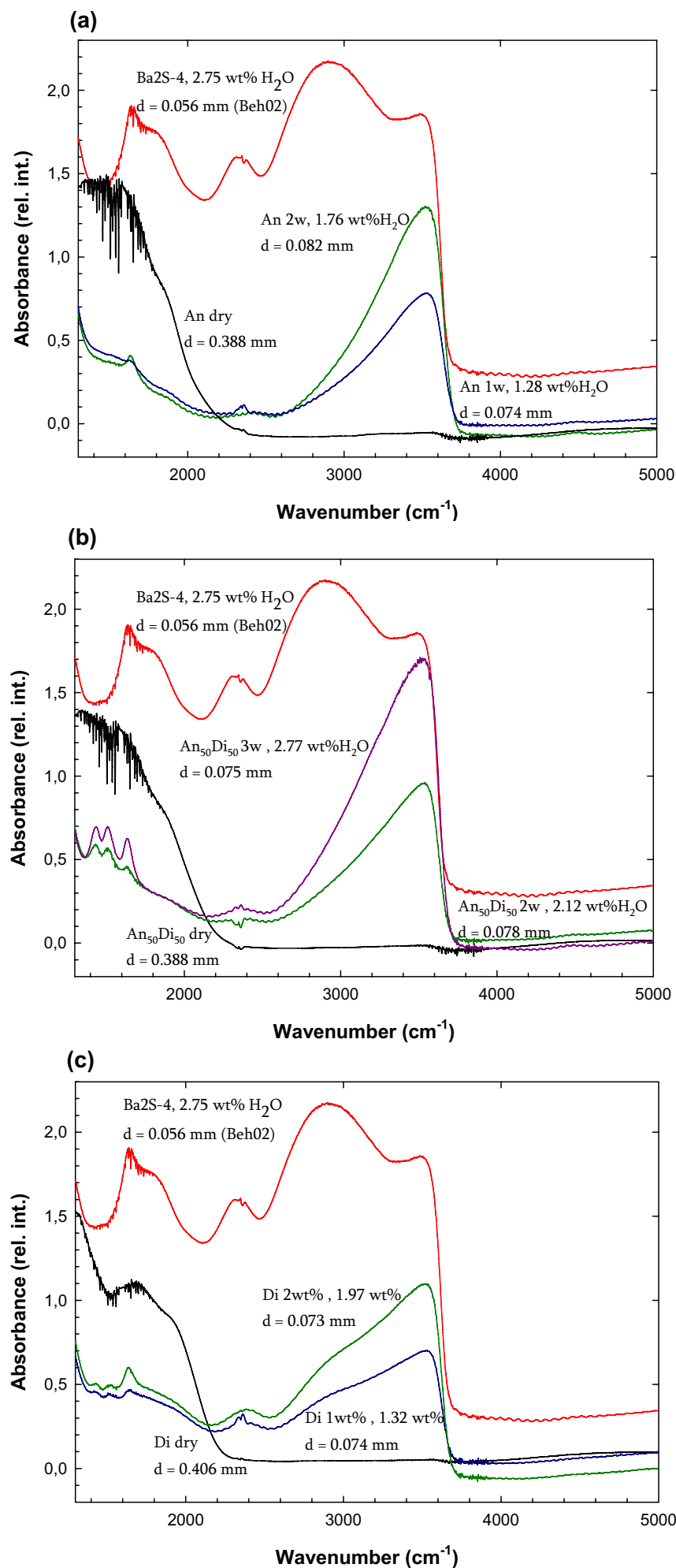


**Fig. 10 (a – b – c):** MIR absorption spectra of An<sub>100</sub>, Di<sub>100</sub> and An<sub>50</sub>Di<sub>50</sub> glasses. Spectra are plotted with an offset for clarity. Thickness and water contents are displayed in the plots.

- 1) MIR spectra of An<sub>100</sub> glasses
- 2) MIR spectra of An<sub>50</sub>Di<sub>50</sub> glasses
- 3) MIR spectra of Di<sub>100</sub> glasses

The bands at 2800–2900, 2350 and 1750 cm<sup>-1</sup> are due to OH stretching vibrations of strongly H-bonded species and the band at 3550 cm<sup>-1</sup> is due to OH stretching vibrations of weakly H-bonded species. In particular, the shoulder at 2900 cm<sup>-1</sup> shown in the Di<sub>100</sub> spectra is consistent with the peak observed for Ba<sub>2</sub>S glass. This band is not visible in An<sub>100</sub> and An<sub>50</sub>Di<sub>50</sub> glasses. The sharp band at 1640 cm<sup>-1</sup> results from bending vibrations of molecular H<sub>2</sub>O.

Small features at 2350 cm<sup>-1</sup> are due to atmospheric CO<sub>2</sub>.

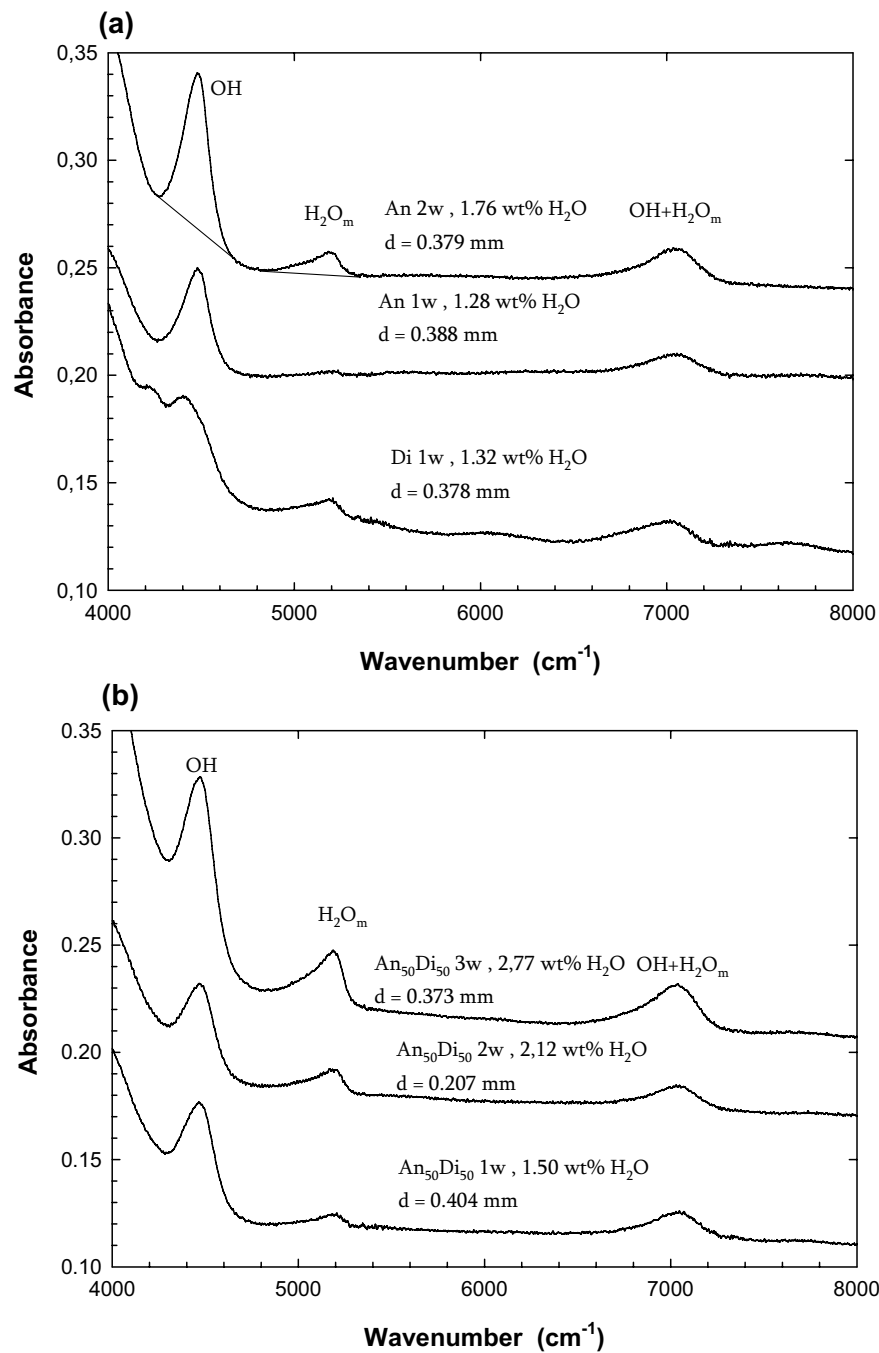


**Fig. 11 (a - b):** NIR absorption spectra of An<sub>100</sub>, An<sub>50</sub>Di<sub>50</sub> and Di<sub>100</sub> glasses. Spectra are plotted with an offset for clarity. Thickness and water contents are displayed in the plots.

- 1) NIR spectra of An<sub>100</sub> and Di<sub>100</sub> glasses
- 2) NIR spectra of An<sub>50</sub>Di<sub>50</sub> glasses

Band assignments are: - 4500 cm<sup>-1</sup> combination mode of OH groups; - 5220 cm<sup>-1</sup> combination mode of H<sub>2</sub>O molecules; - 7000 cm<sup>-1</sup> overtone of OH stretching vibration.

TT baseline is shown in plot (a) for An<sub>100</sub> 2w, 1.76 wt% H<sub>2</sub>O.

In the NIR range, at least two water-related bands at circa 4500 and 5200  $\text{cm}^{-1}$  are visible for hydrous compositions (Fig. 11 a - b). The peak at 4500  $\text{cm}^{-1}$  is due to the combination of stretching and bending mode of Si-OH groups (Scholze, 1966; Bartholomew et al., 1980; Wu, 1980), Al-OH groups probably also absorb in this region, since the minerals kaolinite, muscovite, gibbsite and diaspore have peaks at this wavelength (Hunt and Salisbury, 1970; Hunt et al., 1971). The absorption band at 5200  $\text{cm}^{-1}$  is produced by a combination of stretching and bending modes of H<sub>2</sub>O molecules. The peak at 7010  $\text{cm}^{-1}$  is attributed to the first overtone of the OH stretching vibration and is increasing linearly with water content (Stolper, 1982; Withers and Behrens, 1999). The NIR spectrum of Di<sub>100</sub> shows two discrete bands in the OH range, one at circa 4500 and another at  $\approx 4200$   $\text{cm}^{-1}$ , reflecting the presence of strongly and weakly H-bonded OH groups in the structure as shown by MIR spectra. A weak band is evident also at 6000  $\text{cm}^{-1}$ , possibly an overtone band of strongly H-bonded species, related to the band near 2900  $\text{cm}^{-1}$  in the MIR range.

#### ***1.5.1.1 - Procedure for baseline correction of the combination bands***

To determine the total water content and the water speciation from peak heights or peak areas, an appropriate baseline under the 3550, 4500 and 5200  $\text{cm}^{-1}$  bands must be defined. In precedent works several types of baselines were tested (Withers & Behrens, 1999; Ohlhorst et al., 2001). In this work we choose the so called “Two Tangents (TT)” correction consisting in fit the base of the 4500 and 5200  $\text{cm}^{-1}$  band with a simple straight line. A TT baseline is shown i.e. in Fig. 11 - a for An<sub>100</sub> 2w, 1.76wt% H<sub>2</sub>O. In systems with low iron content, the straight lines are unambiguously defined as tangents through the minima on both sides of each band. On one hand the TT baseline is a rough approximation and presents a systematic error due to the underestimation of area and peak height of OH band. On the other hand this fitting presents a high reproducibility (Stuke et al., 2006).

To the band at 3550  $\text{cm}^{-1}$  in spectra of anorthite glass, a single tangent was fitted.

In the case of pure diopside, the superimposition of the band at 2800 cm<sup>-1</sup> on the band at 3550 cm<sup>-1</sup> is evident. For this reason the tangent baseline is not applicable and for the quantitative evaluation of peak intensity, a constant horizontal baseline is assumed, defined by the absorbance at 4000 cm<sup>-1</sup> (Behrens & Stuke, 2003). Peak heights of both bands at 3550 and 2350 cm<sup>-1</sup> are calculated as  $A_{3550\text{hb}} = A_{3550} - A_{4000}$  and  $A_{2350\text{hb}} = A_{2350} - A_{4000}$  (where hb is the horizontal baseline). This procedure follows the recommendation of the Technical Committee (TC14) of the international Commission of Glass (ICG) (Geotti-Bianchini et al., 1999).

### ***1.5.1.2 - Determination of molar absorption coefficients***

To determine the water content of the nominally dry glasses a calibration of the IR absorption coefficients was necessary. All the samples used for IR calibration were crystal and bubble-free glasses. The water content determined by KFT, the thickness and the density of each sample, the absorbance at ~ 3550, ~ 4500 and ~ 5200 cm<sup>-1</sup> and the NIR calculation of bulk water content and water speciation are summarized in Table 2 - 3.

In the MIR range, the proportionality in the height of the peak at 3550 cm<sup>-1</sup> as a function of total water content allow us to use it as an analytical tool for determining total water content of silicate glasses (Scholze, 1959; Williams et al., 1976, Pearson et al., 1979; Bartholomew et al., 1980).

The Lambert-Beer law is the basis for a quantitative relationship between water concentration and the height of the absorption peak:

$$C_{H_2O_t} = \frac{1802 A_{3550}}{d\rho} \frac{1}{\varepsilon_{3550}} \quad [39]$$

where  $A$  is the peak height, 18.02 is the molecular weight of water,  $d$  is the thickness of the sample in cm,  $\rho$  is the density in g/l,  $\varepsilon$  is the linear molar absorption coefficient in l/mol·cm and  $C_{H_2O_t}$  is the concentration of total water in wt%.

**Table 2** MIR-spectroscopic data

Sample	C <sub>H2O</sub> (wt%)	Thickness (cm)	Density (g/l)	A 3550	A 2350	ε 3550 (l·mol <sup>-1</sup> ·cm <sup>-1</sup> )
<b>An<sub>100</sub>-1w</b>	1.28 ± 0.03	0.0081	2712	0.751 ± 0.011	-	48.4 ± 2.8
<b>An<sub>100</sub>-2w</b>	1.76 ± 0.04	0.0083	2635	1.330 ± 0.022	-	61.4 ± 3.1
<b>An<sub>50</sub>Di<sub>50</sub>-2w</b>	2.12 ± 0.03	0.0078	2701 ± 42	0.923 ± 0.014	-	37.2 ± 1.7
<b>An<sub>50</sub>Di<sub>50</sub>-3w</b>	2.77 ± 0.03	0.0075	2690 ± 49	1.692 ± 0.018	-	54.8 ± 2.2
<b>Di<sub>100</sub>-1w</b>	1.22 ± 0.02	0.0074	2745	0.676 ± 0.005	0.32 ± 0.01	48.9 ± 2.7
<b>Di<sub>100</sub>-2w</b>	1.97 ± 0.03	0.0073	2727	1.057 ± 0.005	0.36 ± 0.01	48.4 ± 2.2

Notes: Total water (C<sub>water</sub>) was determined by pyrolysis and subsequent Karl-Fischer titration. The error in thickness is 0.0002 cm. Densities of anorthite and diopside glasses were calculated with the method of Richet et al. (2000), while for An<sub>50</sub>Di<sub>50</sub> the density measured by Benne & Behrens (2003) was used. Samples were cooled with a rapid quench technique (circa 150 K/s). The absorbance was calculated using a straight line baseline (TT) for An<sub>50</sub>Di<sub>50</sub> and An<sub>100</sub> compositions. For the Di<sub>100</sub> composition, a horizontal was fitted to the spectrum and extrapolated below the 3550 cm<sup>-1</sup> peak.

It has to be noted that the molar absorptivities are, in this work, based on the total water content of the glasses rather than on their OH content, even when OH is the absorbing species. Using bulk water contents measured by KFT and densities estimated with the buoyancy method, ε<sub>3550</sub> values were calculated for samples with different water contents and the average values of 54.9 ± 2.9 l/mol·cm for An<sub>100</sub> and 46.0 ± 8.8 l/mol·cm for An<sub>50</sub>Di<sub>50</sub> were determined. The Di<sub>100</sub> glasses show complex MIR features due to strongly and weakly H-bonded species. In this case a practical absorption coefficient is determined assigning the total water content to the band at 3550 cm<sup>-1</sup> and assuming that all bands appear in constant ratio for a given composition. The obtained value is 48.7 ± 2.5 l/mol·cm. Fig. 12 shows bulk water content versus ε<sub>3550</sub> for the investigated glasses and in Table 4 are reported the average values for ε<sub>3550</sub>. It is emphasized that for Di<sub>100</sub> compositions the obtained ε<sub>3550</sub> values do not account for real species concentrations in glasses because only the weakly H-bond species contributes to the band at 3550 cm<sup>-1</sup>.

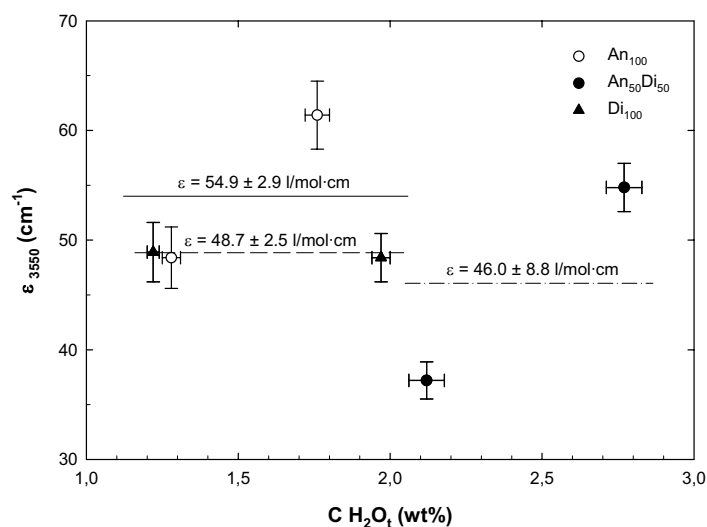


**Fig. 12:** Relationship between the molar absorption coefficient  $\epsilon$  for the fundamental OH stretch band at  $3550\text{ cm}^{-1}$  and the bulk water content for An<sub>100</sub>, An<sub>50</sub>Di<sub>50</sub> and Di<sub>100</sub> glasses. The solid line refers to the average  $\epsilon_{3550}$  for An<sub>100</sub>, the dash-dot line to the average  $\epsilon_{3550}$  for An<sub>50</sub>Di<sub>50</sub> and the dash line to the average  $\epsilon_{3550}$  for Di<sub>100</sub>. Error bars take into account the individual error based on error propagation.

Most of the values in molar absorptivity reported in the literature are for glasses that differ in composition from those examined in this study and there is considerable variation and compositional dependency of molar absorptivities for this peak (e.g., 37 – 86 l/mol·cm; Williams et al., 1976). Most literature values for rhyolitic, basaltic and albitic glasses are ranging from 59 – 74 l/mol·cm  $\pm$  10% (Shaw, 1974; Stolper, 1982). For Fe-bearing andesite a value of  $62.32 \pm 0.42$  l/mol·cm and for Fe-free andesite a value of  $69.21 \pm 0.42$  l/mol·cm were estimated by Mandeville et al. (2002). Previous study has shown that polymerised glasses have normally a higher  $\epsilon_{3550}$  values than the depolymerised ones. This can be recognised in plot of Fig. 12, where anorthite glasses show higher  $\epsilon_{3550}$  values than diopside ones. The An<sub>50</sub>Di<sub>50</sub> samples show lower average values probably due to a dishomogeneity in the glass. That is, the piece of glass analysed by KFT (2.12 wt% of H<sub>2</sub>O) has probably different water content than the piece considered for NIR. Therefore, more reliable is the value of  $54.8 \pm 2.2$  obtained for the sample An<sub>50</sub>Di<sub>50</sub>-3w. Similar situation is present also in the case of An<sub>100</sub>-1w, where higher amount of water was measured by KFT, due to dishomogeneity in the glass.

Using the respective average values of  $\epsilon_{3550}$ , the water contents of the nominally dry glasses were calculated to be  $0.011 \pm 0.003$  wt% (100 ppm by weight) for An<sub>100</sub>,  $0.008 \pm 0.004$  wt% (80 ppm by weight) for An<sub>50</sub>Di<sub>50</sub>, and  $0.005 \pm 0.002$  wt% (50 ppm by weight) for Di<sub>100</sub>.

The concentration of OH and H<sub>2</sub>O can be determined from the intensities of the NIR absorption bands using the Lambert-Beer law:

$$C_{OH} = \frac{1802A_{OH}}{d\rho} \frac{1}{\varepsilon_{OH}} \quad [40]$$

where A is the height of the peaks at 5200 cm<sup>-1</sup>, for molecular water, and at 4500 cm<sup>-1</sup>, for hydroxyl groups,  $C_{H_2O_m}$  and  $C_{OH}$  are the concentrations of molecular water and water dissolved as OH groups in wt%, respectively. When water species are only OH and H<sub>2</sub>O the concentration of total water  $C_{H_2O_t}$  is given by:

$$C_{H_2O_t} = C_{H_2O_m} + C_{OH} \quad [41]$$

Rearranging these equations, we obtain:

$$\left( \frac{1802A_{H_2O_m}}{d\rho C_{H_2O_t}} \right) = \varepsilon_{H_2O_m} - \frac{\varepsilon_{H_2O_m}}{\varepsilon_{OH}} \left( \frac{1802A_{OH}}{d\rho C_{H_2O_t}} \right) \quad [42]$$

**Table 3** NIR-spectroscopic data

Sample	$C_{H_2O_t}$ (wt%)	Thickness (cm)	Density (g/l)	$A_{norm. 5200}$	$A_{norm. 4500}$	$C_{H_2O_m}$ (wt%)	$C_{OH}$ (wt%)	$C_{H_2O_t}$ (wt%)
<b>An<sub>100</sub>-1w</b>	1.28 ± 0.03	0.0389	2712	0.029 ± 0.015	0.548 ± 0.031	-	-	-
<b>An<sub>100</sub>-2w</b>	1.76 ± 0.04	0.0379	2635	0.099 ± 0.012	1.715 ± 0.032	-	-	-
<b>An<sub>50</sub>Di<sub>50</sub>-1w</b>	1.50 ± 0.05	0.0401	2712 ± 36	0.065 ± 0.030	0.461 ± 0.029	0.11 ± 0.03	1.30 ± 0.05	1.41 ± 0.06
<b>An<sub>50</sub>Di<sub>50</sub>-1-b</b>	1.54 ± 0.05	0.0404	2711 ± 36	0.073 ± 0.013	0.450 ± 0.026	0.12 ± 0.02	1.26 ± 0.04	1.38 ± 0.05
<b>An<sub>50</sub>Di<sub>50</sub>-3w</b>	2.77 ± 0.03	0.0373	2690 ± 49	0.152 ± 0.008	0.412 ± 0.014	0.49 ± 0.02	2.28 ± 0.05	2.77 ± 0.06
<b>Di<sub>100</sub>-1w</b>	1.22 ± 0.02	0.0388	2745	0.029 ± 0.030	0.543 ± 0.030	-	-	-

Notes: Total water ( $C_{H_2O_t}$ ) was determined by pyrolysis and subsequent Karl-Fischer titration. The error in thickness is 0.0002 cm. Densities of anorthite and diopside glasses were calculated with the method of Richet et al. (2000), while for An<sub>50</sub>Di<sub>50</sub> the density measured by Benne & Behrens (2003) was used. Samples were cooled with a rapid quench technique (circa 150 K/s). The absorbance was calculated using a straight line baseline (TT).

If the normalized absorbances are plotted one against the other a straight line is obtained, provided that the absorption coefficients are independent on total water and quenching rate. The molar absorption coefficients are determined directly from the intercepts of the obtained lines with both axes. We fitted our data with linear regression considering the individual errors in the determination of each parameter.

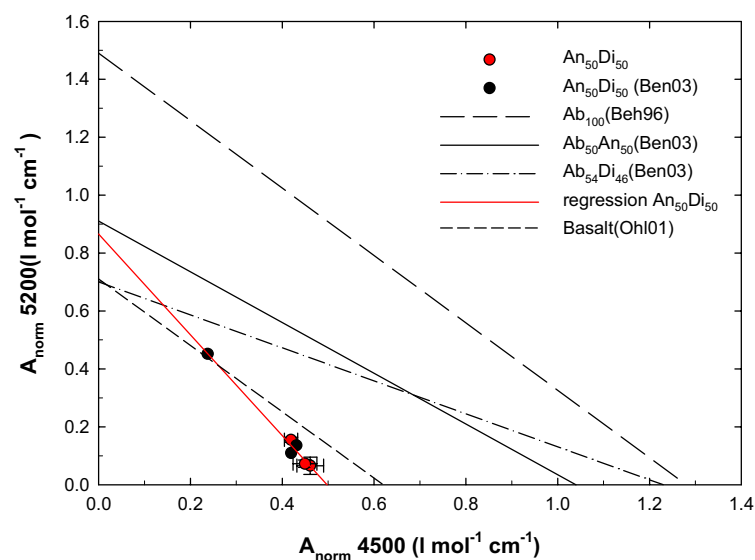


**Fig. 13:** Plot for determination of molar absorption coefficients for the OH combination band at 4500  $\text{cm}^{-1}$  and H<sub>2</sub>O combination band at 5200  $\text{cm}^{-1}$ . The collected data, marked in red, are integrated by that from Benne & Behrens, 2003 (Ben03), in black. For An<sub>50</sub>Di<sub>50</sub>, values of  $A_{\text{norm}}$  for both combination bands were calculated with TT baseline. For comparison data for the join Ab-An and Ab-Di from Benne & Behrens 2003, data for Ab100 glasses from Behrens et al, 1996 (Beh96), and data for basalt from Ohlhorst et al., 2001 (Ohl01) are shown. For this compositions the  $A_{\text{norm}}$  were calculated using a baseline modelled with a Gaussian (GG).

The NIR calibration was possible only for the composition An<sub>50</sub>Di<sub>50</sub> (Table 3). The linear molar extinction coefficients were defined using up to 6 glasses with the same anhydrous composition and water contents ranging from 1 - 5 wt%: three of them, marked in red in Fig. 13, come from this study; the other three are from Benne et al., 2003. The new data are in good agreement with those obtained by Benne & Behrens (2003) for low water content. For high water content, the linear regression is poorly constrained because only one data point from Benne & Behrens (2003) could be used. The other two available points were fitted with a different kind of baseline (GG). This causes a discrepancy in the molar absorptivity coefficients calculated by Benne and Behrens (2003) ( $0.30 \pm 0.06$  l/mol·cm for the combination band of OH<sup>-</sup> at 4500  $\text{cm}^{-1}$  and  $1.09 \pm 0.09$  l/mol·cm for the combination band of H<sub>2</sub>O at 5200  $\text{cm}^{-1}$ ) and those reported in this study. The resulting molar absorptivity coefficients were  $0.50 \pm 0.02$  l/mol·cm for the combination band of OH<sup>-</sup> at 4500  $\text{cm}^{-1}$  and  $0.87 \pm 0.04$  l/mol·cm for the combination band of H<sub>2</sub>O at 5200  $\text{cm}^{-1}$  (Table 4). For the other compositions the prepared samples were too few to have a reliable calibration.

In Fig. 13 our data were plotted for comparison with previous ones from Benne & Behrens (2003), Behrens et al. (1996) and Ohlhorst et al. (2001). It is evident from this

figure that both the NIR absorption combination bands strongly increase with increasing albite content. Albite presents a polymerised structure with a NBO/T value close to 0 as anorthite. Therefore, as already told for  $\epsilon_{3550}$ , the molar absorption coefficients decrease increasing the depolymerisation of the structure. It has to be considered that also the abundance of SiO<sub>2</sub> influences the values of  $\epsilon$ , which increase with the amount of silica content (Ohlhorst et al., 2001).

**Table 4.** Molar absorption coefficients for bands at 5200, 4500 and 3550 cm<sup>-1</sup>

Composition	Range (wt% H <sub>2</sub> O)	$\epsilon_{3550}$ (l mol <sup>-1</sup> cm <sup>-1</sup> )	$\epsilon_{4500}$ (l mol <sup>-1</sup> cm <sup>-1</sup> )	$\epsilon_{5200}$ (l mol <sup>-1</sup> cm <sup>-1</sup> )
An <sub>100</sub>	1.28 – 1.76	54.9 ± 2.9	-	-
An <sub>50</sub> Di <sub>50</sub>	1.5 – 2.77	46.0 ± 8.8	0.50 ± 0.02	0.87 ± 0.04
Di <sub>100</sub>	1.22 – 1.97	48.7 ± 2.5	-	-

## 1.5.2 Impedance spectroscopy

### 1.5.2.1 - Cell Constant

The cell constant  $k$  is calculated by:

$$k = \frac{A}{d} \quad [43]$$

where  $A$  is the electrode area and  $d$  is the sample thickness. Most of the samples have a thickness around 0.400 mm and an area of circa 3 mm<sup>2</sup>, the sample An<sub>50</sub>Di<sub>50</sub>-1wt% has a bigger area of 7.06 mm<sup>2</sup>. Reducing the thickness and enlarging the electrode area improve the results of the conductivity measurements, but in the most cases the samples were too fragile to be cut with a thickness lower than 0.400 mm. Furthermore, thin and large samples were difficult to place in the measurement's cell. The standard error in thickness is 0.002 mm. The error in area was calculated by microscopic observation of a typical mismatch in the overlapping area of the electrodes. The mismatch and eventual others imperfections (areas not covered by gold for several reasons) were calculated by

computer program and give an average error of 0.13 mm<sup>2</sup>. The values of the cell constant k for each sample are reported in Table 5.

### *1.5.2.2 - Ionic Conductivity*

Impedance spectra of imaginary versus real part of specific impedance ( $-Z_s''$  vs  $Z_s'$ ), were recorded for each compositions at different temperatures and are shown in Fig. 14 a-f. The complex impedance plane analysis (Cole-Cole) helps to separate the information about the electrical properties of the sample from the contributions of the sample-electrode interface and of the wires as shown in Fig. 15 (Roling, 1999). In the discussed samples there is no evidence for contributions from wires or sample-electrode interface. In the Cole-Cole plot for polycrystal materials, a single semicircle suggests the bulk and a second semicircle suggests the grain boundary effects (Murugan & Varma, 2002). In the plots of the investigated glasses there are no signs of a second semicircle, i.e. contributions to the electrical conductivity by other processes such as surface conduction. As temperature increases, the enhancement of conductivity is seen from the reduction of diameter of circular arc (Park et al., 2005). The centres of the reported circles are lying on the axis  $Z''$ . The circular plots often display scattering in the low-frequency region (in the plots frequency increases from right to left) probably due to perturbations of the electrical field occurred during measurements by external mechanic and electric agents, able to perturbate the magnetic or electric field. The circular plots present also tails in the low frequency region which may be attributed to electrodes contributions (Park et al., 2005). The data fit reported in the plot were calculated from the measured G values (expressed in  $\Omega$ ), averaging it in the same range of the conductivity plateaux shown in Fig. 16. The diameters ( $\emptyset$ ) of the semicircles are related to G by:

$$\emptyset = 1/G \quad [44]$$

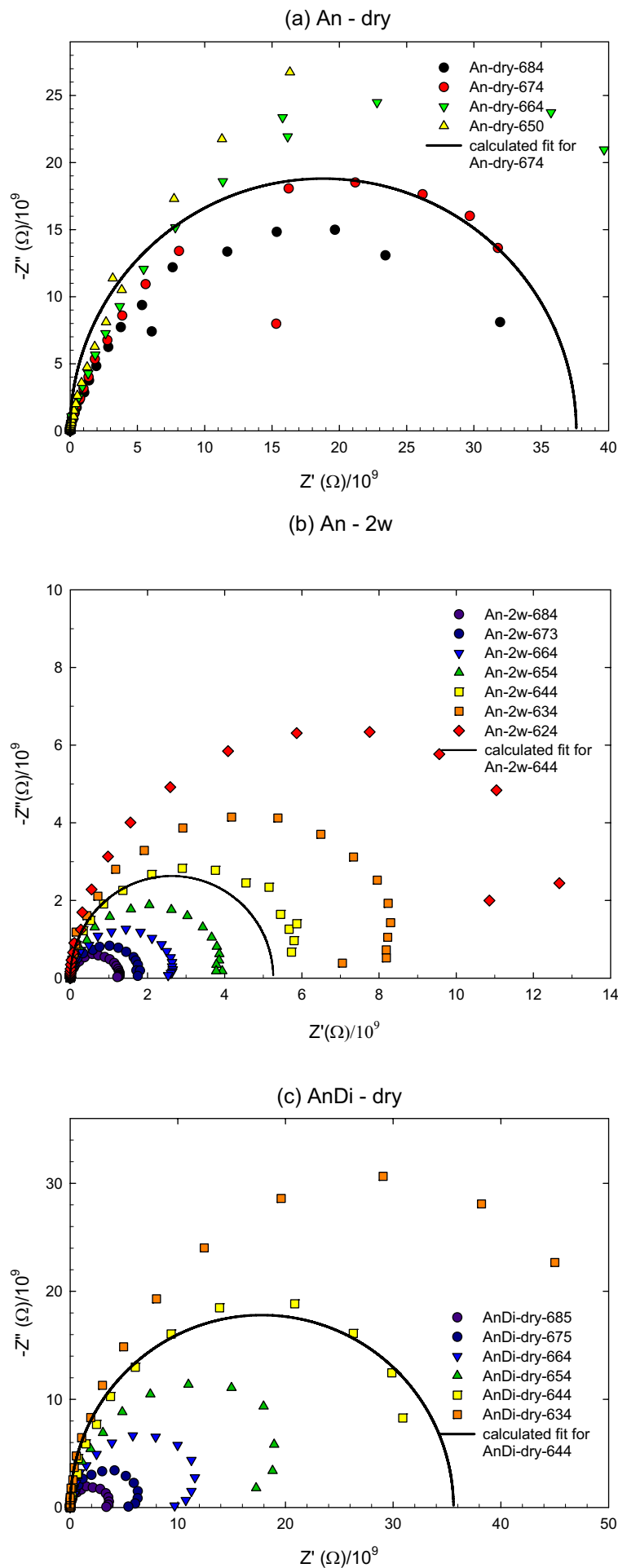
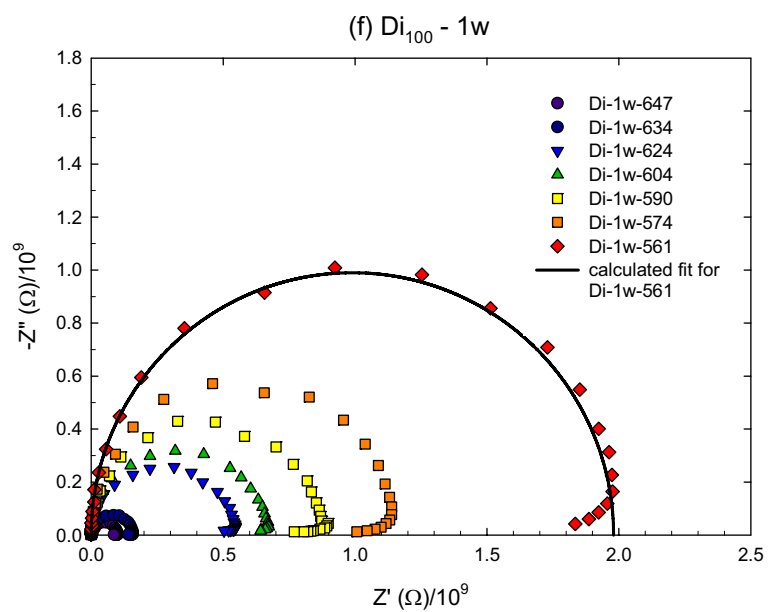
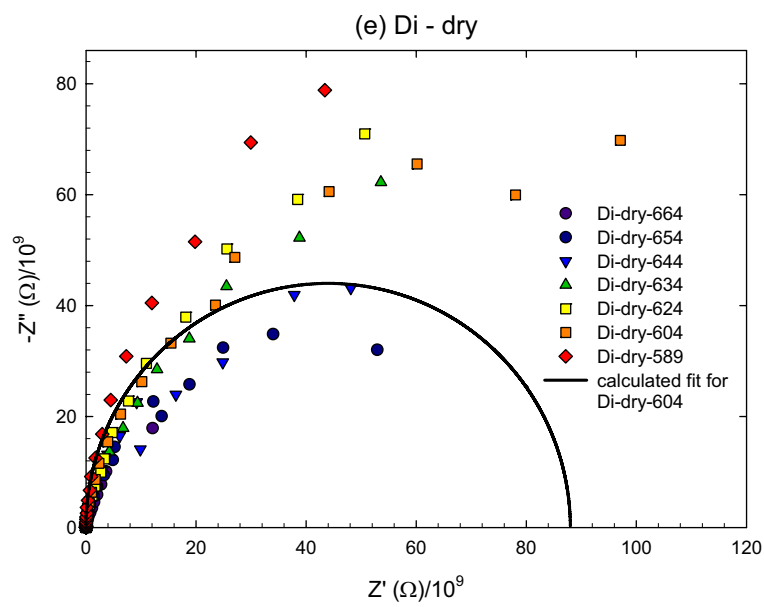
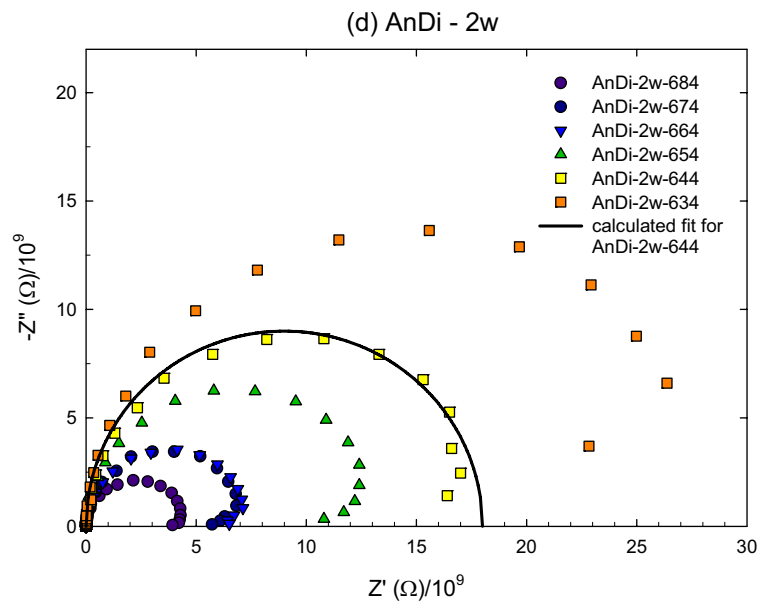


**Fig. 14 (a – f):** complex impedance plots of dry and hydrous glasses. The symbols represent the experimental values and the solid lines show the calculated fit for a chosen temperature. Frequency increases from right to left. Numbers in the legend refer to temperatures of measurements in K.



The calculated fit is close to the real data points for the hydrous compositions, for which it was easy to define the conductivity plateaus; while for the anhydrous An<sub>100</sub> and Di<sub>100</sub> glasses, but also for the An-2w, some deviations are evident, where the plateaux were not properly established, that is, where the average of  $G$  is overestimated or underestimated. Anyway, the arcs of most glasses may be well fitted into the Debye-type, showing behaviour close to the calculated semicircular fitting, as shown in Fig. 14.

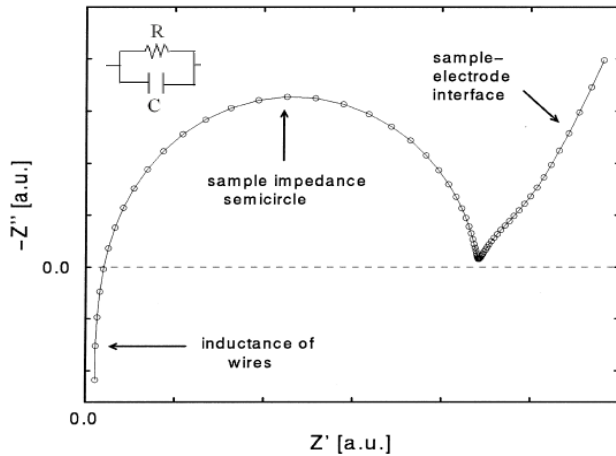


**Fig. 15:** Schematic plot of the complex impedance plane analysis showing the electrical properties of the sample and the contributions of the sample-electrode interface and of the wires. It is also shown, for the sample impedance semicircle, an equivalent circuit R-C parallel (from Roling, 1999).

The specific conductivity  $\sigma_i$  is calculated from the measured  $G$  value as:

$$\sigma_i = G / k \quad [45]$$

where  $G$  is the real part of conductivity.

Conductivity data are plotted as the real part of the complex conductivity versus frequency (Fig. 16 a-h). The hydrous glasses show the typical features of other glasses containing mobile charge carriers (Funke et al., 2000; Behrens et al., 2002). The impedance spectra display plateaux at low frequencies that become more pronounced with increasing temperature. These plateaux are probably caused by thermally activated hopping processes of mobile ions. Comparing the IS spectra of hydrous and dry glasses, it is evident that the plateaux of the anhydrous samples are less wide and less well defined than the ones obtained from the hydrous glasses. The DC conductivity ( $\sigma_{dc}$ ) is calculated by averaging the data in the range of the low frequency plateaux. To define which data of the plateaux have to be considered for  $\sigma$  calculation, the real and the imaginary part of the complex conductivity versus frequency are plotted to comparison; e.g. in Fig.17 data

of the An<sub>50</sub>Di<sub>50</sub>-1w sample at 684 K are shown. At low frequency the imaginary part of conductivity strongly decreases, data in that range are not considered for the calculation of  $\sigma_{dc}$ . The observed decrease is probably related to a contribution of the electrodes and is more pronounced at high temperatures. This is also in good agreement with the observed tail in the low frequency range of the complex impedance plane analysis. In the high frequency range the conductivity strongly increases with frequency which can be attributed to contributions of forward-backward hops of mobile ions (Funke et al., 2000; Behrens et al., 2002).

The intense scattering shown mostly in the high frequency range, but also at low frequency in case of low conductivity, was due to perturbations of the electrical field occurred during measurements by external mechanic and electric agents, able to perturbate the magnetic or electric field.

The error of the dc conductivity was calculated by error propagation considering the errors for the sample thickness and the electrode area, for  $\Delta G$  the standard deviation of  $G$  in the range of the plateau was used. The error for the temperature  $\Delta T$  was estimated to be  $\pm 5$  K. Temperature and conductivity are related by an Arrhenius-type relationship:

$$\sigma_{dc} = \frac{A}{T} e^{\left(\frac{-E_a}{RT}\right)} \quad [46]$$

where  $E_a$ , in kJ/mol, is the activation energy and  $A$ , in K/ $\Omega$ ·m, is a pre-exponential factor.

The overall formula for the error propagation is:

$$\frac{\Delta\sigma_{dc}}{\sigma_{dc}} = \sqrt{\left(\frac{\Delta d}{d}\right)^2 + \left(\frac{\Delta A}{A}\right)^2 + \left(\frac{\Delta G}{G}\right)^2 + \left(-\frac{1}{T} + \frac{E_a}{RT^2}\right)^2 \Delta T^2} \quad [47]$$

If  $E_a \gg RT$ , the last term of eq. 40 become  $\left(-\frac{E_a}{RT^2}\right)^2 \Delta T^2$ .

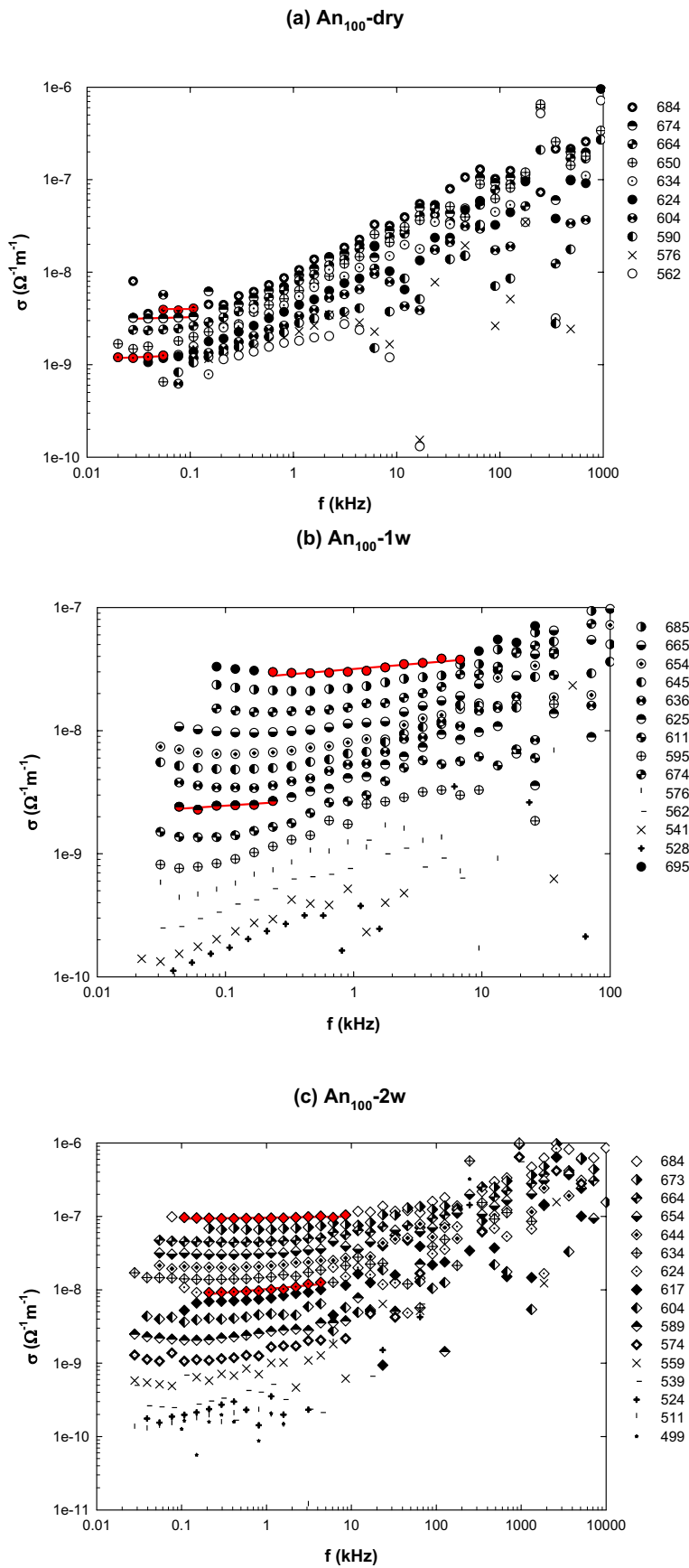
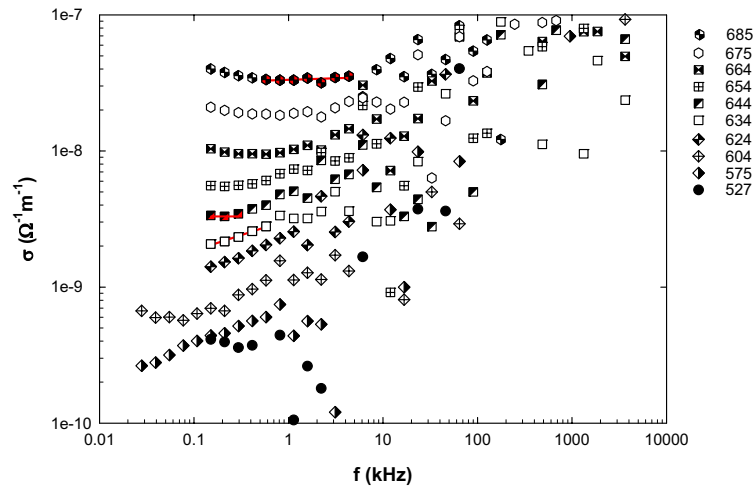


**Fig. 16 (a-h)** – Conductivity spectra of nominally dry and hydrous  $An_{100}$ ,  $Di_{100}$  and  $An_{50}Di_{50}$  glasses. Numbers in the legend refer to temperatures of measurements in K.

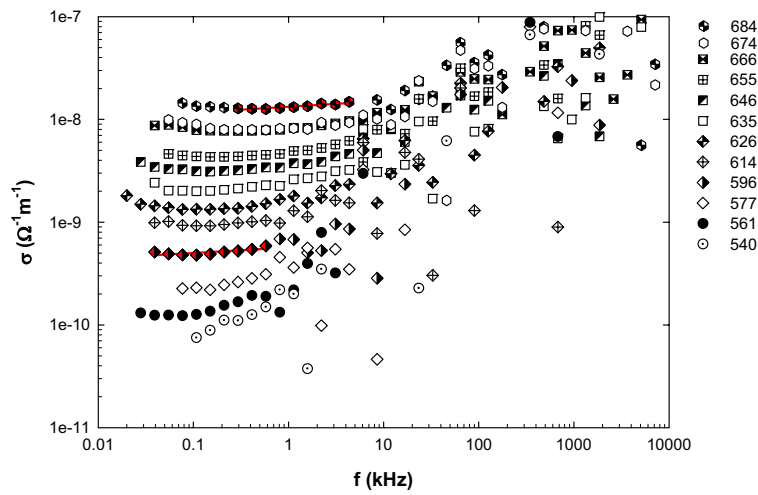
- (a)  $An_{100}$ -dry
- (b)  $An_{100}$ -1w, water content 1,28 wt%
- (c)  $An_{100}$ -2w, water content 1,76 wt%
- (d)  $An_{50}Di_{50}$ -dry
- (e)  $An_{50}Di_{50}$ -1w, water content 1,50 wt%
- (f)  $An_{50}Di_{50}$ -2w, water content 2,12wt%
- (g)  $Di_{100}$ -dry
- (h)  $Di_{100}$ -1w, water content 1,22 wt%

Linear regressions of data used to evaluate dc conductivity are marked in red and define the range of temperature in which the conductivity was calculated.

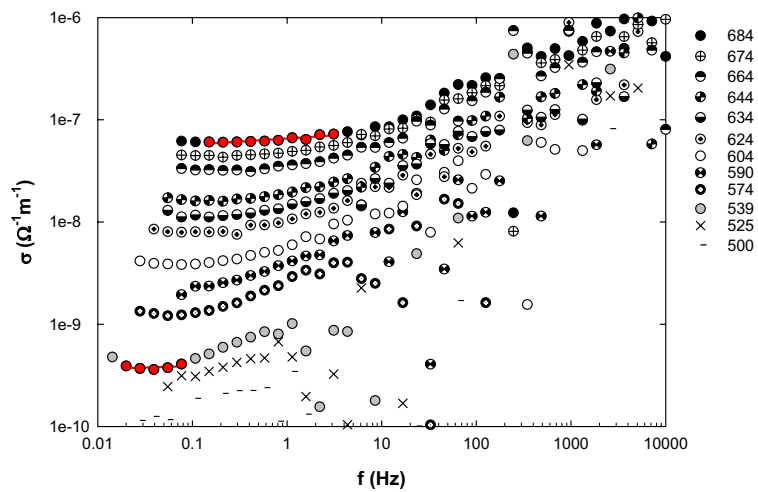
(d) An<sub>50</sub>Di<sub>50</sub>-dry



(e) An<sub>50</sub>Di<sub>50</sub>-1w



(f) An<sub>50</sub>Di<sub>50</sub>-2w



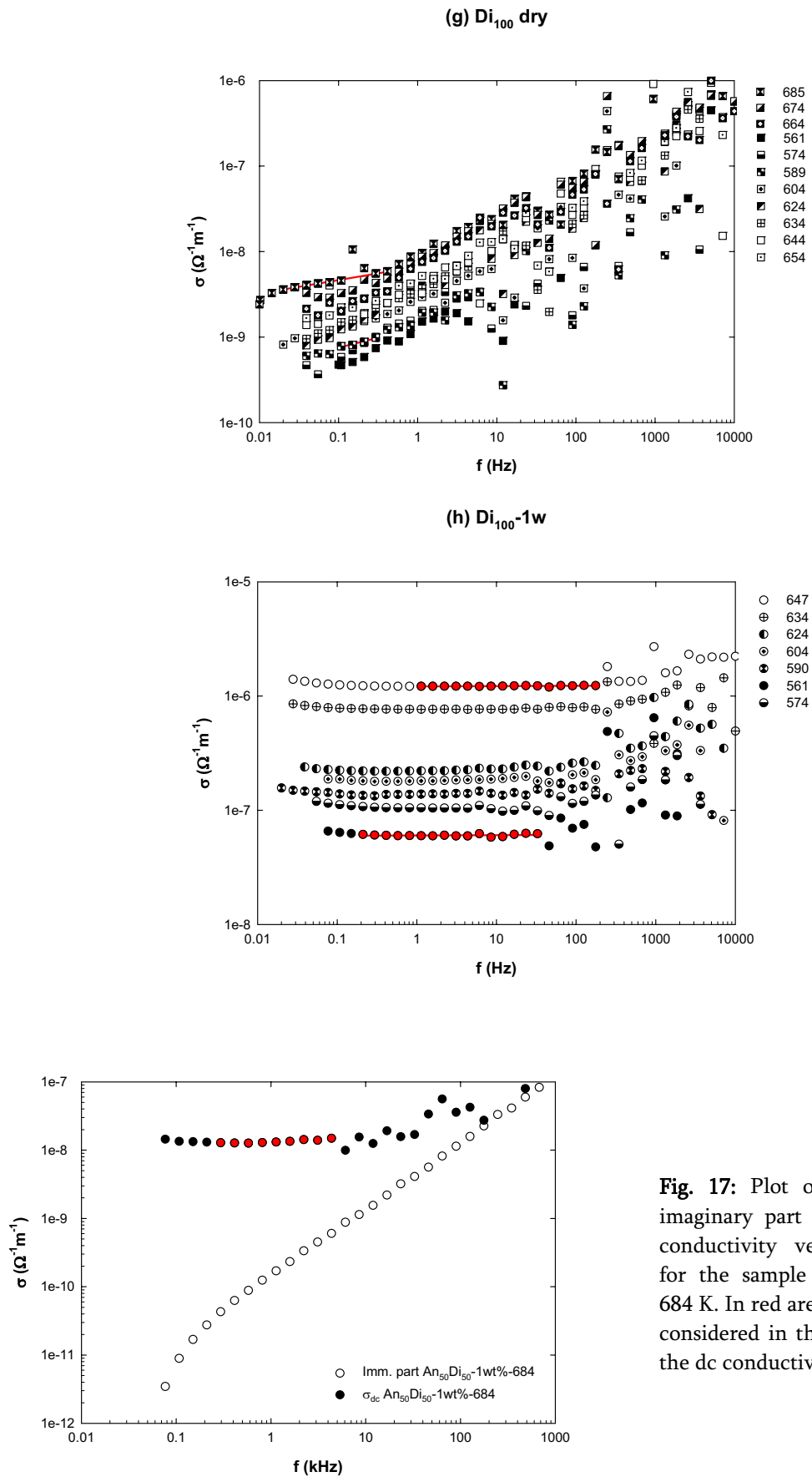


**Fig. 17:** Plot of the real and imaginary part of the complex conductivity versus frequency for the sample  $\text{An}_{50}\text{Di}_{50}$ -1w at 684 K. In red are shown the data considered in the calculation of the dc conductivity.

The error of the measurement is about 20-25% of the measured values, which is a reasonable value concerning the number of variables (thickness, electrode area, temperature, standard deviation of the plateau). The dominating contributions to the error are given by the terms  $(\Delta G/G)^2$  and  $\left(-\frac{1}{T} + \frac{E_a}{RT^2}\right)^2 \Delta T^2$ . Table 5 (p.59) lists, for each sample, the  $\sigma_{dc}$  with the respective errors and the temperature (in K) at which the measurement was done.

A measurable DC conductivity was observed in most cases above 600 K; in the Di<sub>100</sub>-1w and Di<sub>100</sub>-1w-bis a progressive decrease of the DC conductivity with increasing temperature was registered for  $T > 623$  K, due to the water loss. Impedance measurements on dry An<sub>100</sub> and An<sub>50</sub>Di<sub>50</sub> glasses show not a discrete plateau for temperatures below 634-644 K, hydrous An<sub>100</sub> with nominally 1 and 2 wt% of water start to show a reliable plateau at 625 K (Fig. 16). Conductivity data for hydrous Di<sub>100</sub> are not available up to 561 K, while for Di<sub>100</sub>-dry it was not possible to define a proper plateau but an inflection point is visible in Fig.16 (g). In this case, the obtained conductivity values have to be considered just as indicative values. An<sub>50</sub>Di<sub>50</sub>-2w sample shows the first plateau at the lowest temperature of 539 K. It is evident from Fig. 16 that with increasing water content as with increasing temperature the plateaux became more wide and well defined and shift toward higher frequency.

In the nominally dry glasses, the measured conductivity is mostly due to the presence of a small amount of Na, evidenced by microprobe measurements. The amount of Na<sub>2</sub>O is up to 0,15 wt% in the An<sub>100</sub> and decreases to 0,07 wt% in the An<sub>50</sub>Di<sub>50</sub> and finally to 0,05 wt% in the Di<sub>100</sub>. At 685 K,  $\sigma_{dc}$  present values of  $4.05 \pm 0.81 \cdot 10^{-9} \Omega^{-1} \cdot m^{-1}$  for An<sub>100</sub>,  $3.37 \pm 10^{-8} \Omega^{-1} \cdot m^{-1}$  for An<sub>50</sub>Di<sub>50</sub> and  $5.60 \pm 2.30 \cdot 10^{-9} \Omega^{-1} \cdot m^{-1}$  for Di<sub>100</sub> dry glasses. It is inferred that the highest conductivity measured for the An<sub>50</sub>Di<sub>50</sub> dry sample is due to combined effects of increasing NBO/T, compared to An<sub>100</sub> composition, and increasing of Na content, compared to Di<sub>100</sub> composition. Anyway the presence of Na impurities plays a negligible role in the conductivity measurements of the hydrous glasses. It has been shown in previous studies that in silicate glasses containing small cations such as Na or Li the conductivity decreases with increasing the amount of water (Kappes, 2002), while our

measurements show an increase in conductivity with increasing water content. Therefore, we infer that the trends in the Arrhenius plots obtained by the data of the anhydrous glasses indicate the absence of significant amounts of charge carriers, while the DC conductivity observed in the hydrous samples is due to the charge carriers produced by hydration of the glasses. This is particularly evident in the case of Di<sub>100</sub> composition. This interpretation is supported by the higher conductivity shown by the samples with higher amount of water and is in good agreement with a previous study Fig.18 (a-d) (Behrens et al., 2002).

**Table 5.** Sample characterization and dc conductivity data.

Sample k (m)	Temperature (K)	$\sigma_{dc}$ ( $\Omega^{-1}\cdot m^{-1}$ )	logD
<b>An<sub>100</sub>-dry</b> k = 0.0083	684	$4.05 \pm 0.81 (10^{-9})$	
	674	$3.21 \pm 0.59$	
	664	$2.43 \pm 0.47$	
	650	$1.44 \pm 0.54$	
	634	$1.21 \pm 0.25$	
<b>An<sub>100</sub>-1w</b> k = 0.0081 C <sub>H<sub>2</sub>O</sub> =1.28wt%	695	$3.24 \pm 0.66 (10^{-8})$	$-13.80 \pm 0.10$
	685	$2.36 \pm 0.51$	$-13.95 \pm 0.10$
	674	$1.53 \pm 0.32$	$-14.14 \pm 0.10$
	665	$1.04 \pm 0.21$	$-14.32 \pm 0.10$
	654	$0.68 \pm 0.14$	$-14.51 \pm 0.10$
	646	$0.52 \pm 0.11$	$-14.63 \pm 0.10$
	636	$0.427 \pm 0.093$	$-14.72 \pm 0.11$
	625	$0.246 \pm 0.054$	$-14.97 \pm 0.11$
<b>An<sub>100</sub>-2w</b> k = 0.0083 C <sub>H<sub>2</sub>O</sub> =1.76wt%	611	$0.142 \pm 0.033$	$-15.22 \pm 0.10$
	684	$9.60 \pm 1.80 (10^{-8})$	$-13.48 \pm 0.09$
	673	$6.79 \pm 1.30$	$-13.63 \pm 0.09$
	664	$4.62 \pm 0.91$	$-13.81 \pm 0.010$
	654	$3.19 \pm 0.66$	$-13.97 \pm 0.10$
	644	$2.29 \pm 0.55$	$-14.13 \pm 0.12$
	634	$1.45 \pm 0.31$	$-14.33 \pm 0.11$
	624	$1.03 \pm 0.25$	$-14.49 \pm 0.12$
	617	$0.78 \pm 0.19$	$-14.61 \pm 0.12$
	604	$0.422 \pm 0.096$	$-14.89 \pm 0.12$
589	$0.221 \pm 0.055$	$-15.18 \pm 0.13$	

Sample k (m)	Temperature (K)	$\sigma_{dc}(\Omega^{-1}\cdot m^{-1})$	logD
<b>An<sub>50</sub>Di<sub>50</sub>-dry</b>  k = 0.0079	685	$3.37 \pm 0.57 (10^{-8})$	
	675	$1.87 \pm 0.32$	
	664	$0.97 \pm 0.17$	
	654	$0.57 \pm 0.11$	
	644	$0.357 \pm 0.072$	
<b>An<sub>50</sub> Di<sub>50</sub>-1w</b>  k = 0.0176  C <sub>H<sub>2</sub>O</sub> =1.50wt%	684	$1.34 \pm 0.23 (10^{-8})$	$-14.26 \pm 0.08$
	674	$0.80 \pm 0.13$	$-14.49 \pm 0.08$
	666	$0.80 \pm 0.13$	$-14.50 \pm 0.08$
	655	$0.48 \pm 0.10$	$-14.73 \pm 0.10$
	646	$0.341 \pm 0.067$	$-14.88 \pm 0.11$
	635	$0.214 \pm 0.042$	$-15.09 \pm 0.10$
	626	$0.144 \pm 0.031$	$-15.27 \pm 0.11$
	614	$0.974 \pm 0.019$	$-15.45 \pm 0.10$
	596	$0.051 \pm 0.011$	$-15.74 \pm 0.11$
	<b>An<sub>50</sub> Di<sub>50</sub>-2w</b>  k = 0.0080  C <sub>H<sub>2</sub>O</sub> =2.12wt%	684	$6.42 \pm 1.10 (10^{-8})$
664		$3.59 \pm 0.74$	$-14.00 \pm 0.10$
654		$2.62 \pm 0.58$	$-14.14 \pm 0.11$
644		$1.92 \pm 0.48$	$-14.28 \pm 0.12$
634		$1.38 \pm 0.36$	$-14.43 \pm 0.13$
624		$0.92 \pm 0.23$	$-14.62 \pm 0.13$
604		$0.411 \pm 0.086$	$-15.00 \pm 0.10$
590		$0.249 \pm 0.054$	$-15.21 \pm 0.19$
574		$0.128 \pm 0.028$	$-15.51 \pm 0.53$
539		$0.038 \pm 0.011$	$-16.06 \pm 0.53$
<b>An<sub>50</sub> Di<sub>50</sub>-3w</b>  k = 0.0078  C <sub>H<sub>2</sub>O</sub> =2.77wt%	685	$3.00 \pm 0.59 (10^{-6})$	$-12.16 \pm 0.10$
	667	$1.77 \pm 0.32$	$-12.40 \pm 0.09$
	645	$0.71 \pm 0.18$	$-12.81 \pm 0.13$
	627	$0.60 \pm 0.14$	$-12.90 \pm 0.11$

Sample k (m)	Temperature (°K)	$\sigma_{dc}(\Omega^{-1}\cdot m^{-1})$	logD
<b>Di<sub>100</sub>-dry</b> k = 0.0083	685	$5.60 \pm 2.30 (10^{-9})$	
	674	$3.16 \pm 0.51$	
	664	$3.05 \pm 0.57$	
	654	$2.78 \pm 0.99$	
	644	$2.37 \pm 0.56$	
<b>Di<sub>100</sub>-1w</b> k = 0.0083 C <sub>H<sub>2</sub>O<sub>t</sub></sub> =1.22wt%	647	$12.20 \pm 1.90 (10^{-7})$	$-12.24 \pm 0.07$
	634	$7.72 \pm 1.20$	$-12.45 \pm 0.08$
	624	$2.33 \pm 0.41$	$-12.97 \pm 0.08$
	604	$1.84 \pm 0.32$	$-13.08 \pm 0.08$
	590	$1.39 \pm 0.26$	$-13.22 \pm 0.08$
	574	$1.05 \pm 0.20$	$-13.36 \pm 0.09$
	561	$0.60 \pm 0.12$	$-13.61 \pm 0.09$
<b>Di<sub>100</sub>-1w-bis</b> k = 0.0083 C <sub>H<sub>2</sub>O<sub>t</sub></sub> =1.22wt%	689	$2.16 \pm 0.39 (10^{-7})$	$-12.96 \pm 0.06$
	675	$1.74 \pm 0.31$	$-13.06 \pm 0.05$
	665	$2.78 \pm 0.69$	$-12.87 \pm 0.10$
	655	$3.06 \pm 0.49$	$-12.83 \pm 0.03$
	645	$14.3 \pm 2.2$	$-12.91 \pm 0.04$
	633	$10.2 \pm 1.6$	$-12.32 \pm 0.08$
	614	$7.14 \pm 1.20$	$-12.49 \pm 0.08$
	604	$4.95 \pm 0.85$	$-12.66 \pm 0.08$
	594	$3.49 \pm 0.62$	$-12.82 \pm 0.09$
585	$2.39 \pm 0.45$	$-12.99 \pm 0.10$	

Notes: Di<sub>100</sub>-1w and Di<sub>100</sub>-1w-bis were from the same glass body. In the table are reported the values of the cell constant k for each sample. The standard error in thickness is 0.2 mm. The error in area is 0.13 m<sup>2</sup>. The C<sub>H<sub>2</sub>O<sub>t</sub></sub> reported was calculated by KFT.

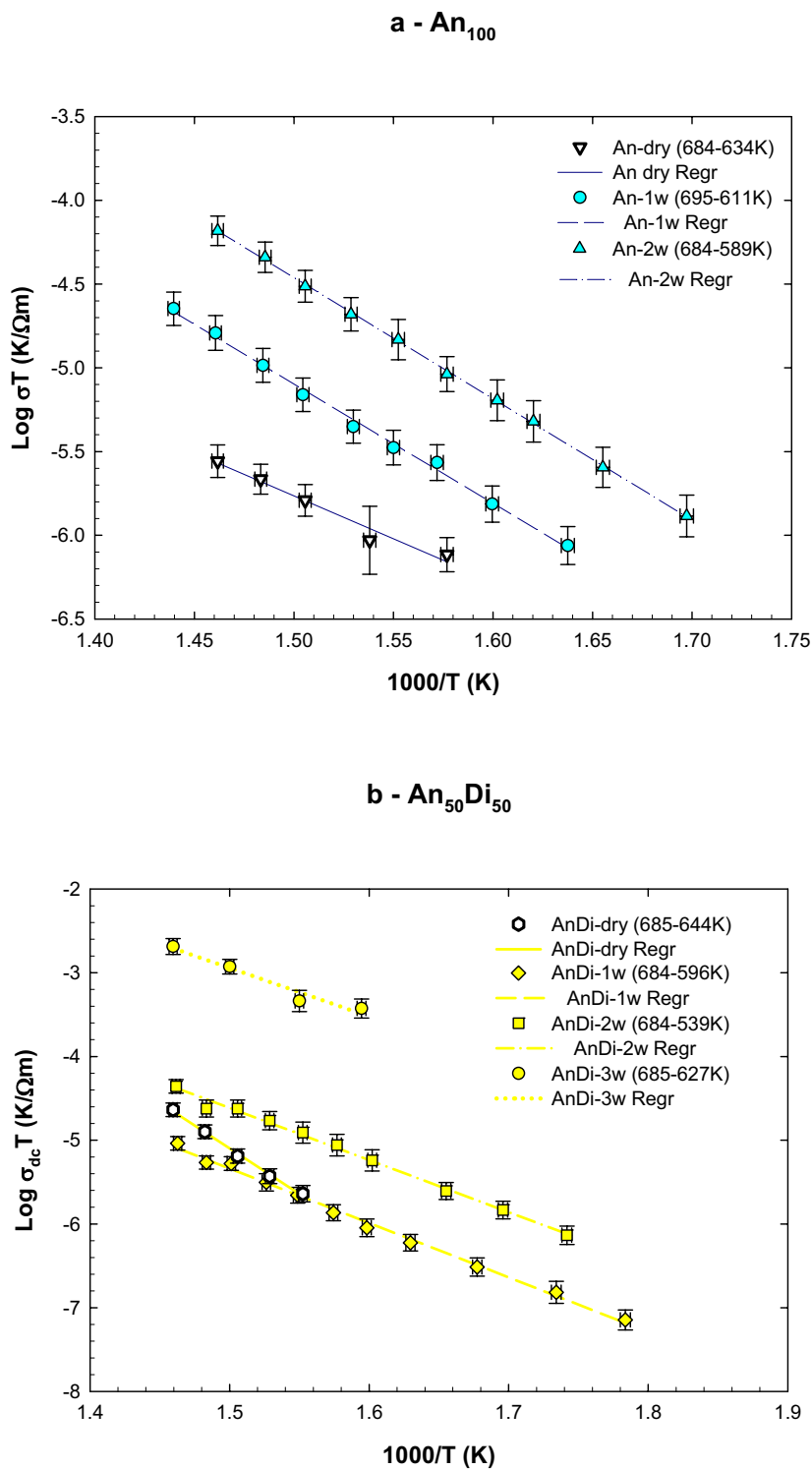


**Fig. 18 (a-d)** – Plot of  $\text{Log}(\sigma_{\text{dc}}T)$  as a function of reciprocal temperature for:

(a) An<sub>100</sub> glasses (An-1w: 1.28wt% $\text{H}_2\text{O}_t$ ; An-2w: 1.76wt%  $\text{H}_2\text{O}_t$ )

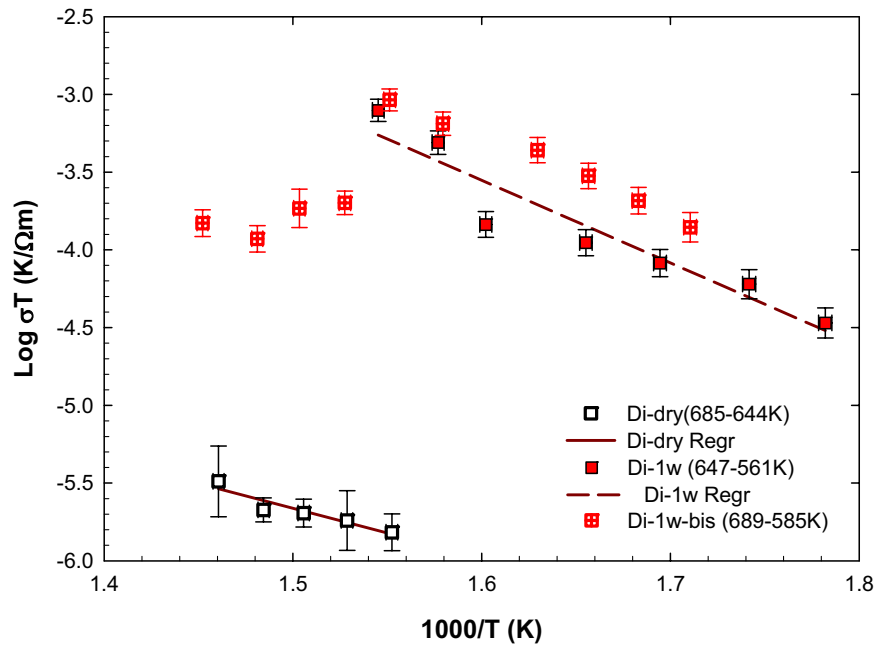
(b) An<sub>50</sub>Di<sub>50</sub> glasses (AnDi-1w: 1.22wt% $\text{H}_2\text{O}_t$ ; AnDi-2w: 2.12wt%  $\text{H}_2\text{O}_t$ ; AnDi-3w: 2.77wt%  $\text{H}_2\text{O}_t$ )

(c) Di<sub>100</sub> glasses (Di-1w: 1.22wt% $\text{H}_2\text{O}_t$ )

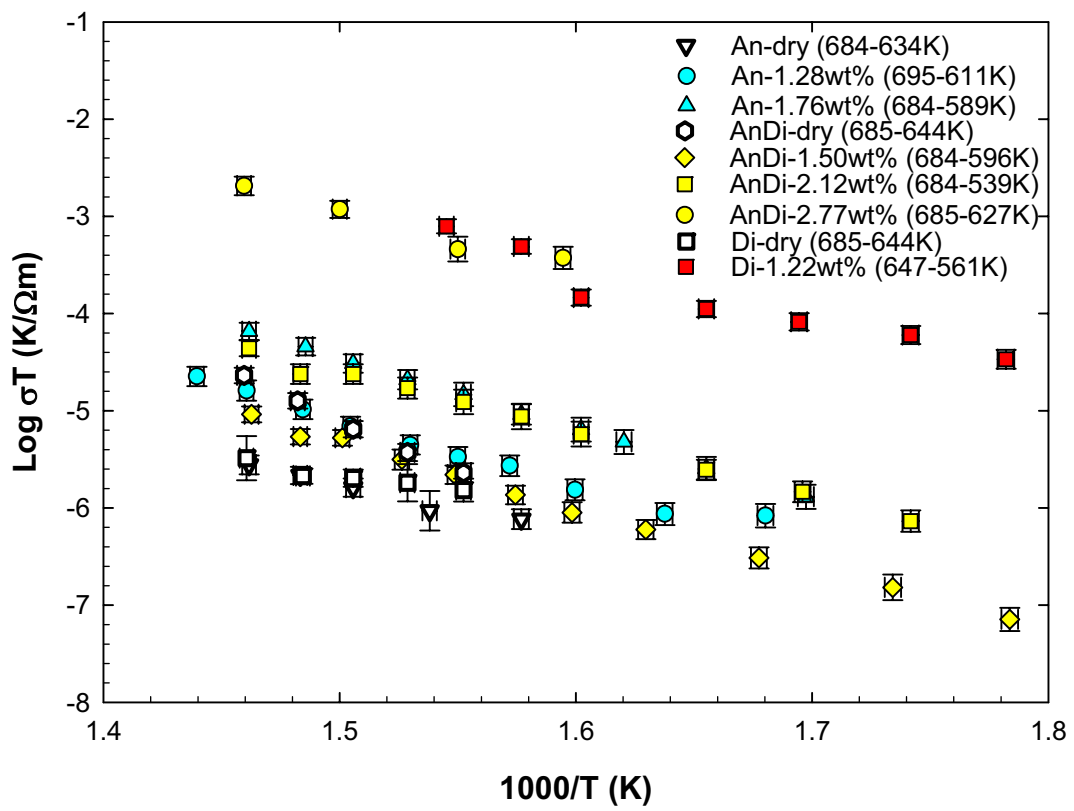
(d) comparative plot

The numbers refer to the temperature range of measurements used for the linear regression. Note the shift to lower conductivity for the sample Di<sub>100</sub>-1w-bis at temperature above 623 K, indicating a loss of charge carriers or structural changes of the glass. In plot d, all compositions are shown together for comparison. Note that Di<sub>100</sub>-1w shows values comparable with that of An<sub>50</sub>Di<sub>50</sub>-3w. Besides, the conductivity of An<sub>50</sub>Di<sub>50</sub>-dry and An<sub>50</sub>Di<sub>50</sub>-1wt% are similar. In the case of dry glasses, the measured conductivity is attributed to minor amounts of dissolved  $\text{Na}_2\text{O}$ .

c - Di<sub>100</sub>



d



### 1.5.2.3 - Stability of samples during impedance measurements

During impedance measurements, the samples were exposed to a heating treatment, as described in paragraph 1.4.3.2. Therefore, the samples were optically checked before and after the measurements for eventual changes. No fractures or holes or crystals were found in the glasses after heating. The electrode surfaces were a bit damaged, as shown in Fig.7b, but this was happening at the end of the measurements, during the removal of the sample from the cell, due to the reaction of the gold electrodes surfaces with the platinum cell at the highest temperatures, as stated in paragraph 1.4.3.1.

The amount of water for each sample was measured before conductivity experiments by KFT, NIR and MIR spectroscopy and after conductivity measurements by NIR and MIR spectroscopy, after removing the coated gold electrodes. The obtained values for An<sub>50</sub>Di<sub>50</sub> compositions are reported in Table 6.

**Table 6.** Water content before and after conductivity experiments for An<sub>50</sub>Di<sub>50</sub> compositions.

Sample	KFT-C <sub>H2O</sub>	NIR C <sub>H2O in.</sub>	NIR C <sub>H2Om-in</sub>	NIR C <sub>OH-in.</sub>	NIR C <sub>H2O-fin.</sub>	NIR C <sub>H2Om-fin</sub>	NIR C <sub>OH-in.</sub>	Water loss
<b>An<sub>50</sub>Di<sub>50</sub>-1w</b>	1.50 ± 0.05	1.50 ± 0.05	0.12 ± 0.03	1.38 ± 0.05	1.30 ± 0.04	0.05 ± 0.02	1.25 ± 0.04	13 %
<b>An<sub>50</sub>Di<sub>50</sub>-2w</b>	2.12 ± 0.03	2.50 ± 0.05	0.38 ± 0.02	2.12 ± 0.05	2.29 ± 0.04	0.20 ± 0.02	2.09 ± 0.04	8 %
<b>An<sub>50</sub>Di<sub>50</sub>-3w</b>	2.77 ± 0.03	2.81 ± 0.05	0.49 ± 0.02	2.32 ± 0.05	2.59 ± 0.23	0.35 ± 0.18	2.24 ± 0.13	8 %

Notes: The bulk water content was measured before the conductivity experiments by KFT and NIR-MIR spectroscopy. After conductivity measurements, samples were tested again with NIR-MIR spectroscopy.

It has to be considered that the samples measured by KFT were glass pieces adjacent to the ones chosen for impedance measurements. Therefore, small dishomogeneities in the glasses are the cause of differences in initial bulk water content measured by KFT and the one measured by NIR for An<sub>50</sub>Di<sub>50</sub>-1w and An<sub>50</sub>Di<sub>50</sub>-3w. It was calculated that the water loss during measurements was varying from the 8% of An<sub>50</sub>Di<sub>50</sub>-2w and An<sub>50</sub>Di<sub>50</sub>-3w to the 18% of the An<sub>100</sub>-1w. The Di<sub>100</sub>-1w-bis shows the highest water loss of 46% relative. Where possible (An<sub>50</sub>Di<sub>50</sub> composition), it was also evaluated the speciation of water and it was found that the water is mainly present as OH specie.

It is expected that the dehydration of the samples during conductivity experiments produces a decrease in conductivity. This is evident in plot c of Fig.18 for the sample Di<sub>100</sub>-1w-bis, where a water loss of 0.55 wt% H<sub>2</sub>O<sub>t</sub> produces a decrease in conductivity of circa 0.7 log units, while it is not visible for other samples. Furthermore, the dehydration will be not uniform over the sample length, but will be more marked along the rim than in the centre of the sample. In that case, the sample should be considered as constituted by a series of resistors.

To have more information about loss of charge carriers and/or structural changes of the glasses, conductivity measurements during cooling at the same temperature effectuated during heating are required. For these measurements, analysis during cooling could not be done due to the long time cooling required (50 min for 10 K + 1h waiting before temperature starts to decrease).

### ***1.5.3 Temperature dependence of $\sigma_{dc}$***

The temperature dependence of electrical conductivity described by the Arrhenius relationship was shown in chapter 1.5.2.2 as:

$$\sigma_{dc}T = Ae^{\left(\frac{-E_a}{RT}\right)} \quad [48]$$

where  $E_a$ , in kJ/mol, is the activation energy and  $A$ , in K/ $\Omega$ ·m, is a pre-exponential factor. Arrhenius parameters are given in Table 7 and in Fig. 18 the log ( $\sigma_{dc} \cdot T$ ) is plotted as a function of reciprocal temperature. The activation energy is similar for the An<sub>100</sub>-1w and the An<sub>100</sub>-2w glasses: 136 and 137 kJ/mol respectively. For the compositions An<sub>50</sub>Di<sub>50</sub> is ranging from 110 kJ/mol for the nominally 3 wt% to 124 kJ/mol for the sample An<sub>50</sub>Di<sub>50</sub>-1w. The  $E_a$  for the Di<sub>100</sub> hydrous glasses is around 100 kJ/mol. These values resemble the ones found for molecular water diffusion and bulk water diffusion in other silicate glasses, varying from 60 - 120 kJ/mol (Scholze et al., 1959; Zhang and Behrens, 2000; Behrens et al., 2002).

**Table 7.** Arrhenius parameters

<b>Sample</b>	<b>Exp. No.</b>	<b>Temperature in. - fin. (K)</b>	<b>Log (A) (A in K/Ωm)</b>	<b>Log D<sub>0</sub> (D<sub>0</sub> in m/s)</b>	<b>E<sub>a</sub> (kJ/mol)</b>
<b>An<sub>100</sub>-dry</b>	5	684 - 634	3.17 ± 0.24	n.d.	114 ± 12
<b>An<sub>100</sub>-1w</b>	9	695 - 611	5.59 ± 0.12	-3.56 ± 0.22	136 ± 3
<b>An<sub>100</sub>-2w</b>	11	684 - 589	6.30 ± 0.10	-2.99 ± 0.19	137 ± 1
<b>An<sub>50</sub>Di<sub>50</sub>-dry</b>	5	685 - 644	4.09 ± 0.12	n.d.	219 ± 5
<b>An<sub>50</sub>Di<sub>50</sub>-1w</b>	11	684 - 561	4.42 ± 0.12	-4.81 ± 0.21	124 ± 3
<b>An<sub>50</sub>Di<sub>50</sub>-2w</b>	11	684 - 525	3.77 ± 0.11	-7.43 ± 0.22	117 ± 3
<b>An<sub>50</sub>Di<sub>50</sub>-3w</b>	4	685 - 627	5.75 ± 0.23	-3.73 ± 0.34	111 ± 17
<b>Di<sub>100</sub>-dry</b>	5	685 - 644	-2.70 ± 0.12	n.d.	68 ± 7
<b>Di<sub>100</sub>-1w</b>	7	647 - 561	4.95 ± 0.21	-5.31 ± 0.32	102 ± 15
<b>Di<sub>100</sub>-1w-bis</b>	6	647 - 561	4.74 ± 0.16	-4.39 ± 0.26	96 ± 5

Notes: The first column refers to the number of measurements considered in the calculation of the activation energy.

## 1.6 - Discussion

### 1.6.1 Water diffusion

In Fig. 18 a-d there are shown the conductivity values of dry and hydrous glasses versus the reciprocal temperature. It is noteworthy that the dry glasses show a measurable dc conductivity that is probably due to the presence of small amount of Na<sup>+</sup>, as already reported in chapter 1.5.2.2. Knowing the amount of water in the dry samples, it is possible to distinguish the contribution of H<sup>+</sup> from the contribution of Na<sup>+</sup>, considering:

$$\sigma_{dct} = \sigma_{dcH^+} + \sigma_{dcNa^+}, \quad [49]$$

where  $\sigma_{dct}$  is the total electrical conductivity and  $\sigma_{dcH^+}$  and  $\sigma_{dcNa^+}$  are respectively the contributions to the electrical conductivity given by H<sup>+</sup> and Na<sup>+</sup>.  $\sigma_{dcNa^+}$  is calculated assuming that  $\sigma_{dcH^+}$  is given by the equation:

$$\sigma_{dcH^+} = \frac{C_{H^+(dry)}}{C_{H^+(hydrous)}} \sigma_{dcH^+(hydrous)} \quad [50]$$

where  $C_{H^+(dry)}$  and  $C_{H^+(hydrous)}$  are the concentration of H<sup>+</sup> in the anhydrous and hydrous glass and  $\sigma_{dcH^+(hydrous)}$  is the electrical conductivity in the hydrous glass. The values of  $\sigma_{H^+}$  and  $\sigma_{Na^+}$  with the referring temperatures for dry glasses are listed in Table 8. To calculate the  $C_{dcH^+}$ , the samples An<sub>100</sub>-1w, An<sub>50</sub>Di<sub>50</sub>-1w and Di<sub>100</sub>-1w were used, because it is known that the increase of the water content reduces the mobility of alkali. It is emphasized that there is no contribution of Na conductivity for the Di<sub>100</sub> dry glass, in which the measured conductivity of protons is lower than the calculated one. Hence, it is inferred that not all the protons contribute to the total conductivity. The Na contribution to the total dc conductivity becomes predominant in An<sub>100</sub> and An<sub>50</sub>Di<sub>50</sub> dry glasses where the conductivity of protons is respectively circa 1-2 orders of magnitude and 2-3 orders of magnitude lower than the conductivity of Na. This finding is in good agreement with the measured Na content in glasses reported in Table 1, where it is shown that the Na content is at the detection limit for Di<sub>100</sub> and increases for An<sub>100</sub> dry glasses. The An<sub>50</sub>Di<sub>50</sub> dry sample show intermediate values of Na content but the strongest contribution of Na to conductivity. This may be due to a different network structure; anyway a more detailed knowledge on the structural dependence of proton diffusivity in glasses is

required in this case. The calculated values for Na<sup>+</sup> conductivity in An<sub>100</sub> dry glass are circa 3 orders of magnitude higher than the one evaluated by Jambon (1980) and Behrens et al. (1992) by the residual activity method.

**Table 8.** H<sup>+</sup> and Na<sup>+</sup> dc conductivity data.

Sample C (wt%)	Temperature (K)	$\sigma_{dc-dry}$	$\sigma_{dcNa^+}$	$\sigma_{dcH^+}$
	684.65	4.05 (10 <sup>-9</sup> )	3.84 (10 <sup>-9</sup> )	2.02 (10 <sup>-10</sup> )
<b>An<sub>100</sub>-dry</b>	673.65	3.21	3.08	1.31
C = 0.01	664.65	2.43	2.34	0.89
	653.65	1.44	1.38	0.58
	684.15	3.37 (10 <sup>-8</sup> )	3.36 (10 <sup>-8</sup> )	7.09 (10 <sup>-11</sup> )
<b>An<sub>50</sub>Di<sub>50</sub>-dry</b>	673.15	1.87	1.87	4.23
C = 0.008	664.15	0.97	0.97	4.23
	654.15	0.57	0.57	2.54
	644.15	0.36	0.35	1.80
<b>Di<sub>100</sub>-dry</b>	647.15	2.37 (10 <sup>-9</sup> )	-	5.23 (10 <sup>-9</sup> )
C = 0.005				

Notes: In the table are listed the values of dc conductivity of Na<sup>+</sup> and H<sup>+</sup> for the analysed dry glasses at different temperatures. To calculate the  $C_{dcH^+}$ , the samples An<sub>100</sub>-1w, An<sub>50</sub>Di<sub>50</sub>-1w and Di<sub>100</sub>-1w were used. The water concentration in wt% calculated by MIR is reported for each sample. The factor in parentheses applies to all data for the respective sample.

Using the Nernst-Einstein relationship it is possible to evaluate conductivity data in terms of diffusivity of protons:

$$D_i = \frac{f\sigma_i RT}{C_i z_i^2 F^2} \quad [51]$$

where  $\sigma_i$  is the partial dc conductivity in 1/Ω·m,  $C_i$  the concentration in wt% and  $z_i$  the charge of i ion. T is the temperature in K, R is the gas constant in J/K·mol, F is the Faraday constant in C/mol and f is a correlation factor depending on diffusion mechanism and is in this case, for simplicity, considered as to 1. Evaluated diffusivity values are reported in Table 5 and displayed in Fig. 19 (a-d).

At temperatures far below the glass transition it has been inferred from previous studies that the structures of glasses are quite rigid and the structural relaxation is too slow to allow the formation of a transient OH group pair (Doremus, 1969; Wasserburg, 1988; Doremus, 1995; Zhang et al., 1991). Therefore, water molecules migrate through the silicate network by direct jumps from one available space to another and are immobilised by reaction with the oxygens of the silicate structure (Zhang et al., 1991; Doremus, 2000). In particular, protons of OH groups are considered responsible for the electrical conductivity and they move through the glass network jumping from one non-bridging oxygen to another:



It was possible to estimate the concentration of mobile protons by NIR spectra for the composition An<sub>50</sub>Di<sub>50</sub>: the initial concentration of OH groups is 1.38 wt% in the glass containing 1.50 wt% of H<sub>2</sub>O<sub>t</sub> and 2.32 wt% in the sample with bulk water content of 2.81 wt% (Table 6). In the sample An<sub>50</sub>Di<sub>50</sub> with 2.12 wt% H<sub>2</sub>O<sub>t</sub> (by KFT), a discrepancy in the water content measured with KFT and NIR is evident. With NIR measurements, values of 2.50 wt% of H<sub>2</sub>O<sub>t</sub> and 2.12 wt% of OH were calculated. It has to be considered that the samples measured by KFT were glass pieces adjacent to the ones chosen for impedance measurements. Therefore, small dishomogeneities in the glasses are the cause of differences in initial bulk water content measured by KFT and the one measured by NIR. Therefore, the values measured by NIR were considered more accurate and taken into account for further calculations and data elaborations.

For An<sub>100</sub> and Di<sub>100</sub> a calibration for NIR is not available yet and in first approximation it is assumed that the whole water content will be taken into account when considering diffusion. With this approximation an error of < 8% will be introduced, when compared with the partition of H<sub>2</sub>O molecules and OH groups in An<sub>50</sub>Di<sub>50</sub> glasses. Anyway, this depends whether only OH groups contribute to the charge transport, or H<sub>2</sub>O molecules as well.

### ***1.6.2 Mechanism of proton conduction***

In Fig. 19 (a-c) there are reported for better understanding diffusivity plots for each of the analysed compositions. The plot of Fig.19 – a, shows that the diffusion of An-1.76 wt% H<sub>2</sub>O<sub>t</sub> is circa 0.5 log units higher than An-1.28 wt% H<sub>2</sub>O<sub>t</sub>. In Fig. 19 – b, it is shown that the diffusion of An<sub>50</sub>Di<sub>50</sub>-1.50 wt% H<sub>2</sub>O<sub>t</sub> is circa 0.6 log units lower than An<sub>50</sub>Di<sub>50</sub>-2.50 wt% H<sub>2</sub>O<sub>t</sub>. An increase in diffusion is shown for the glass An<sub>50</sub>Di<sub>50</sub> with 2,77 wt% of H<sub>2</sub>O<sub>t</sub>, which presents diffusion values circa 1,5 log units higher than the one containing 2,50 wt% of H<sub>2</sub>O<sub>t</sub>.

In Fig. 19-d data of all analysed compositions are plotted together for comparison. It is evident that the diffusion is faster in the Di sample, which shows values at 1.22 wt% of H<sub>2</sub>O<sub>t</sub> comparable to those of An<sub>50</sub>Di<sub>50</sub> at 2.77wt% H<sub>2</sub>O<sub>t</sub>. In general, the diffusion is faster in the depolymerised Di<sub>100</sub> than in the polymerised An<sub>100</sub> glasses. In particular, the bulk water diffusivity in the Di<sub>100</sub> sample with 1.22 wt% H<sub>2</sub>O<sub>t</sub> is 2 orders of magnitude faster than in the An<sub>100</sub> sample with circa the same total water content. This is in good agreement with the idea of Haider and Roberts (1970) that in the depolymerised silicate and aluminosilicate glasses, coupled motion of H<sup>+</sup> and OH<sup>-</sup> is the predominant mechanism for diffusion of water. This finding was also supported by the work on hydrous BaSi<sub>2</sub>O<sub>5</sub> glass of Behrens et al., 2002. In fact, single bonded oxygens, able to react with diffusing protons forming OH groups, are more abundant in depolymerised glasses. In this case, binding of a diffusing OH<sup>-</sup> to one of the associated (Al,Si)-O-(Al,Si) bonds will be facilitated by a local charge imbalance (Haider and Roberts, 1970; Behrens et al., 2002). In 1993, Helmich and Rauch demonstrated that, below 473 K, H<sub>2</sub>O<sub>m</sub> diffuses as an entity into silica glass without isotopic exchange with network oxygens. Consequently, it was inferred that a mechanism involving H<sup>+</sup> and OH<sup>-</sup> is more important for depolymerized glasses than for polymerized ones.

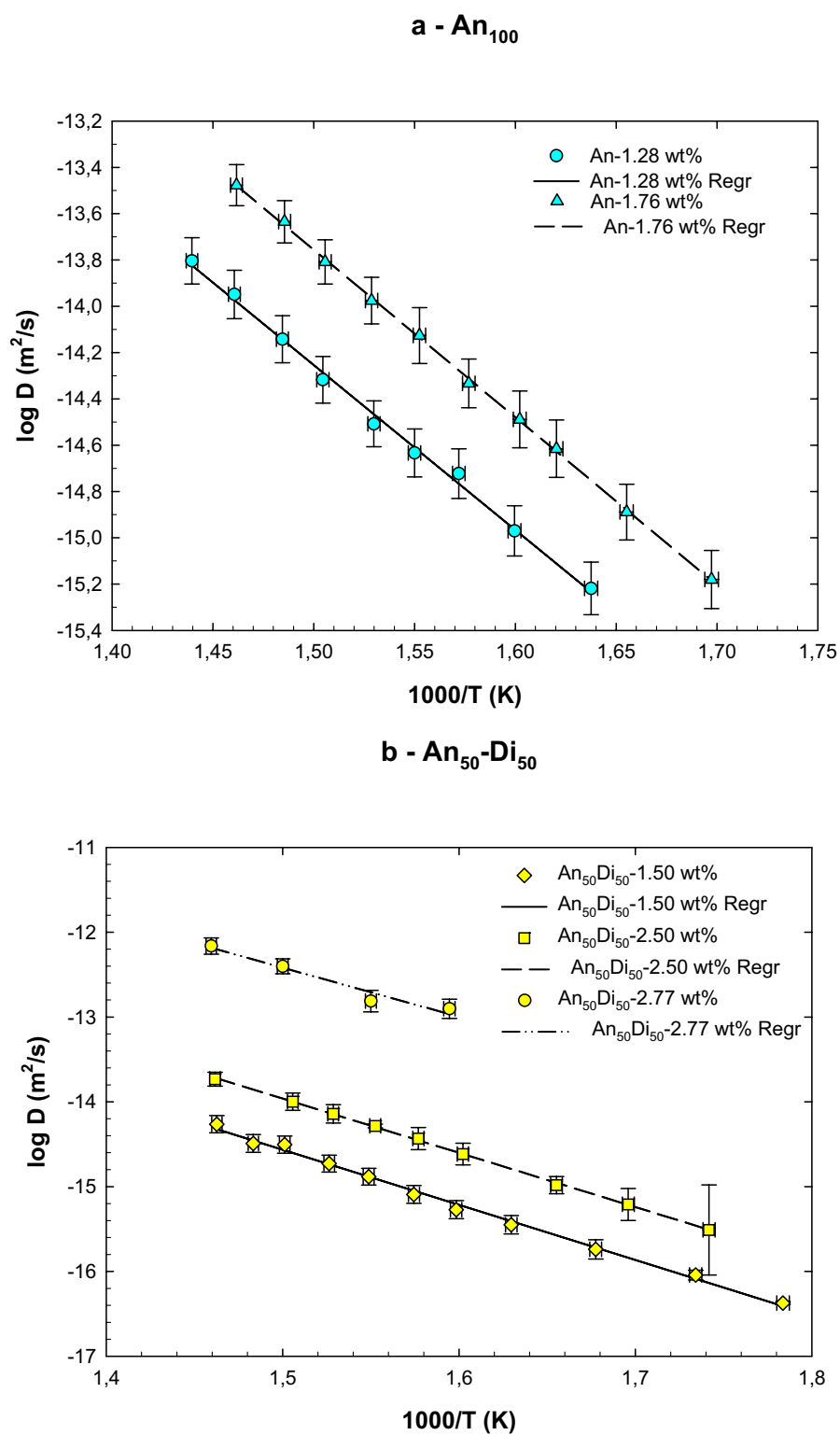
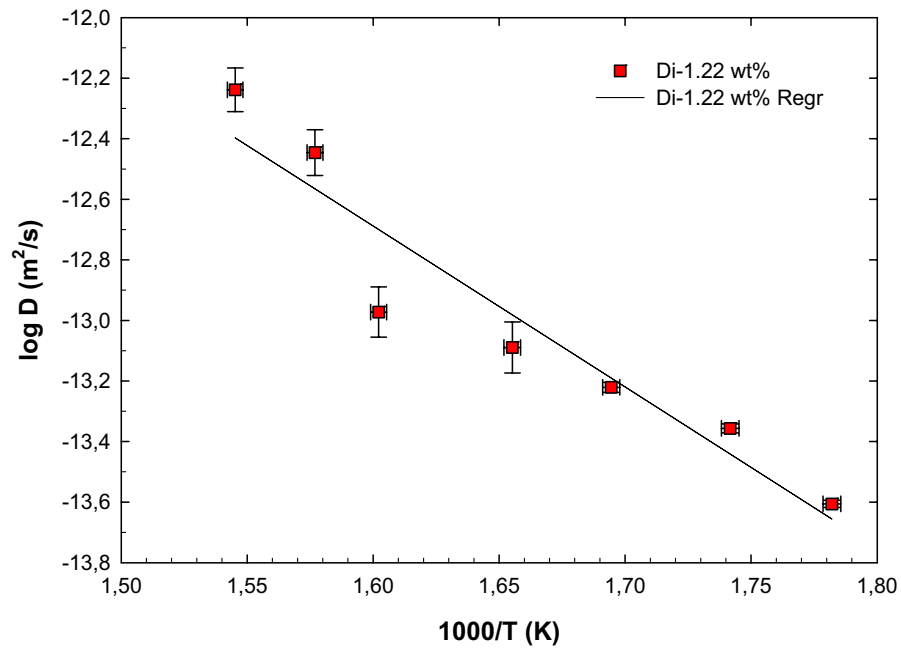


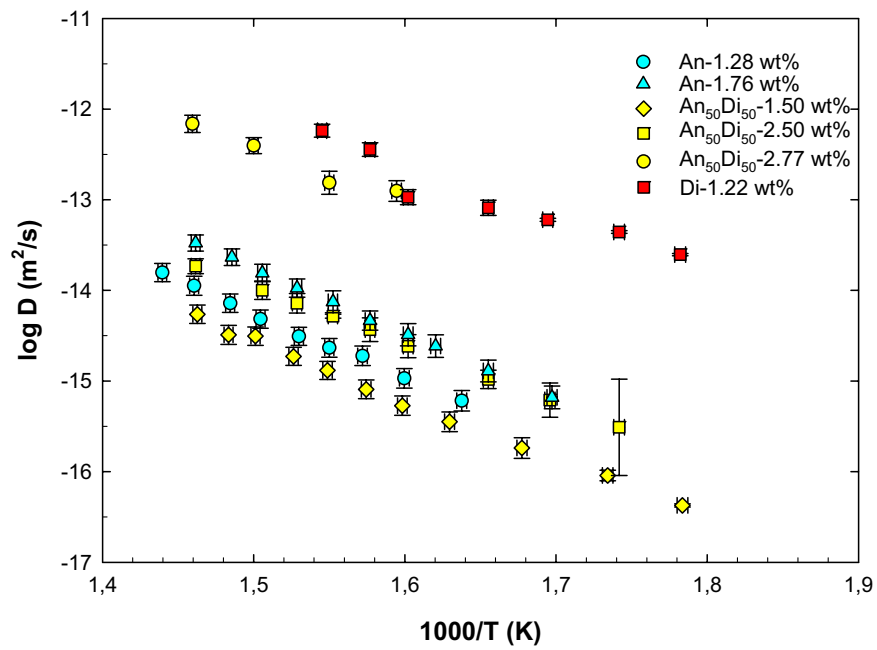
**Fig. 19 (a-d)** – Plot of  $\log D$  as a function of reciprocal temperature for:

- (a) An<sub>100</sub> glasses
- (b) An<sub>50</sub>Di<sub>50</sub> glasses
- (c) Di<sub>100</sub> glasses
- (d) comparative plot

c - Di<sub>100</sub>



d



This idea is supported by impedance measurements on silica glass containing up to 3,16 wt% dissolved water that show no measurable dc conductivity at temperatures up to 576 K (Behrens et al., 2002). Anyway, due to the availability of an improved impedance apparatus with lower detection limit, a measurable conductivity was found for the nominally totally polymerized pure Anorthite composition with 1-2wt% H<sub>2</sub>O<sub>t</sub>, in this study.

The lowest conductivity and diffusion values are reported for the composition An<sub>50</sub>Di<sub>50</sub>, which presents an intermediate polymerization degree and an intermediate Na<sup>+</sup> content. It is inferred that this may be due to a different, less dense glass structure that facilitates the Na<sup>+</sup> conductivity. This is evident in Fig. 18-b, where the Na<sup>+</sup> conductivity masks the proton conductivity in dry and 1wt% H<sub>2</sub>O glasses. However, more detailed investigations are required to prove this.

In a PhD work on silicate melts in 1990, it was suggested by Stanton that the group H<sub>3</sub>O<sup>+</sup> could contribute to the water diffusion. The H<sub>3</sub>O<sup>+</sup> molecule presents a high symmetry and has four vibration modes; some of these could be seen by IR spectroscopy. According to Christie et al. (1975) the size of hydronium is similar to K<sup>+</sup> and, hence, it could be inferred a similar diffusivity. However, most likely the proton is associated in glasses with network oxygen having higher electron density (i.e. NBO) and not to H<sub>2</sub>O. From mid-infrared spectra of the studied glasses there is no direct evidence for hydronium ions. Spectra are easily explained by OH groups and H<sub>2</sub>O molecules. No features inconsistent with these species are found.

However, to gain information about the presence of this molecule in the studied glasses and to investigate its contribution to the water diffusion further analyses with Raman investigation method should be performed.

### *1.6.3 Comparison to literature*

The proton diffusivity of the studied glasses is shown in Fig.20 in comparison to data for bulk water and molecular H<sub>2</sub>O diffusion. Proton diffusivity in Di<sub>100</sub> with 1.22 wt% H<sub>2</sub>O<sub>t</sub> and An<sub>50</sub>Di<sub>50</sub> with 2.77 wt% H<sub>2</sub>O<sub>t</sub> is about one order of magnitude faster than the diffusion data for hydrous species in sodium silicate glasses. It is noteworthy that the values of proton diffusion for BaSi<sub>2</sub>O<sub>5</sub> with 2.75 wt% of H<sub>2</sub>O<sub>t</sub> at 1 atm (Behrens et al., 2003) are comparable to the values extrapolated to temperatures around 500 K for the An<sub>50</sub>Di<sub>50</sub> with 2.77 wt% of H<sub>2</sub>O<sub>t</sub> at 1 atm. The proton diffusivity for An<sub>100</sub> and An<sub>50</sub>Di<sub>50</sub> with circa 2 wt% of bulk water content is similar to the bulk water diffusivity of NaSi<sub>4</sub>O<sub>9</sub>. The proton diffusivity for An<sub>100</sub> and An<sub>50</sub>Di<sub>50</sub> with circa 1wt% of bulk water content is similar to the H<sub>2</sub>O<sub>m</sub> diffusivity in rhyolite. Anyway, molecular H<sub>2</sub>O diffusivity in rhyolite glass could not be measured directly at high temperature, because in this range water-related species rapidly inter-convert, but was derived by modelling the concentration distance curves of total water (Zhang & Behrens, 2000). At low temperature in SiO<sub>2</sub> glass, H<sub>2</sub>O molecules migrate without reaction with the silicate network and thus its diffusivity can be directly measured (Helmich & Rauch, 1993).

In conclusion, hydrous depolymerised Di<sub>100</sub> glasses and polymerised An<sub>50</sub>Di<sub>50</sub> glasses with more than 2.50 wt% of H<sub>2</sub>O<sub>t</sub> show proton conductivity 1-2 orders of magnitude faster than the other investigated glasses, which present values of proton conductivity close to those of bulk water diffusion in polymerised glasses. To explain the higher mobility in the polymerised glasses with H<sub>2</sub>O<sub>t</sub> > 2.50 wt%, a site memory effect with the formation of conducting pathways could be postulated as suggested by Maass et al., in 1992, for alkali glasses. However, a more detailed knowledge on mechanism of proton mobility in glasses is required to prove this.

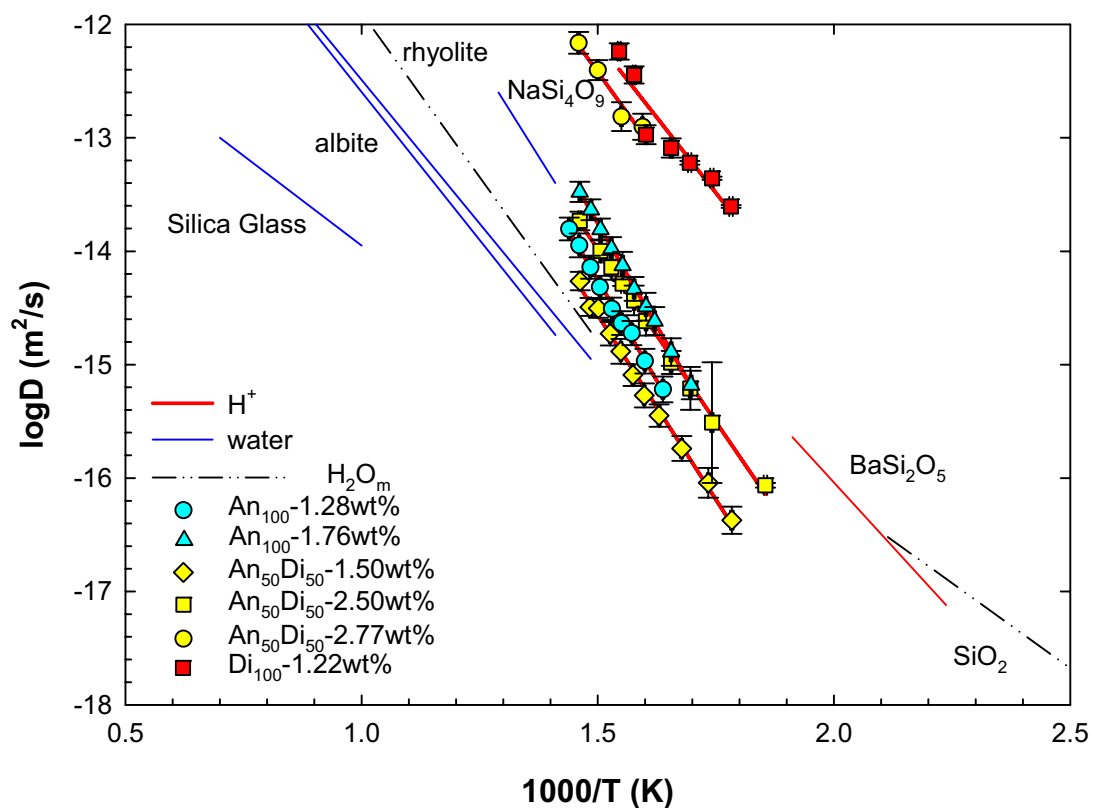


**Fig. 20: Diffusion Plot.** Comparison of diffusivities of water-related species in silicate glasses. Data for bulk water diffusion are labelled in blue, dot-dashed lines are for molecular water diffusion and proton diffusion is marked in red.

Data sources:

- rhyolite, 1 wt% water, 500 MPa (Zhang & Behrens, 2000)
- albite, 1 wt% water, 500 MPa (Behrens et al., 2000)
- $\text{SiO}_2$ , <0.5 wt% water, <2 MPa, low temperature (Helmich & Rauch, 1993)
- $\text{SiO}_2$ , low water content, high temperature (Moulson & Roberts, 1960)
- $\text{NaSi}_4\text{O}_9$ , low water content, 1 atm (Haider and Roberts, 1970)
- $\text{BaSi}_2\text{O}_5$ , 2,75wt%  $\text{H}_2\text{O}$ , 1 atm (Behrens et al., 2002)

## Chapter 2 – Diffusion of water in Phonolite and Trachyte melts

### 2.1 - Abstract

Knowledge on water diffusion behavior is especially needed for silica rich melts to model magma degassing and fragmentation during volcanic eruptions and bubble growth. The diffusion of water might be also affect processes in the magma chamber before eruption such as fluid-melt interaction and magma mingling and mixing.

As starting materials synthetic analogues of potassium-rich trachyte from the Phlegrean Fields, Italy, and potassium-rich phonolite from Laacher See, Germany, were used. The diffusion of water in phonolitic and trachytic melts was investigated at temperature of 1373 K to 1673 K and pressure between 2 and 25 kbar using the diffusion couple technique. Pairs of water poor and water rich glasses with water content ranging from nominally dry to 6 wt% of dissolved  $H_2O_t$  were heated for 108 to 1186 s. The experiments were performed in a Piston Cylinder apparatus (PCA) (University of Michigan) or in an Internally Heated Gas Pressure Vessel (IHPV) (University of Hannover). Concentration profiles of hydrous species (OH groups and  $H_2O$  molecules) and total water ( $C_{H_2O_t}$  as sum of OH and  $H_2O_m$ ) were measured along the cylindrical axis of the diffusion sample using IR microspectroscopy.

The IR spectroscopic technique was calibrated using a set of samples with bulk water contents measured by Karl-Fischer titration. The resulting molar absorptivity coefficients for the combination band of OH<sup>-</sup> at 4500  $cm^{-1}$  are  $0.94 \pm 0.05$   $Lmol^{-1}cm^{-1}$  for phonolite and  $1.05 \pm 0.04$   $Lmol^{-1}cm^{-1}$  for trachyte. For the combination band of  $H_2O$  at 5200  $cm^{-1}$  we determined absorption coefficients of  $1.18 \pm 0.03$  for phonolite and  $1.13 \pm 0.02$   $Lmol^{-1}cm^{-1}$  for trachyte.

Electron microprobe traverses show no significant change in relative proportions of anhydrous components along H<sub>2</sub>O profiles, indicating that our data can be treated as effective binary interdiffusion between H<sub>2</sub>O and the rest of the silicate melt. Bulk water diffusivity ( $D_{H_2O_t}$ ) was derived from profiles of total water using a modified Boltzmann-Matano method as well as using fittings assuming a functional relationship between  $D_{H_2O_t}$  and  $C_{H_2O_t}$ . In case of phonolite melts fitting of the profiles indicate that the water diffusivity is proportional to the total water content up to 4 wt% H<sub>2</sub>O<sub>t</sub>.

The following formulation was derived to estimate  $D_{H_2O_t}$  (m<sup>2</sup>/s) at 1 wt% H<sub>2</sub>O<sub>t</sub> in melts with phonolitic composition, as a function of T (K):

$$\log D_{H_2O_t} = -7.11 - 2.07 \log C_{H_2O_t} - \frac{(4827 - 4620 \log C_{H_2O_t})}{T}$$

The experimental data are reproduced by this relationship with a standard error of 0.07 log units. A pressure effect on water diffusivity could not be resolved for phonolitic melt in the range 2 to 25 kbar, while for trachyte composition smaller diffusivities at higher pressures were registered, indicating a negative pressure effect.

For phonolite and trachyte, water diffusivity lower than in trachyte of Freda et al. (2003) but faster than in rhyolite of Zhang et al. (2000) and Ni and Zhang (2008) was determined. In particular, the  $D_{H_2O_t}$  for phonolite at high temperature show values very close to that of the peralkaline rhyolite analysed by Behrens & Zhang (2009).

## 2.2 - Introduction

The behaviour of magmas during volcanic eruptions depends on various parameters like the melt viscosity, the solubility, and the concentrations of dissolved volatiles and their diffusivity. The diffusion of water is an important property of magmas playing a crucial role in several volcanic processes such as magma degassing during volcanic eruptions, magma fragmentation and bubble growth (Navon et al., 1998; Zhang, 1999; Liu and Zhang, 2000; Martel et al., 2000). In the first instance, exsolution of dissolved water during magma decompression provides a major driving force for subaerial explosive volcanism. Knowledge on water diffusion behaviour is especially needed for silica rich melts to model volcanic eruptions. However, processes in the magma chamber before eruption such as fluid-melt interaction and magma mingling and mixing might be also affected by water diffusion. The diffusion of water in silicate melts is some orders of magnitude faster than Si and Al diffusion but is slower than fast elements diffusion like sodium (Watson, 1994). So, for a given time scale, H<sub>2</sub>O can migrate quite deeper into a contiguous melt than other melt components. On the other hand, dissolved water reduces the melt viscosity and supports diffusion of the slow elements. In order to study bubble growth, degassing and other volcanological and magmatic processes, H<sub>2</sub>O diffusion data for melts of various compositions are required.

The diffusion of H<sub>2</sub>O in dacitic, andesitic, rhyolitic, and basaltic melts has been extensively studied and is well understood, as shown in the next paragraph.

The aim of this work is to study water diffusion in trachytic and phonolitic melts at high temperature and pressures. Furthermore, by combining our new data with previous results, we attempt to discuss the mechanism of water diffusion and to describe its dependence on temperature and pressure.

## 2.3 - Precedent studies

Understanding  $H_2O$  diffusion in silicate melts is important in two aspects:

- the first is the importance of data to understand and model volcanological and magmatic processes like bubble growth and degassing during volcanic eruptions ( e.g. Navon et al., 1998; Proussevitch and Sahagian, 1998).
- the second is that this is a diffusion problem for a multi-species component with one species more mobile than the other (Zhang et al., 1991). There were other systems in which mobile and immobile species (e.g. network-modifying cations) were inferred but could not be directly measured (e.g. silica glass in Moulson and Roberts, 1961; silica glass in Doremus, 1995; olivine-basalt glass in Cooper et al., 1996; Pyrope crystals in Wang et al., 1996). Therefore, a detailed understanding of the role of  $H_2O_m$  and  $OH$  in  $H_2O$  diffusion, where both can be measured even if not as species in the melt at least in quenched glasses, may be instructive for these other systems in which mobile and immobile species are not directly measurable.

Several studies were carried out on rhyolitic, basaltic, andesitic and dacitic melts.

The diffusion of water in natural rhyolitic melts has been well investigated in the past. Shaw in 1974 carried out the first study on water diffusion in a rhyolitic melt. There he proved that the  $H_2O$  diffusivity is high compared to that of other components and increases with the increasing amount of total water dissolved in the melt. Following investigations confirmed these conclusions (Friedman and Long, 1976; Jambon, 1979, 1983; Delaney and Karsten, 1981; Karsten et al., 1982; Lapham et al., 1984). Delaney and Karsten (1981) carried out hydration experiments and found that  $H_2O$  diffusion profiles are best modelled if the diffusivity of the  $H_2O$  component increases exponentially with total  $H_2O$  concentration. Karsten et al. (1982) showed that the activation energy for total  $H_2O$  diffusivity is low.

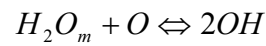
In silicate melts and glasses the total water is dissolved at least in two water species: OH groups and H<sub>2</sub>O molecules (H<sub>2</sub>O<sub>m</sub>). It is important to consider the role of speciation in diffusion because H<sub>2</sub>O<sub>m</sub> and OH possess different diffusivities. Wasserburg (1988) presented a formal analysis on treatment of the diffusion of H<sub>2</sub>O component when the H<sub>2</sub>O<sub>m</sub> is the diffusing species.

Based on dehydration experiments on rhyolitic glasses containing from 0.1 to 1.8wt% of dissolved water at 0.1 MPa and 400-550°C, Zhang et al. (1991) modelled the H<sub>2</sub>O diffusion mechanism in rhyolitic melts considering explicitly the role of water speciation in the melt:

$$\frac{\partial X}{\partial t} = \frac{\partial}{\partial x} \left\{ D_{H_2O_m} \frac{\partial X_m}{\partial x} + D_{OH} \frac{\partial X_{OH} / 2}{\partial x} \right\}$$

[53]

where  $D_{H_2O_m}$  is the diffusivity of molecular H<sub>2</sub>O,  $D_{OH}$  is the diffusivity of OH groups, and  $X$ ,  $X_m$  and  $X_{OH}$  are mole fractions of H<sub>2</sub>O<sub>t</sub>, H<sub>2</sub>O<sub>m</sub> and OH on a single oxygen basis (Stolper, 1982; Zhang, 1999). The species concentrations are related to each other by the interconversion reaction:



[54]

where O is an anhydrous oxygen. H<sub>2</sub>O<sub>t</sub>, H<sub>2</sub>O<sub>m</sub> and OH profiles are measured from diffusion experiments.  $D_{H_2O_m}$  and  $D_{OH}$  can be obtained by fitting the measured profiles to the equation above if species concentrations at the experimental temperature are preserved and if the diffusivities are assumed to be constant (this is applicable to melts only at temperature near T<sub>g</sub>). They found that the diffusion coefficient of OH groups is negligible and the molecular water is the most diffusing species. That leads to:

$$D_{H_2O_t} = D_{H_2O_m} dX_m / dX$$

[55]

where  $D_{H_2O_t}$  is the total H<sub>2</sub>O diffusivity. They have shown also that  $D_{H_2O_m}$  is constant for low total water content and the  $D_{H_2O_t}$  is proportional to the total water

concentration. The diffusion model of Zhang et al. (1991) was applied to calculate the concentration dependent on  $D_{H_2O_t}$  for rhyolitic melts at low  $H_2O_t$  as long as internal consistency is maintained (Jambon et al., 1992; Zhang, 1999).

Zhang and Behrens (2000) extended the study on water diffusion to rhyolitic melts at high pressure (8.1 Kbar) and temperature, with a large range of water concentration (from 0.08 wt% up to 7.7 wt%). They used improved experimental techniques where short-duration diffusion experiments with well controlled thermal history were realized. In most of the diffusion experiments of Nowak and Behrens (1997), the run times were probably too long, and water was lost from the hydrous half of the diffusion couple by diffusion to the surface. They found that their formulation for  $D_{H_2O_t}$  can predict  $D$  to within a factor of two at 0-800 MPa, developing a model to calculate water diffusivity in rhyolitic melts for different geological situations.

Okumura & Nakashima (2004) reported new H<sub>2</sub>O diffusion data for rhyolitic compositions using in situ measurements of dehydration experiments. The obtained diffusion coefficients showed dependences on both the temperature and the initial water content, and their values were similar to the results of previous studies.

Ni & Zhang (2008) investigated H<sub>2</sub>O diffusion in rhyolitic melt with the diffusion-couple method extending the pressure range from 0.95–1.9 GPa, at 673–1902 K and 0.2–5.2 wt% total water content. Comparing their results to previous data at 0.1–500MPa, they found that H<sub>2</sub>O diffusivity is smaller at higher pressures, indicating a negative pressure effect. A new computation model that covers a wide range of geological conditions was elaborated.

Nowak and Behrens (1997) and Behrens and Nowak (1997) investigated haplogranitic melts, compositionally similar to the natural rhyolite used by Zhang et al. (1991), and other synthetic melts at high T, from 800 to 1200°C, and 50-500MPa, with very high content of  $H_2O_t$ , up to 8.5wt%. They found that at water contents higher than 2 wt% the water diffusivity varies exponentially with total

water content. Especially when the  $H_2O_t$  is greater than 3wt%, they found that the shape of  $D_{H_2O_t}$  vs.  $H_2O_t$ , showing a roughly exponential dependence, does not follow that of Zhang et al. (1991), with a linear or less than linear dependence. Instead, at water contents below 3 wt% it was observed that water diffusivity varies linearly with total water content, as shown by Zhang et al. (1991).

Zhang and Stolper (1991) investigated  $H_2O$  diffusion in basaltic melts with 0.04-0.4 wt%  $H_2O_t$  at 1000 MPa and at 1300-1500°C. It was found that  $D_{H_2O_t}$  in basaltic melt is significantly higher, circa two orders of magnitude, than that in rhyolitic melts under similar conditions. Although the concentration of molecular water could not be measured directly, basing on the observed proportionality between the total water diffusion and total water concentration, they suggest that molecular water can also be a diffusing species.

Freda et al. (2003) studied water diffusion in trachytic melts at high pressure (1GPa) and temperatures from 1373 to 1673 K in a piston cylinder apparatus. They found that the total water diffusion increases linearly with total water concentration up to 2 wt% and that the values of water diffusion are intermediate between those of rhyolitic and basaltic melts.

Behrens et al. (2004) examined the diffusion of water in dacitic and andesitic melts at high temperatures (from 1458 to 1858 K) and pressures (between 0.5 to 1.5 GPa) using the diffusion couple technique. The diffusion profiles were derived using a modified Boltzmann-Matano method. It was found that the diffusivity of total water in dacitic melts is proportional to the total water concentration, whereas in andesitic melts the dependence of diffusion on concentration is less pronounced. By combining new and previous results they showed that the water diffusion increases monotonically with increasing melt polymerization at temperatures up to 1500 K and for certain water contents. A pressure effect on water diffusivity could not be resolved for both dacitic and andesitic melts. It was also shown that below 1000 K, depending also on water content and pressure, water diffusion may be faster in rhyolite than in dacite than in andesite melts.

Liu et al. (2004) performed dehydration experiments at 824–910 K and 0.1–145 MPa to determine the water diffusivity in dacitic melts. The obtained diffusivity of total water depended on total water contents and was smaller than water diffusivity in rhyolitic melts, whereas water diffusivity in dacitic melts was larger than that in rhyolitic melts at higher temperatures (Behrens et al., 2004). Liu et al. (2004) suggested that the mobility of water appeared to be reduced by introducing alkaline earth elements in the melts at low temperatures.

Dehydration experiments for basaltic, andesitic and dacitic glasses with 1.1, 0.7 and 1.0 wt% of total water were carried out at 673–948 K by Okumura & Nakashima (2006). The diffusivities of total water in basalt and dacite were found to be linearly dependent on total water contents, but that in andesite was weakly dependent on or independent of total water contents. It was shown that the total water diffusivity decreases from rhyolite to andesite, but the total diffusivity in basalt is higher than that in dacite and lower than that in rhyolite. Furthermore, it was inferred that the diffusivities of total water in basalt to rhyolite increase with depolymerization of silicate structures at higher temperatures.

## 2.4 - Starting Materials

As starting materials for the diffusion couple experiments we used synthetic analogues of potassium-rich phonolite and potassium-rich trachyte: for the phonolite was used a composition from Laacher See Volcano, Germany; for the trachyte we took the composition of an obsidian from the basal unit of the Breccia Museo deposit from Phlegrean Field, Italy (Ricci, 2000; Di Matteo et al., 2004). A same composition has been used in a study on trace element diffusion in trachytic and phonolitic melts (Behrens & Hahn, 2009).

Dry glasses were synthesized by fusion of oxide and carbonates at 1873 K in platinum open crucibles at ambient pressure in a conventional chamber furnace (Ohlhorst et al., 2001). In the case of the phonolitic material, after 2 hours, the melt was quenched crushed and melted again for another 2 h at the same temperature. The glass was finally rapidly quenched onto a brass plate. In the case of trachytic composition, the high viscosity of the melt did not allow to pour it out of the crucible. Furthermore, the obtained glass was characterized by high internal tension if the melt was quenched too fast. Therefore, after the same melting procedure described above, the trachytic melt was slowly cooled down directly in the platinum crucible.

The composition of glasses, displayed in Table 9, was analysed by electron microprobe, Cameca SX100, which was already described in Chapter 1, paragraph 3. The measurements were realised using 5 nA beam current, 15 kV accelerating voltage, a defocused beam with 20  $\mu\text{m}$  in diameter and 8 s counting time with the exception of Na and K for which 2 s counting time was used to avoid eventual alkali loss in particular for the wet samples.

Each listed composition is the average of at least 30 electron microprobe analyses made on 3 different fragments of dry phonolite and trachyte glass. To test the homogeneity of the glasses, the 3 fragments analysed for each compositions were cut from the two ends and the inner part of the dry glass piece. The total iron is given as FeO.

**Table 9:** Composition of starting materials (in wt %) by electron microprobe

Sample	SiO <sub>2</sub>	Al <sub>2</sub> O <sub>3</sub>	Na <sub>2</sub> O	K <sub>2</sub> O	CaO	TiO <sub>2</sub>	FeO	MgO	Total
<b>Phonolite</b>	58.89	19.87	5.96	6.87	3.90	0.76	3.61	0.69	100.55
1σ	0.42	0.19	0.44	0.25	0.15	0.02	0.35	0.04	0,65
<b>Trachyte</b>	60.53	17.83	5.22	7.28	1.72	0.48	7.14	0.21	100.45
1σ	0.39	0.24	0,24	0.19	0.14	0.04	0.43	0.04	0.79

Notes: The microprobe analyses were effectuated on 3 dry fragments of phonolite and trachyte. For each sample, ten measurements were collected. Values of standard deviations (1σ) are reported.

The ratio of non-bridging oxygen over tetrahedral cations (NBO/T) was calculated by the equation:

$$\frac{NBO}{T} = \frac{Na^{+} + K^{+} + 2Ca^{2+} + 2Mg^{2+} + 2Fe^{2+} - Al^{3+} - Fe^{3+}}{Si^{4+} + Ti^{4+} + Al^{3+} + Fe^{3+}} \quad [56]$$

modified after Mysen et al. (1985) and was found close to zero for both melts: 0.06 for phonolite and 0.11 for trachyte.

In the calculation of NBO/T the Fe<sup>3+</sup>/Fe<sub>total</sub> ratios reported in Table 14 for air melted glasses was used and it was considered Fe<sup>3+</sup> as network former and Fe<sup>2+</sup> as network modifier. In the phonolite the atomic ratio of Na/K is 1.59, while in the trachyte is 1.09.

## 2.5 - Experimental Procedures

### 2.5.1 - Hydrous glasses

For diffusion experiments several hydrous samples of both phonolite and trachyte compositions with various water contents, from 0.5 wt% to 5.5 wt% of  $H_2O_t$ , were produced. Dry glasses were crushed in an agatha mortar and sieved to obtain two fine powder fractions with grain size of 200 - 500  $\mu m$  and < 200  $\mu m$ . The two fractions were mixed in weight ratio of 1:1 to get a powder with a low pore volume. The obtained mixture was heated at 1073 K to remove organic material and subsequently loaded in gold palladium capsules (30 – 35 mm long, 4 mm in diameter, 0.2 mm wall thickness)



**Fig. 21:** Gold-palladium capsule for hydrous glass syntheses (35 mm long, 4 mm in diameter)

(Fig. 21), to avoid iron loss. To obtain large and homogeneous glass pieces, water and glass powder were added in turns in several steps and compressed with a steel piston. For syntheses of almost dry glasses, the loaded capsules were heated in an oven at 573 K for two hours to remove absorbed water and rapidly welded when capsules were still hot. All the capsules

containing water were externally cooled by water during welding. The water bearing capsules were stored in oven at 383 K for one night after welding; afterwards the weights were controlled to test for possible leakage. Syntheses were performed at 1473 K and 4 kbar for circa 20 h in an internally heated gas pressure vessel (IHPV), pressurized with Ar. Sample assemblages were always  $H_2O$  - under saturated at run conditions so that water was completely dissolved in the melt and bubble free glass pieces were obtained. The samples were quenched isobarically by automatic pumping after opening to the pressure line. To avoid high stress in the glasses, the melt was cooled down with a ramp (50 K/min. to 673 K, 10 K/min. from 673 to 573 K and finally 5 K/min. to room temperature). The synthesis products were showing at microscope analyses some oxides

crystals but were completely bubbles free. Anyway, only crystals and bubbles free samples were used for IR calibrations.

## 2.5.2. Diffusion couple experiments

### 2.5.2.1 – Piston Cylinder Apparatus



**Fig. 22:** Piston Cylinder Apparatus (PCA) at Michigan University

A set of samples for diffusion couple experiment were prepared and carried out in a piston cylinder apparatus (PCA) (Fig. 22) at University of Michigan. For both compositions, in each diffusion couple experiment, two glass cylinders of the same diameter, one containing high  $\text{H}_2\text{O}_t$  and one containing low  $\text{H}_2\text{O}_t$ , were prepared. Cylinders of 2.8 mm of diameter were drilled out from the prepared glasses and cut to a length of 3.00 mm. One of the base planes of each cylinder was polished. Then the two cylinders were placed together with the polished surfaces in direct contact. The two half cylinders were loaded together in a platinum tube, sealed on both ends with a “coning” system. It

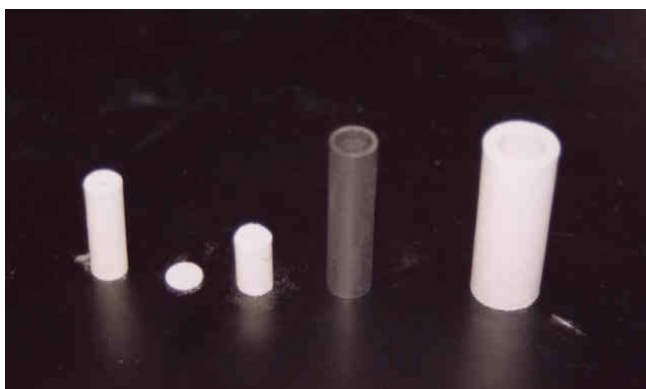


**Fig. 23:** components of the sample assemblage. From right to left, there are shown the  $\text{BaCO}_3$  tube, the graphite heater and the crushable alumina cylinder, which consists of three pieces. Dimensions are 32 mm in length for the  $\text{BaCO}_3$  tube.

consists in a rotating sphere that allows deforming the platinum tube giving to it the shape of a cone. The cone can be flattened minimizing air and free space inside. Then the sample assemblage was prepared, it measures 0.5 inches of diameter and 32 mm in length (Fig. 23). It consists of a  $\text{BaCO}_3$  tube as the outer pressure medium, a graphite

heater and crushable alumina as the inner pressure medium. The diffusion couple was placed in the centre of the heater so that the interface was at the hottest point and the water-rich half was above the water-poor half. The temperature was measured on top of the platinum capsule using a type-D thermocouple.

A “piston out” procedure was used to bring the cold assemblage to the final pressure. The assemblage was initially over pressurized by circa 0.1 kbar and allowed to relax at 473 K for at least 2 or 3 hours. Then the pressure was released to the required one, and

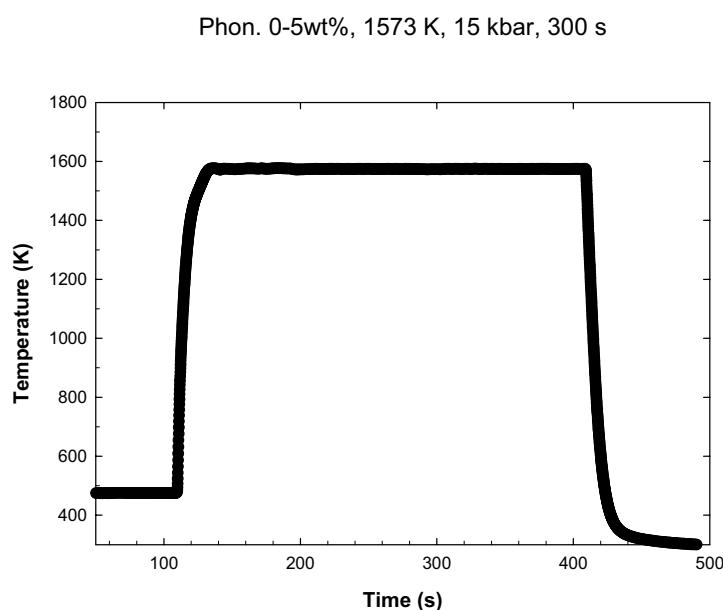
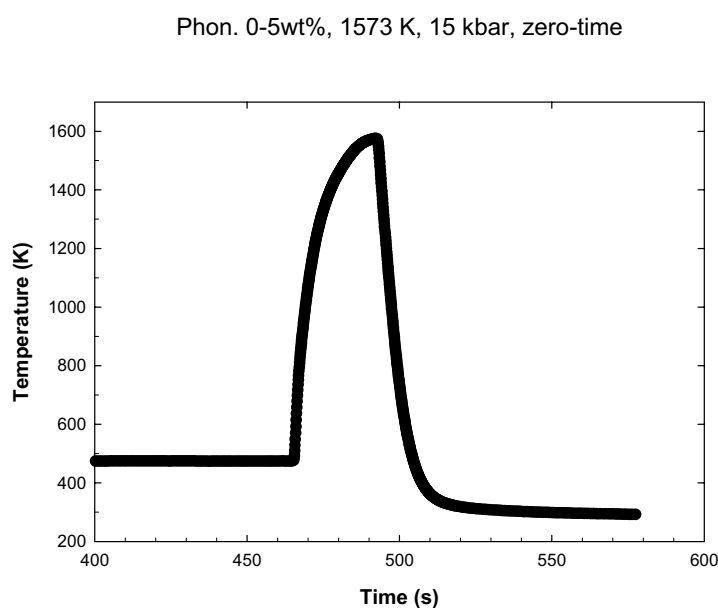


**Fig. 24:** time-temperature plot for diffusion couple experiments with nominally 0 and 300 s time duration. The effective run duration was typically 11 s longer than the dwell at high temperature.

temperature was increased at a rate of 20 K/s or faster. Overshooting and fluctuation in temperature was < 10 K. Runs at 1573 K lasted mostly 300 s, but also two 15 h runs at low temperatures and two nominally “zero-time” experiments at 1573 K were run. Cooling was initiated by turning off the heating power resulting in an initial quench rate of circa 150 K/s. During the cooling, the pressure was hold constant by manual pumping. After the run, the diffusion couple shows numerous cracks perpendicular to the cylindrical axis indicating non hydrostatic stress during cooling. A slower rate in the final stage of cooling, with a rate of 100 K/s

to 573 K and then 1 K/s to room temperature, did not prevent crack formation (Behrens et al., 2004).

To check redox changes at experimental conditions, six additional experiments were run. Dry and hydrous glass cylinders of 2.8 mm of diameter were drilled out from the prepared glasses and cut to a length of circa 5.00 mm. Sample assembly and run conditions were the same described above for the diffusion couple experiments. Run parameters were: 1573 K, 15 kbar, 300 s. At these conditions, an iron loss was expected.

Since almost all our experiments were very short in time, it was necessary to estimate the contributions to the diffusion profiles due to the heating and cooling time. Therefore the time-temperature history of each experiment was recorded by computer (examples are displayed in Fig. 24) and the effective run duration at the dwell temperature was evaluated. An average correction of 11 s has to be added to the dwell in account for heating, cooling and overshooting. The correction time was calculated taking into account the time-temperature plots of the experiments and of the zero time experiments for each composition.

Error in temperature is fundamentally determined by sample setting: the thermocouple is in contact with the basal part of the capsule, therefore the measured temperature does not correspond with the real one at the capsule's centre. To correct the temperature the distance of the thermocouple to the interface of the diffusion couple was measured, ranging typically from 3.00 to  $3.50 \pm 0.2$  mm. This value was confronted with a calibration plot displaying  $\Delta T$  (in K) versus the distance from the capsules centre (in mm). It is calculated that 35 K has to be added to the measured temperature.

The pressure uncertainty of the PCA is not exactly known, but is roughly estimated 10% of the pressure in the used range (Behrens et al., 2004).

### ***2.5.2.2 – Internal Heated Gas Pressure Vessel***

Another set of samples for diffusion couple experiments was prepared and carried out in an IHPV equipped with a rapid heat-rapid quench device (RHQ) at University of Hannover (Fig. 25). The dimension of the glass cylinders and the sample's assemblage in platinum capsules were the same described for the previous experiments, but in few cases

larger cylinder were used with a diameter of circa 4 mm. The samples were placed in platinum capsules manually enlarged to minimize air and free space, welded shut, and compressed in Ar gas at few hundred bars at room temperature in a cold-seal pressure vessel (CSPV). The compressed platinum capsules were placed in the sample holder of the IHPV, pressurized and kept in the cold part of the furnace, while the hot zone was reaching the required temperature.

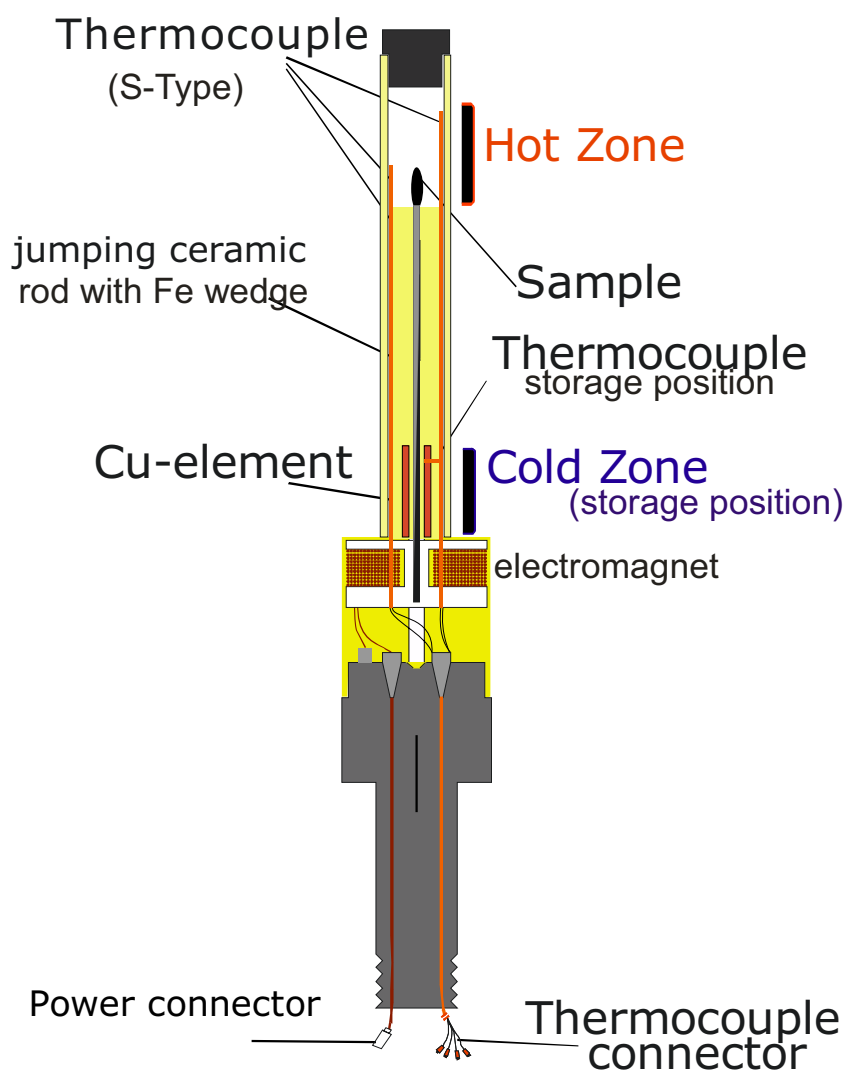


**Fig. 25:** Schematic cross section of the IHPV sample holder equipped with rapid heat-rapid quench (RHQ) device. The sample is represented in the hot zone, as during an experiment, but it can rapidly move from the cold zone to the hot zone and backwards by the application of a magnetic field produced by an electrical current.

In that case, Ar was used as the pressure medium outside the capsule. When the programmed temperature was reached in the hot zone, the sample holder was brought in the hot zone position by an applied magnetic field, as shown in Fig.25. The sample was kept in the hot zone for the experimental time and then released to the cold zone position by removing the applied magnetic field. Some technical problems were registered during the backwards jumps of the capsules in the cold part of the furnace. During

several high temperature (more than 1373 K) or long time (more than 8 min) experiments, the capsule could not be released in the bottom of the oven. That was due

to the softening of the glue used to fix the capsule on the jumping ceramic rod and to the consequent inclination of the capsule that was finally sticking to the outer ceramic tube. The temperature distribution was controlled by melting experiments of gold wires. It was found that a piece of gold wire placed in the sample holder was molten at 1373 K within 60 s. The time correction is based on a temperature relaxation time of 6 s for the inner part of the samples. Circa 20 s are required to reach the final temperature. The temperature fluctuation was  $\leq 3$  K during the dwell (private communication Jan Stelling and Markus Oelze). A Eurotherm - controller/programmer was controlling the heating programme. The temperature in the sample holder was measured over a distance of 3 cm by S-type thermocouples with an accuracy of  $\pm 10^\circ\text{C}$ . The initial cooling rate was estimated around 150 K/s. The pressure was automatically controlled within  $\pm 25$  bar during the all experiment duration, including quench. At the chosen P – T conditions the melts were undersaturated with respect to volatile, therefore the diffusion experiments were not affected by bubble formation or dehydration.

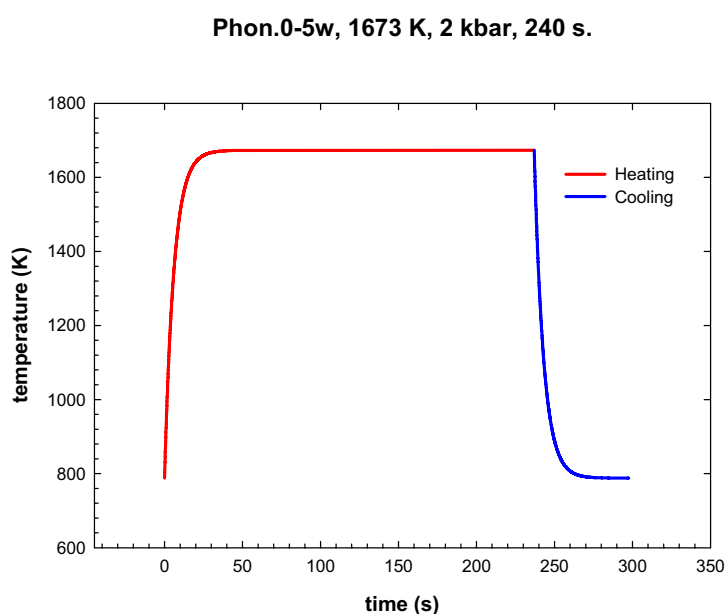


**Fig. 26:** Modeled time-temperature trend for diffusion couple experiments with nominally 240 s time duration. The effective run duration was typically 15 - 14 s shorter than the prefixed experimental time.

As for PCA experiments, it was necessary to estimate the contributions to the diffusion profiles due to the heating and cooling time. Therefore, the time-temperature history of each experiment was recorded by computer (examples are displayed in Fig. 26) and was evaluated the effective run duration by the formula:

$$t_{eff} = \int D_{T(t)} / D_{T_1} dt = \int \exp(-E_a / R \cdot (1/T(t) - 1/T_1)) dt \quad [57]$$

where  $E_a$  (kJ/mol) is the activation energy,  $R$  is the gas constant and  $T_{(t)} = T_{\text{final}} + (T_{\text{initial}} - T_{\text{final}}) \cdot \exp(-t/\tau)$  where  $T_{\text{final}}$  (K) is the temperature before the jump,  $T_{\text{initial}}$  (K) is the dwell temperature and  $\tau$  is the relaxation time (typically 6 s). It was found that the calculated effective run duration was 15 s shorter than the prefixed experimental time, for temperature around 1673 K, and 14 s shorter when the dwell temperature is around 1373 K.

## 2.6 - Analytical Procedures

### *2.6.1. Karl-Fischer Titration*

The water content of hydrous Trachyte and Phonolite glasses was measured by Karl-Fischer Titration. The homogeneity of the water distribution was checked for each glass block by analysing two pieces, from 20 to 50 mg in accord to the amount of water, from the ends and from the centre of each block. Each sample were wrapped into a platinum foil to avoid fragments loss after explosive dehydration and heated up to 1573 K. This temperature was reached with the “rapid heat” mode in 4-6 min by stepwise, increasing the power of the HF-generator used for heating the Pt sample holder. The analytical procedure is described by Behrens et al. (1996), results are given in Table 11. Differences in water content were typically below 5 % relative. Just for one block (phon.1-2w) a larger difference of 14 % relative was measured over the 30 mm length. However, this corresponds only to a 0.24 wt% in a sample with an average of 2.42 wt% of water.

### *2.6.2 Colorimetric determination of ferrous iron*

To control the redox state of the melts, the different iron species were determined using a colorimetric method described by Schlüssler et al., 2008 (Table 14). The air-molten trachyte and phonolite and the hydrous glasses synthesised by IHPV were analysed. Furthermore, the series of 6 additional experiments run in the PCA, as already described in paragraph 2.5.2.1, were analysed. For each sample an amount ranging from 4 mg to 10 mg was used. Glass samples were decomposed in an HF-H<sub>2</sub>SO<sub>4</sub> solution in the presence of excess pentavalent vanadium. It oxidizes ferrous iron released from the sample. After complete sample dissolution ferrous iron is regenerated from tetravalent vanadium by increasing the pH value to  $\approx 5$ . The regenerated Fe<sup>2+</sup> forms a very stable complex with 2:2'bipyridyl in the solution, which shows an intensive absorption band in the visible spectrum.

### 2.6.3 Infrared analyses

After quenching, each capsule was sectioned along the cylindrical axis, perpendicular to

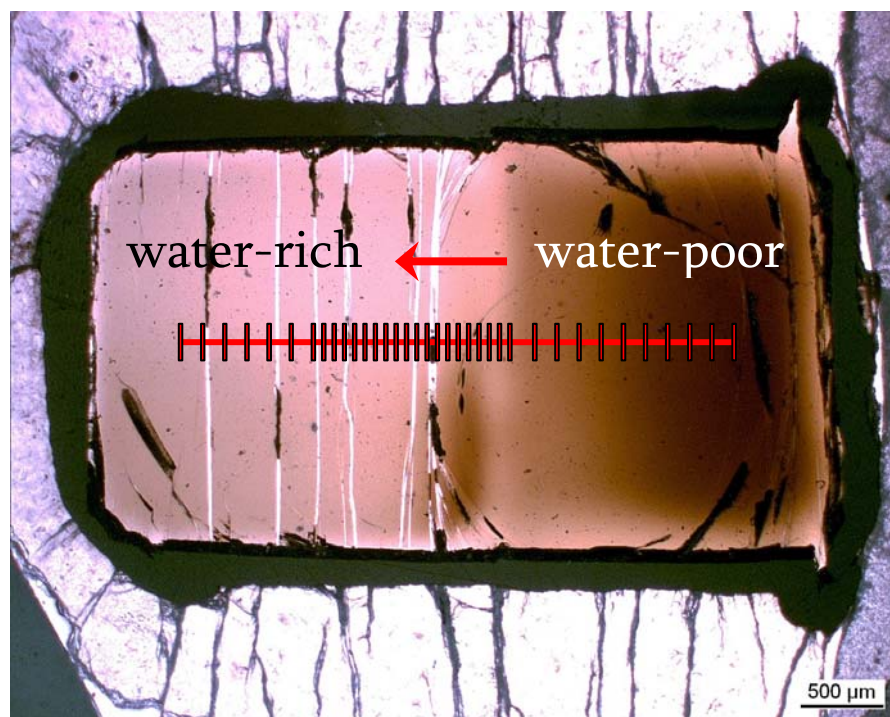


**Fig.26:** micro-photograph of the sample Phon.2-5wt%; 1573 K; 15 kbar; 300s. The water rich part shows darker color than the water poor one. In red are marked the points of the NIR course where data were collected.

the polished sample's surface. One or two slices per capsule were cut, fixed on a glass plate, and polished on both sides to a thickness of 200  $\mu\text{m}$  for near infrared analyses (NIR) and 80  $\mu\text{m}$  for mid infrared analyses (MIR).

Sections were optically tested with a microscope after

the run. Some of them showed no significant deformation: the surface transition between the two halves was planar and parallel to the original one, suggesting that any significant convection was present in melt during the experiments (i.e. P4, P9, P10, T1 and T9, see Appendix B for pictures). In other samples, as shown in Fig. 26, some deformations at the interface of the two cylinders were showing a deviation from the one-dimensional conditions (see also P2, P3, P6, P9, T3 and T5 in Appendix B). In most cases it was possible to measure the diffusion profiles of these samples but often the fitting was not successful. Typically, both halves of the samples were brown in colour, more intensely coloured as the amount of water decreases. Micro-photographs are shown in the Appendix B.

IR spectra were collected with an IR microscope Bruker IR scope II connected to an FTIR spectrometer Bruker IFS88 to determine the water concentration-distance profiles. Operation conditions were: light source, W lamp for NIR and globar light for MIR;

beamsplitter, CaF<sub>2</sub> for NIR and KBr for MIR. To limit the volume of sample analyzed, a rectangular focus area of 30 μm wide and 100 μm long was chosen. Spectra were collected in 100 μm steps in the regions far from the transition surface, and in 50 μm to 30 μm as we get more close to transition plane (Fig.26). Typically 100 scans were accumulated for each spectrum, with a spectral resolution of 4 cm<sup>-1</sup> for NIR and 2 cm<sup>-1</sup> for MIR.

To determine the concentrations of water species, the IR calibration for both phonolite and trachyte was done. The linear molar extinction coefficients for each composition was defined using for each composition up to 6 rapid quenched glasses, purpose-made produced according to the previous description, with the same anhydrous composition and water contents ranging from 0.5 to 6 wt%.

## 2.7 - Results

### 2.7.1 IR spectroscopy

#### 2.7.1.1 Band assignment and peak positions

In Fig. 27 a-b and 28 a-b typical middle and near-infrared spectra of phonolitic and trachytic glasses are shown. In the MIR range, a pronounced, asymmetric absorption peak is visible around  $3520\text{ cm}^{-1}$  for hydrous samples. It is attributed to OH stretching vibrations of weakly H-bonded hydrous species (Scholze, 1959), as already discussed in paragraph 1.5.1. This peak is visible also in the spectra of dry glasses and was used to estimate the bulk water content. At least two water-related bands at circa  $4500$  and  $5200\text{ cm}^{-1}$  are visible in the NIR range from  $4000$  to  $6000\text{ cm}^{-1}$ .

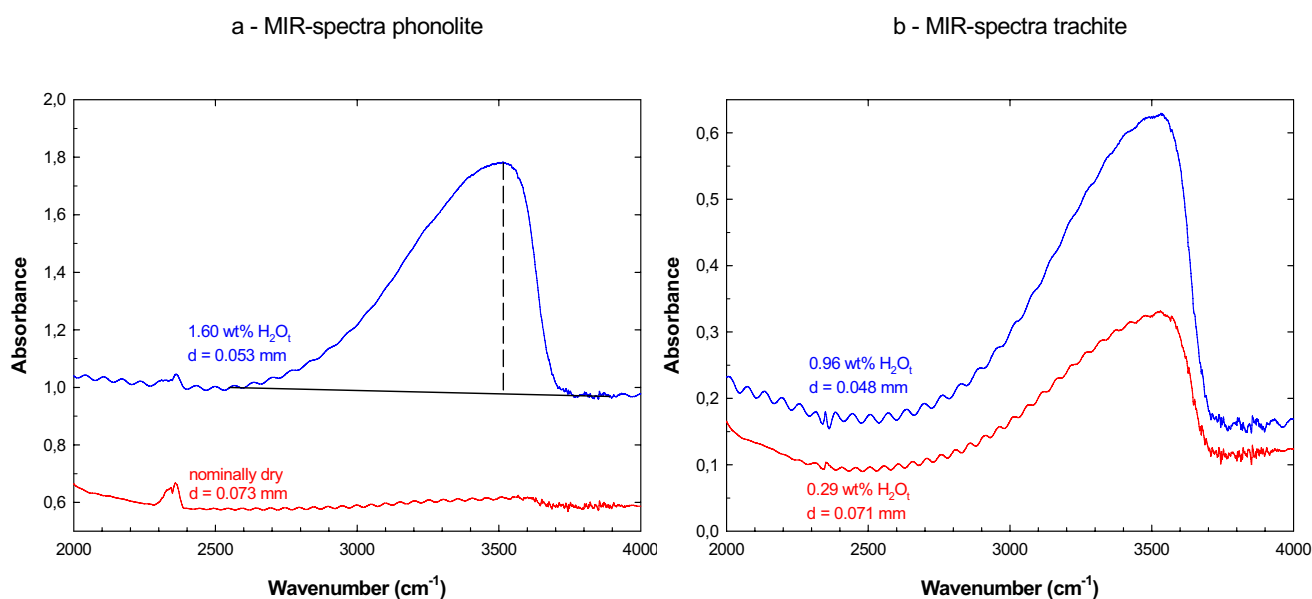


**Fig. 27 (a-b)** Mid infrared spectra of phonolite and trachyte glasses with different amount of bulk water content. Thickness and water contents are displayed in the plots. The TT type baseline is shown for the phonolite hydrous spectra. In the phonolite plot, the spectrum of hydrous glass is shown for comparison with the spectrum of a nominally dry glass. The main peak at circa  $3520\text{ cm}^{-1}$  is due to OH stretching vibrations of weakly H-bonded species. Small features at  $2350\text{ cm}^{-1}$  are due to atmospheric  $\text{CO}_2$ .

The peak at around  $4500\text{ cm}^{-1}$  is due to the combination of stretching and bending of OH groups bonded to tetrahedral cations, the absorption band at  $5200\text{ cm}^{-1}$  is produced by a combination of stretching + bending modes of  $\text{H}_2\text{O}$  molecules (Stolper, 1982).

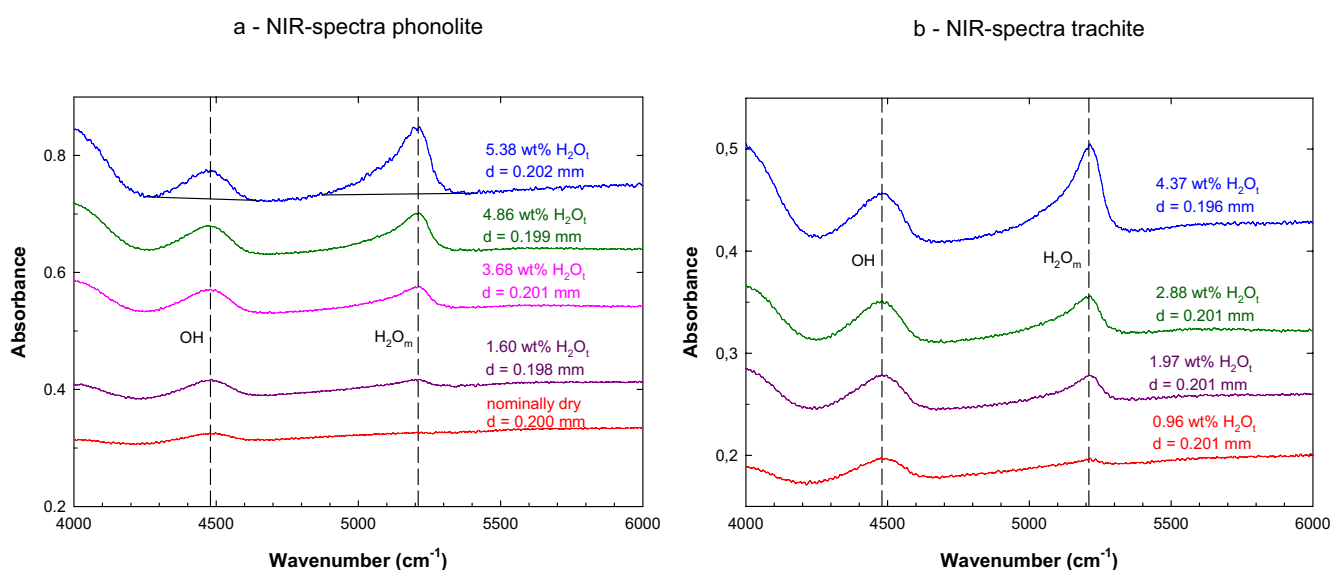


**Fig. 28 (a-b)** Near infrared spectra of phonolite and trachyte glasses with different amount of bulk water content. Spectra are plotted with an offset for clarity. Thickness and water contents are displayed in the plots. The TT type baseline is shown for phonolite hydrous spectra with 5.38 wt%  $\text{H}_2\text{O}_1$ . In the phonolite plot, the spectrum of a nominally dry glass is shown for comparison. Band assignments are: -  $4500\text{ cm}^{-1}$  combination mode of OH groups; -  $5220\text{ cm}^{-1}$  combination mode of  $\text{H}_2\text{O}$  molecules.

### 2.7.1.2 Procedure for baseline correction of the combination bands

To determine the total water content and the water speciation from peak heights or peak areas, an appropriate baseline under the  $4500$  and  $5200\text{ cm}^{-1}$  band must be defined. In precedent works several types of baselines were tested (Withers & Behrens, 1999; Ohlhorst et al., 2001). In this work we choose the so called “Two tangents (TT)” correction consisting in fitting the base of the  $4500$  and  $5200\text{ cm}^{-1}$  band with a simple straight line. In systems with low iron content, the straight lines are unambiguously defined as tangents through the minima on both sides of each band. The iron content of the studied samples is not low, however the total amount of ferrous iron is often low and, thus, the intensity of the band at  $5600\text{--}6000\text{ cm}^{-1}$ . On one hand the TT baseline is a rough approximation and may have a systematic error due to the underestimation of area and peak height of the OH band. On the other hand this fitting has a high reproducibility.

### 2.7.1.3 Determination of molar absorption coefficients

All the samples used for IR calibration were crystal and bubble-free glasses. The syntheses conditions, the water content determined by KFT, the thickness and the density of each sample and the absorbances at  $\approx 3520$ ,  $\approx 4500$  and  $\approx 5200$   $\text{cm}^{-1}$  are summarized in Table 10 and 11.

**Table 10** - MIR spectroscopic data

Sample	$C_{\text{H}_2\text{O}_t}$ (wt%)	Thickness (mm)	Density (g/l)	A 3520	$\epsilon_{3520}$ ( $\text{l}\cdot\text{mol}^{-1}\text{cm}^{-1}$ )
Phonolite	$1.26 \pm 0.03$	0.055	2498	$0.38 \pm 0.01$	$40.0 \pm 2.5$
	$1.6 \pm 0.02$	0.053	2494	$0.38 \pm 0.01$	$32.6 \pm 1.8$
Trachyte	$0.96 \pm 0.02$	0.048	2434	$0.47 \pm 0.01$	$75.1 \pm 5.6$
	$1.97 \pm 0.03$	0.053	2410	$0.98 \pm 0.01$	$70.3 \pm 3.6$

**Notes:** total water ( $C_{\text{H}_2\text{O}_t}$ ) for hydrous glasses was determined by pyrolysis and subsequent Karl-Fischer titration. The absorbance was calculated using a straight line baseline (TT). The error in thickness is 0.002 mm. Densities were calculated using the equations  $\rho = 2512 - 11.4 C_{\text{H}_2\text{O}_t}$  for phonolite and  $\rho = 2457 - 24.0 C_{\text{H}_2\text{O}_t}$  for trachyte derived from data of Behrens & Hahn, 2009; the error in density was estimated around 1 - 2%.

As already illustrated in Chapter 1, the Lambert-Beer law is the basis for a quantitative relationship between water concentration and the height of the absorption peak:

$$C_{\text{H}_2\text{O}_t} = \frac{1802 A_{3520}}{d \rho \epsilon_{3520}} \quad [49]$$

where A is the peak height, 18.02 is the molecular weight of water, d is the thickness of the sample in cm, measured by a Mitutoyo digital instrument,  $\rho$  is the density in g/l,  $\epsilon$  is the linear molar absorption coefficient in  $\text{l mol}^{-1} \text{cm}^{-1}$  and  $C_{\text{H}_2\text{O}_t}$  is the concentration of total water in wt%.

Using the density determined by Behrens & Hahn, 2009:

$$\rho = 2512 - 11.4 C_{\text{water}} \text{ (phonolite)} \quad [50]$$

$$\rho = 2457 - 24.0 C_{\text{water}} \text{ (trachyte)} \quad [51]$$

Table 11 - NIR spectroscopic data

Sample	C <sub>H<sub>2</sub>O<sub>t</sub></sub> (wt%)	Thickness (mm)	Density (g/l)	A 5200	A 4500
Phonolite	1.60 ± 0.02	0.198	2494	0.014 ± 0.002	0.028 ± 0.002
	2.65 ± 0.06	0.199	2482	0.038 ± 0.002	0.038 ± 0.002
	3.68 ± 0.06	0.201	2470	0.065 ± 0.003	0.044 ± 0.003
	4.86 ± 0.06	0.199	2457	0.097 ± 0.003	0.047 ± 0.003
	5.38 ± 0.07	0.202	2451	0.115 ± 0.004	0.048 ± 0.004
Trachyte	0.96 ± 0.02	0.201	2399	0.006 ± 0.002	0.021 ± 0.002
	1.97 ± 0.02	0.201	2382	0.025 ± 0.002	0.032 ± 0.002
	2.88 ± 0.05	0.201	2367	0.047 ± 0.002	0.038 ± 0.002
	4.37 ± 0.02	0.196	2342	0.076 ± 0.003	0.045 ± 0.003
	4.59 ± 0.02	0.200	2338	0.085 ± 0.003	0.044 ± 0.003

**Notes:** total water (C<sub>H<sub>2</sub>O<sub>t</sub></sub>) was determined by pyrolysis and subsequent Karl-Fisher titration. The absorbance was calculated using a straight line baseline (TT). The standard error in thickness is 0.002 mm. Densities were calculated using the equations  $\rho = 2512 - 11.4 C_{\text{water}}$  for phonolite and  $\rho = 2457 - 24.0 C_{\text{water}}$  for trachyte derived from data of Behrens & Hahn, (2009); the error in density was estimated around 1 - 2%.

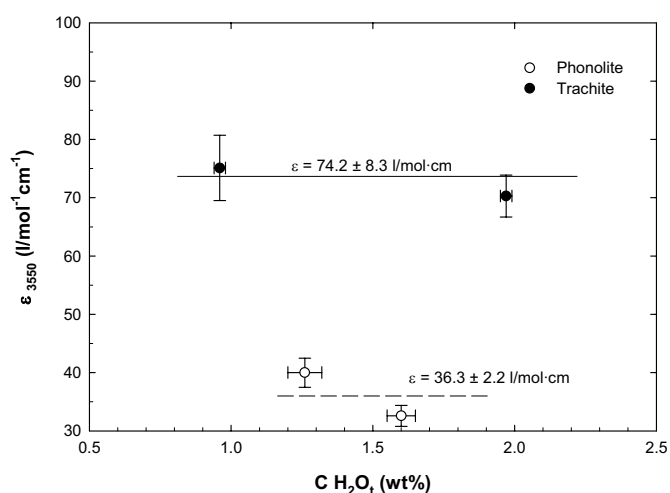


**Fig.29:** Relationship between the molar absorption coefficient  $\epsilon$  for the fundamental OH stretch band at  $3520 \text{ cm}^{-1}$  and the bulk water content for phonolitic and trachytic glasses. The solid line refers to the average  $\epsilon_{3520}$  for the trachyte and the dash line to the average for phonolite. Error bars take into account the individual error based on error propagation.

and bulk water contents measured by KFT,  $\epsilon_{3520}$  values were calculated for samples with different water contents. The average of  $36.3 \pm 2.2$  for phonolite and  $74.2 \pm 8.3 \text{ l/mol}\cdot\text{cm}$  for trachyte were determined (Table 10, Fig. 29). The values obtained for phonolitic melt are significantly lower than other  $\epsilon_{3500}$  values measured for aluminosilicate glasses showing similar band features. The absorption coefficients

determined by Behrens & Hahn (2009) are  $67.9 \pm 4.1 \text{ L}\cdot\text{mol}^{-1}\cdot\text{cm}^{-1}$  for phonolite and

$66.9 \pm 5.8 \text{ L}\cdot\text{mol}^{-1} \text{ cm}^{-1}$  for trachyte. The  $\epsilon_{3520}$  value obtained in this study for trachyte is comparable with those reported from Behrens and Hahn (2009). The  $\epsilon_{3520}$  values measured in this study for phonolite is too low; this is probably due to dishomogeneity in the synthesized samples and/or to partial crystallization.

The concentrations of  $\text{H}_2\text{O}_m$  and OH were determined from the heights of the absorption bands at  $5230 \text{ cm}^{-1}$  and at  $4500 \text{ cm}^{-1}$ , respectively, using the Lambert-Beer law:

$$C_{\text{H}_2\text{O}_m} = \frac{1802 A_{\text{H}_2\text{O}_m}}{d\rho} \frac{1}{\epsilon_{\text{H}_2\text{O}_m}} \quad [58]$$

$$C_{\text{OH}} = \frac{1802 A_{\text{OH}}}{d\rho} \frac{1}{\epsilon_{\text{OH}}} \quad [59]$$

where  $C_{\text{H}_2\text{O}_m}$  and  $C_{\text{OH}}$  are respectively the concentrations of water dissolved as molecular water and OH groups in wt%. When water species are only OH and  $\text{H}_2\text{O}_m$  the concentration of total water  $C_{\text{H}_2\text{O}_t}$  is given by:

$$C_{\text{H}_2\text{O}_t} = C_{\text{H}_2\text{O}_m} + C_{\text{OH}} \quad [60]$$

Rearranging these equations, gives:

$$\left( \frac{1802 A_{\text{H}_2\text{O}_m}}{d\rho C_{\text{H}_2\text{O}_t}} \right) = \epsilon_{\text{H}_2\text{O}_m} - \frac{\epsilon_{\text{H}_2\text{O}_m}}{\epsilon_{\text{OH}}} \left( \frac{1802 A_{\text{OH}}}{d\rho C_{\text{H}_2\text{O}_t}} \right) \quad [61]$$

If the normalized absorbances are plotted one against the other a straight line is obtained, providing the absorption coefficients are independent on total water and quench rate. The molar absorption coefficients are determined directly from the intercepts of the obtained lines with both axes. The calculated data were fitted with linear regression considering the individual errors in the determination of each parameter. It is evident in Fig. 30 that the uncertainty of the normalized absorption is increasing with decreasing of water content. This is a direct consequence of the lower precision in measuring the peak heights and of the increasing of the relative error of KFT. The resulting molar absorptivity coefficients for the combination band of  $\text{OH}^-$  at  $4500 \text{ cm}^{-1}$  are  $0.94 \pm 0.05 \text{ Lmol}^{-1}\text{cm}^{-1}$  for phonolite and  $1.05 \pm 0.04 \text{ Lmol}^{-1}\text{cm}^{-1}$  for

trachyte. For the combination band of  $\text{H}_2\text{O}_m$  at  $5200\text{ cm}^{-1}$  we determined absorption coefficients of  $1.18 \pm 0.03$  for phonolite and  $1.13 \pm 0.02\text{ Lmol}^{-1}\text{cm}^{-1}$  for trachyte.

The  $\epsilon$  values obtained in this study from linear regression are listed in Table 12 and displayed in Fig.30 in comparison with other values from previous studies.

**Table 12** - Molar absorption coefficients for OH and  $\text{H}_2\text{O}$  combination bands for hydrous silicate glasses.

Composition	Range (wt% $\text{H}_2\text{O}$ )	$\epsilon_{\text{OH}}$ ( $\text{l mol}^{-1}\text{ cm}^{-1}$ )	$\epsilon_{\text{H}_2\text{O}}$ ( $\text{l mol}^{-1}\text{ cm}^{-1}$ )	Source of data
Rhyolite	1.0-6.2	$1.41 \pm 0.07$	$1.66 \pm 0.05$	Withers & Behrens (1999)
Trachyte	0.9-4.5	$1.05 \pm 0.04$	$1.13 \pm 0.02$	this study
Phonolite	1.5-5.3	$0.94 \pm 0.05$	$1.18 \pm 0.03$	this study
Phonolite	1.3-6.3	$1.1 \pm 0.12$	$1.25 \pm 0.33$	Carroll et al. (1997)
Dacite	1.5-5.9	$0.97 \pm 0.04$	$1.11 \pm 0.05$	Ohlhorst et al. (2001)
Andesite	1.9-6.3	$0.68 \pm 0.05$	$0.86 \pm 0.05$	Ohlhorst et al. (2001)
Basalt	1.6-6.3	$0.56 \pm 0.05$	$0.56 \pm 0.05$	Ohlhorst et al. (2001)

**Notes:** Baseline: TT (except for phonolite from Carroll et al. where the baseline is GG type).

The molar absorption coefficients determined in this study cannot be directly compared with those reported by Carroll et al. (1997) for phonolite composition because of differences in baseline determination and in chemical composition. However, slightly higher  $\epsilon$  values are expected for the flexicurve applied by Carroll et al. (1997) compared to the TT baselines (Withers and Behrens, 1999). Therefore, the two calibrations are in good agreement. It is evident from Fig.30 that the  $\epsilon$  values systematically increase from basaltic over andesitic to dacitic to trachytic and phonolitic and finally rhyolitic compositions.

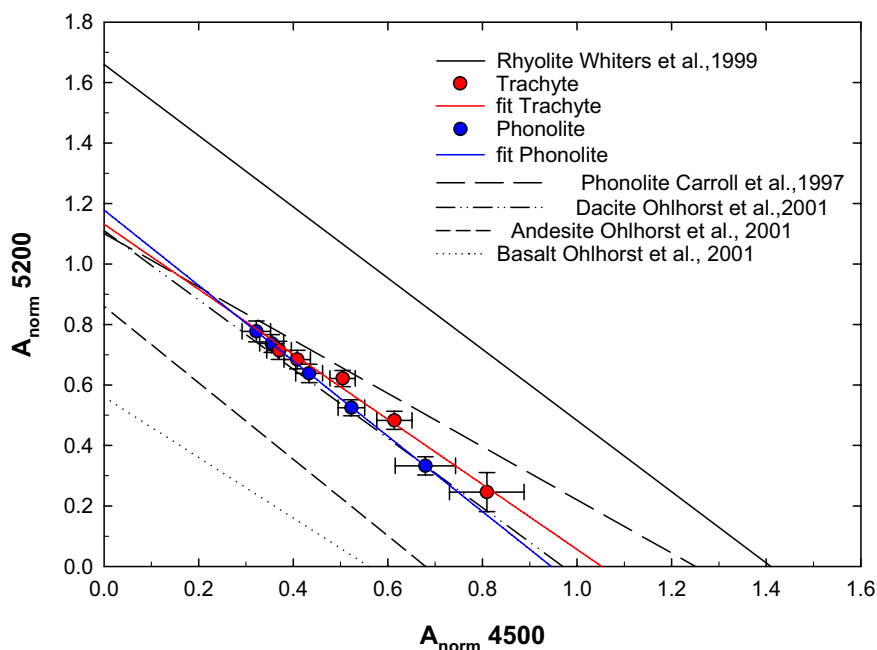


**Fig. 30:** Plot for determination of molar absorption coefficients for the OH combination band at  $4500\text{ cm}^{-1}$  and H<sub>2</sub>O combination band at  $5200\text{ cm}^{-1}$ . Lines were obtained by the linear regression of the data in plot. Intercepts of the lines with the axes define the molar absorption coefficients for OH (x-axes) and H<sub>2</sub>O (y-axes). For comparison data for dacite, andesite and basalt from Ohlhorst et al., 2001, data for rhyolite from Whiters et al, 1999, and data for phonolite from Carroll et al., 1997 are shown.

### 2.7.2 Evaluation of diffusion profiles

All successful diffusion experiments are summarized in Table 14. Four other runs with phonolitic and trachytic compositions at 773 and 873 K and 2 kbar with duration ranging from 48 to 15 h failed because of partial crystallization as shown in Fig.31.

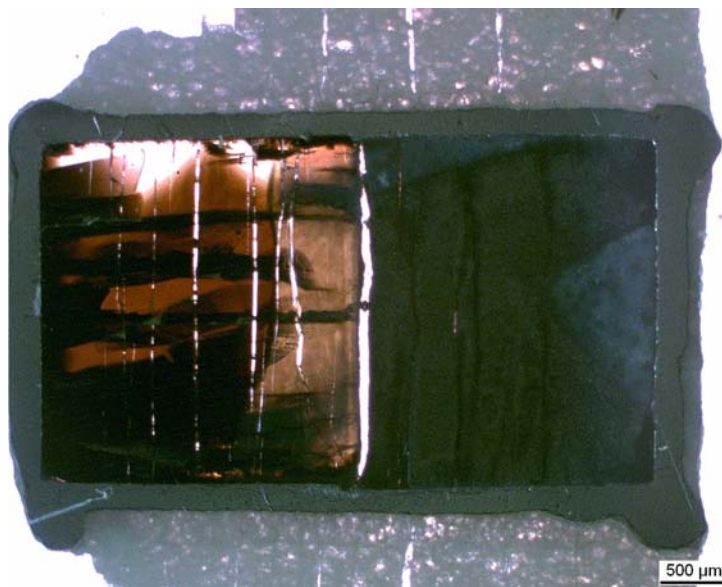


**Fig.31:** Microscope photo of cross section of the sample Phon.0-5wt%; 773K; 15 kbar; 15h. The dry part (right) is crystallised (micro-photo of crystals are shown in Fig.32) and the wet part (left) shows presences of oxides.

Table 13-a. Results of water diffusion experiments for phonolite.

Sample	Composition	C <sub>H<sub>2</sub>O</sub> in. KFT (wt%)	Pressure (bar)	T <sub>meas.</sub> (K)	T <sub>corr.</sub> (K)	Dwell (s)	Eff. Time (s)	Cooling	C <sub>H<sub>2</sub>O</sub> -fin. NIR (wt%)	D <sub>water</sub> at 1 wt% H <sub>2</sub> O (μm <sup>2</sup> /s)	D <sub>water</sub> at 3.5 wt% H <sub>2</sub> O (μm <sup>2</sup> /s)	D <sub>water</sub> at 1 wt% H <sub>2</sub> O (μm <sup>2</sup> /s)
phonolite												
PHDC6	phon. 0-5w	0.22/4.95	3000	1677	1677	240	228	RHQ	0.10/5.00	86.4 ± 17.3	293.2 ± 58.6	77.5 ± 4.1
P8	phon. 0-5w	0.22/4.95	2000	1673	1673	240	225	RQ	0.18/4.50	91.5 ± 18.3	n.d.	85.0 ± 3.0
PHDC5	phon. 0-5w	0.22/5.43	3000	1673	1673	120	108	RHQ	0.20/6.20	182.4 ± 36.5	474.1 ± 94.8	n.d.
P1*	phon. 0-5w	0.57/4.95	25000	1573	1598	300	311	RQ	0.41/3.64	69.1 ± 13.8	n.d.	71.2 ± 4.5
P4*	phon. 2-5w	2.42/5.43	25000	1573	1598	300	311	RQ	2.14/5.63	n.d.	184.2 ± 36.8	57.0 ± 1.8
P5*	phon. 2-5w	2.42/5.43	15000	1573	1598	300	311	RQ	2.46/6.05	54.6 ± 10.9	93.0 ± 18.6	n.d.
P2*	phon. 0-5w	0.57/4.95	15000	1573	1598	300	311	RQ	0.49/5.36	73.9 ± 14.8	n.d.	63.8 ± 1.9
P3*	phon. 0-5w	0.57/4.95	5000	1573	1598	300	311	RQ	0.80/4.70	75.9 ± 15.2	n.d.	53.5 ± 1.5
PHDC2	phon. 0-5w	0.22/5.43	3000	1573	1573	240	224	RHQ	0.30/5.70	70.2 ± 14.0	146.6 ± 29.3	n.d.
PHDC3	phon. 0-5w	0.22/5.43	3000	1573	1573	120	108	RHQ	0.25/5.60	43.7 ± 8.7	183.6 ± 36.7	n.d.
PHDC4	phon. 0-5w	0.22/4.95	3000	1573	1573	480	468	RHQ	0.18/4.10	68.2 ± 13.6	371.0 ± 74.2	71.8 ± 4.2
P6	phon. 0-5w	0.22/4.95	2000	1473	1473	900	886	RQ	0.09/4.14	42.1 ± 8.4	n.d.	43.5 ± 0.7
P10	phon. 2-5w	2.42/4.95	2000	1473	1473	900	886	RQ	2.49/4.46	n.d.	179.3 ± 35.9	58.8 ± 2.4
PHDC1	phon. 0-5w	0.22/5.43	3000	1473	1473	300	323	NQ	0.14/5.80	n.d.	241.6 ± 48.3	n.d.
P9	phon. 2-5w	2.42/5.43	2000	1373	1373	1200	1186	RQ	2.02/5.32	n.d.	212.8 ± 42.6	n.d.
P7	phon. 0-5w	0.22/5.43	2000	1373	1373	900	886	RQ	0.09/4.98	19.0 ± 3.8	n.d.	20.3 ± 0.8

Mod. Boltzmann-Matano method

Num. fitting

**Table 13-b.** Results of water diffusion experiments for trachyte.

Sample	Composition	C <sub>H<sub>2</sub>O</sub> <sub>T</sub> in. KFT (wt%)	Pressure (bar)	T <sub>meas.</sub> (K)	T <sub>corr.</sub> (K)	Dwell (s)	Eff. Time (s)	Cooling	C <sub>H<sub>2</sub>O</sub> -fin. NIR (wt%)	D <sub>water</sub> at 1 wt% H <sub>2</sub> O ( $\mu\text{m}^2/\text{s}$ )	D <sub>water</sub> at 3.5 wt% H <sub>2</sub> O ( $\mu\text{m}^2/\text{s}$ )	D <sub>water</sub> at 1 wt% H <sub>2</sub> O ( $\mu\text{m}^2/\text{s}$ )
<b>trachyte</b>												
<b>T5</b>	trach. 1-6w	1.29/6.50	3000	1673	1673	240	226	RHQ	1.52/6.64	n.d.	208.0 ± 41.6	n.d.
<b>T1*</b>	trach. 0-5w	0.29/5.34	25000	1573	1598	300	311	RQ	0.54/5.41	39.2 ± 7.8	n.d.	n.d.
<b>T4*</b>	trach. 2-5w	2.64/5.34	25000	1573	1598	300	311	RQ	2.65/5.43	n.d.	95.5 ± 19.1	n.d.
<b>T3</b>	trach. 1-6w	1.29/6.50	3000	1573	1573	240	225	RHQ	1.48/6.51	n.d.	154.8 ± 31.0	n.d.
<b>T2</b>	trach. 2-5w	2.64/5.34	2000	1473	1473	900	886	RHQ	2.72/5.34	n.d.	304.5 ± 60.9	n.d.
<b>T8</b>	Trach. 1-6w	1.29/6.50	2000	1473	1473	480	466	RHQ	1.47/7.48	n.d.	158.5 ± 31.6	n.d.
<b>T6</b>	Trach. 2-5w	2.64/5.34	2000	1373	1373	900	886	RHQ	2.63/5.30	n.d.	129.1 ± 25.8	n.d.
<b>T7</b>	Trach. 1-5w	1.29/5.34	2000	1373	1373	480	466	RHQ	1.43/5.23	n.d.	56.3 ± 11.3	n.d.

**Notes:** Water diffusivities are determined using a modified Boltzmann Matano method. (\*) samples run in the PCA; the other experiments were effectuated in the IHPV. In the columns C<sub>H<sub>2</sub>O</sub> in. KFT and C<sub>H<sub>2</sub>O</sub>-fin. NIR, the two values reported refers respectively to the bulk water content of the water poor side and the water rich side. RQ: rapid quench; RHQ: rapid heat rapid quench; NQ: normal quench. Errors of the diffusion coefficient is an estimation based on the quality of fit and on the uncertainty of experimental (T, P, t) and analytical (C<sub>water</sub>, distance) parameter and is calculated around 20% (Behrens et al., 2004). Initial water contents are measured by KFT (and MIR in case of H<sub>2</sub>O<sub>i</sub> < 0.5wt%)

In general, it was easy to obtain clear glasses after experiments for phonolitic composition, while for the trachyte glasses often numerous, small, acicular crystals were present in samples with water content ranging from 0 to 3wt%. In many cases the amount of the small crystals, with the size of few  $\mu\text{m}$  and visible only with microprobe, was too high and the glasses were not transparent. In this case it was not possible to analyse the water concentration-distance profile by IR spectrometer. Acicular crystals were also present in some phonolitic samples but were too small in size to have

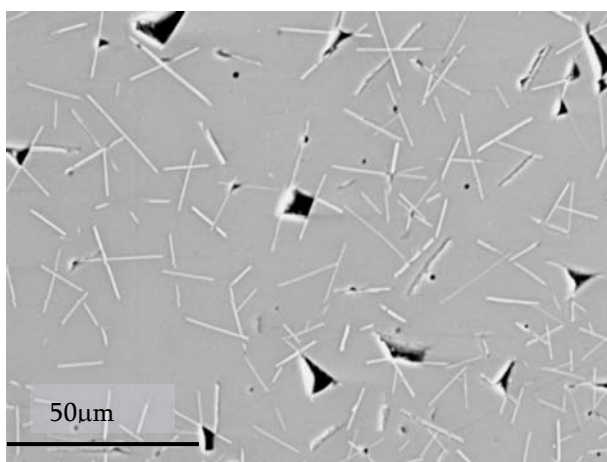


**Fig. 37:** Small acicular crystals in the sample P8. In this case, their amount was low enough to enable a proper determination of the concentration-distance profiles.

composition analyses by microprobe (Fig.37).

Extraction of iron from the melt into the platinum walls of the capsule was a minor problem in these experiments because run duration was short compared to cation diffusion rates in the melt (cf. Baker, 1990; Zhang, 1993; Kress and Ghiorso, 1995; Koepke and Behrens, 2001). This finding is supported by microprobe analyses shown in Fig.39 where it is evident that

the iron loss interests just 200-300  $\mu\text{m}$  along the capsules wall. This is in good agreement with the observations in Behrens & Zhang (2004).

To obtain the water concentration-distance profiles (Fig.38), the concentrations of  $\text{H}_2\text{O}$  and OH were determined from the heights of the absorption bands at  $5230\text{ cm}^{-1}$  and at  $4500\text{ cm}^{-1}$ , respectively, using the Lambert-Beer law. The total water was obtained by summing up both species concentration. The diffusion profile of each successful experiment is reported in the Appendix. In some cases (i.e. P6 and P7), in the dry part the concentration of dissolved water was below the detection limit for the NIR combination band ( $<0.1\text{ wt}\%$ ). Scatter in concentration of hydrous species is particularly evident for

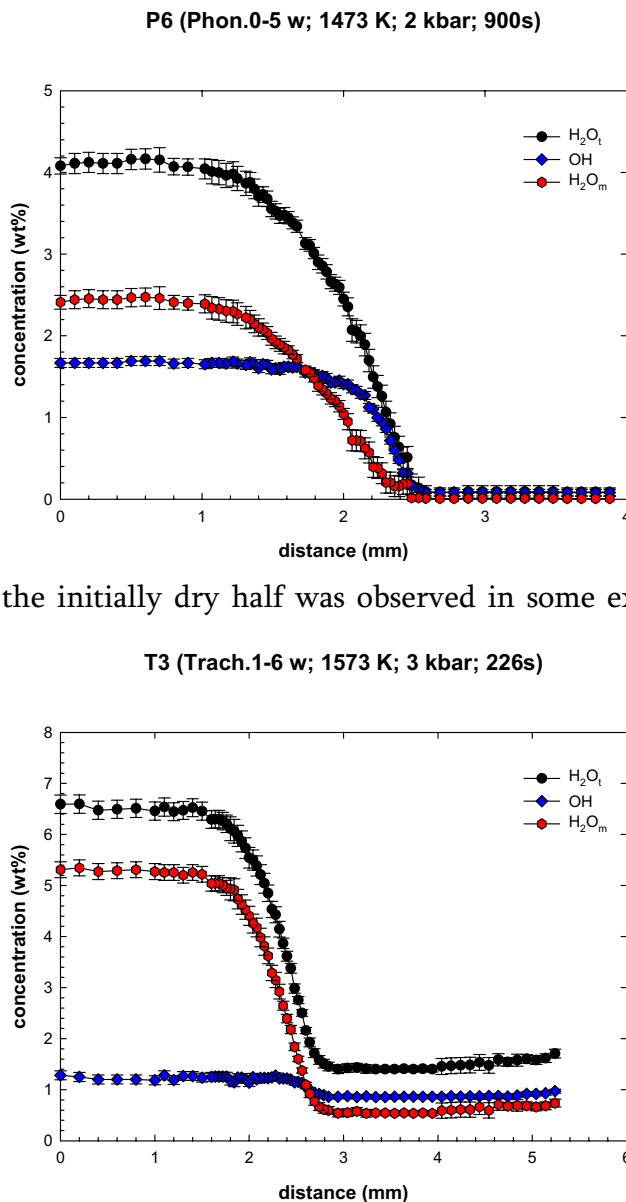


**Fig. 38:** Examples of water concentration profile for phonolite and trachyte melts. Black dots: bulk water content – blue dots: OH group – red dots: molecular water. Error bars refers calculated by error propagation considering error in thickness (0.002 mm) and in the absorbance for peak at 4500 and 5200  $\text{cm}^{-1}$ .

experimental conditions but those near the glass temperature, during cooling. Therefore, the total water concentration profile was used to model the diffusion process. According with Silver et al. (1990) and Behrens et al. (1996), OH<sup>-</sup> groups are the dominating species

the samples P1, P4, P10, T1 and T4 and is attributed to the presence of fractures and cracks (Behrens et al., 2004). If the IR beam passes a crack in the sample, the measurements often yield too low concentrations. The samples with more cracks are those run in the PCA at a pressure of 25 kbar. An increase of  $\text{H}_2\text{O}_t$  at the end of the initially dry half was observed in some experiments (i.e. P4 and T3) indicating fast transport of  $\text{H}_2\text{O}$  along the capsule walls. In other experiments (i.e. P3, P9 and T6) a decrease in  $\text{H}_2\text{O}_t$  near the end of the hydrous sample was observed. However, these processes affected only a small portion of the sample near the rim and had no influence on the diffusion profiles measured in the centre region of the couple.

It is emphasised that the abundance of OH and  $\text{H}_2\text{O}_m$  does not reflect the equilibrium concentration at

at low water content, increasing the water content the OH<sup>-</sup> group concentration reaches a nearly constant value while the molecular water becomes the dominating species.

The errors in the concentration measured by NIR were calculated by error propagation considering the error in the sample thickness ( $\Delta d = 0.002$  mm), in the evaluated absorbance for peaks at  $4500\text{ cm}^{-1}$  ( $\Delta A_{4500}$ ) and  $5200\text{ cm}^{-1}$  ( $\Delta A_{5200}$ ) and in the density  $\rho$  (0.02 g/l). The formula for the error calculation is:

$$\Delta C_{OH} = C_{OH} \sqrt{\left(\frac{\Delta d}{d}\right)^2 + \left(\frac{\Delta A_{4500}}{A_{4500}}\right)^2 + \left(\frac{\Delta \rho}{\rho}\right)^2} \quad [62]$$

$$\Delta C_{H_2O} = C_{H_2O} \sqrt{\left(\frac{\Delta d}{d}\right)^2 + \left(\frac{\Delta A_{5200}}{A_{5200}}\right)^2 + \left(\frac{\Delta \rho}{\rho}\right)^2} \quad [63]$$

In Table 13, initial and post-experimental water contents are shown. In most cases an increase or decrease of circa 0.5 wt% were measured, due to small dishomogeneity of the glasses within the large synthesised batches and to changes in the redox state of the iron. Anyway some samples were showing relatively higher or lower water content at the end of the experiments (P1, P5, PHDC4, PHDC5, T5 and T8).

### ***2.7.3 Results from colorimetric determination of ferrous iron***

To control the redox state of the melts, the different iron species were determined by colorimetric technique (Schlüssler et al., 2008). Values of Fe<sup>3+</sup>/Fe<sub>tot</sub> for glasses synthesised in air at ambient pressure (a.P.), in the IHPV and in the PCA are reported in Table 14. In the IHPV, at constant T, P and fH<sub>2</sub>, the redox state of iron in the melt is controlled by the water content of the melt by the equations:



The air-molten phonolite has a  $Fe^{3+}/Fe_{total}$  value of  $0.73 \pm 0.02$ . In most of the experiments, the hydrous glasses were more oxidised than the dry one, showing higher values of  $Fe^{3+}/Fe_{tot}$ . This is in contrast with the funding of Behrens et al. (2004) for dacitic and andesitic glasses. The samples processed in the PCA, with values ranging from 0.09 to 0.41 for phonolite and from 0.27 to 0.47 for trachyte, are more reduced than the one synthesised in the IHPV, showing  $Fe^{3+}/Fe_{total}$  values ranging from 0.35 to 0.59 for phonolite and from 0.08 to 0.19 for trachyte. These funding are unusual, being the oxygen fugacity lower in the IHPV than in PCA. Anyway, the amount of each sample processed in the PCA available for iron determination was often too few (4-7 mg).

#### ***2.7.4 – Major oxide concentration profile***

To verify that in the studied systems water was the unique mobile species and that no contribution from other components was given to the water transport, major oxides concentration profile were determined by microprobe. In Fig. 39, the oxide concentration profile in comparison with the  $H_2O_t$  profile is shown for the sample P2. Data points were collected along the same route used to determine the water concentration profile by NIR. No significant variations in the relative abundance of cations are visible.

Therefore the concentration gradient or diffusive flux of any anhydrous component due to  $H_2O$  diffusion is minimal and cannot be resolved within the precision of microprobe data. Hence, the coupling of  $H_2O$  to other components was considered of minor importance and  $H_2O$  transport could be treated as binary inter-diffusion of  $H_2O$  and the rest of the silicate melt. A small Fe loss is visible in a narrow rim ( $\approx 200 - 300 \mu m$ ) in the dry side at the contact with the capsule wall.

**Table 14:** Iron determination by colorimetric analyses

Sample	$\text{Fe}^{3+}/\text{Fe}_{\text{tot}}$		$\text{H}_2\text{O}$ (wt%)	
Phon.dry-a.P.	$0.73 \pm 0.02^*$		n.d.	
Trach.dry-a.P.	n.d.		n.d.	
	IHPV	PCA	$\text{C}_{\text{H}_2\text{O}_t}$ IHPV	$\text{C}_{\text{H}_2\text{O}_t}$ PCA
Phon.dry	$0.35 \pm 0.07^*$	$0.41 \pm 0.05$	$0.57 \pm 0.03$	$0.45 \pm 0.06$
Phon.-2wt%	$0.59 \pm 0.04^*$	$0.11 \pm 0.11$	$2.42 \pm 0.05$	$2.45 \pm 0.07$
Phon.-5wt%	$0.45 \pm 0.03^*$	$0.09 \pm 0.06$	$5.43 \pm 0.06$	$5.31 \pm 0.09$
Trach.dry	$0.31 \pm 0.05^*$	$0.08 \pm 0.07$	$0.29 \pm 0.02^{**}$	$0.54 \pm 0.03$
Trach.-2wt%	$0.27 \pm 0.03^*$	$0.19 \pm 0.07$	$2.64 \pm 0.04$	$2.72 \pm 0.05$
Trach.-5wt%	$0.47 \pm 0.03^*$	$0.12 \pm 0.05$	$5.34 \pm 0.03$	$5.43 \pm 0.04$

**Notes:** the amount of sample used to perform these analyses was varying from 4 to 7 mg for the PCA samples and 10 mg for the IHPV samples. Run parameters: -PCA: 1598 K; 15 kbar; 311s; -IHPV: 1473 K, 4 kbar, 20 h. (\*) the reported value is the average of two measurements. A second analyse was not possible for the samples run in the PCA. Water content after IHPV syntheses was analysed by KFT. Water content after PCA syntheses was analysed by NIR. (\*\*) water content analysed by MIR.

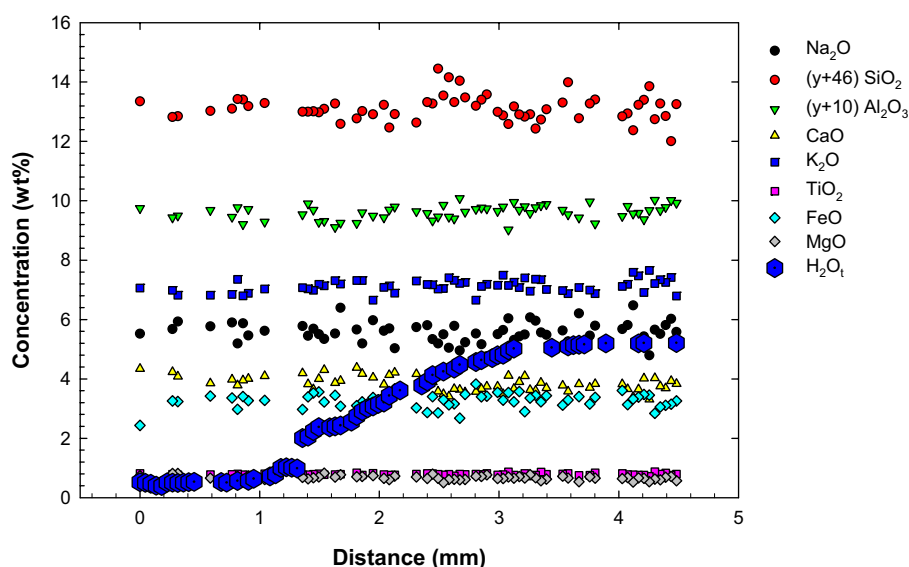


**Fig. 39:** Major oxide concentration profile for the sample P2 along cylindrical axis. Oxide contents are normalized to anhydrous composition to identify changes in relative abundance of cations. The  $\text{H}_2\text{O}_t$  profile is shown for comparison.

## 2.8 – Discussion

### *2.8.1 The effect of redox state on water transport*

In silicate melts containing H and Fe, redox interactions occur between H<sub>2</sub>-H<sub>2</sub>O and Fe<sup>3+</sup>-Fe<sup>2+</sup> (Behrens et al., 1994; Gaillard et al., 2002). Gaillard et al., 2003, demonstrated that:

- reduction of Fe<sup>3+</sup> in the melt by H<sub>2</sub> ( $\text{Fe}_2\text{O}_3 + \text{H}_2 = 2\text{FeO} + \text{H}_2\text{O}$ ) operates by the progression of a redox front that is accompanied by an increase in the concentration of OH-groups;
- H<sub>2</sub> diffusion in silicate melts is much more rapid than the observed rate of reduction of Fe<sup>3+</sup>;
- the velocity of the redox front within the melt is faster than the mobility of molecular H<sub>2</sub>O, suggesting that various hydrogen-bearing species with different diffusivities may exist in a silicate melt.

It is evident from Table 14 that starting glasses of the diffusion couples were already relatively reduced and that the samples processed in the PCA are more reduced than the ones synthesised in the IHPV.

Redox state of iron can influence the water transport in two ways:

- One possibility is hydrogen diffusion from the pressure medium into the diffusion capsule, which may interfere with the water diffusion profile. This would be possible in the PCA, where the graphite tube heater creates reducing conditions. IR measurements show that the H<sub>2</sub>O content in the dry half of samples is mostly decreasing of 0.1 wt% relative to the initial glass for phonolitic samples, except in few samples for a narrow rim ( $\approx 200 - 300 \mu\text{m}$  in thickness) near the capsule wall. In P3 and T1 glasses, a bulk water content increase of circa 0.3 wt% was registered.
- A second possibility is internal transport of molecular H<sub>2</sub> from the hydrous part to the anhydrous part. Such a profile would be superimposed on the measured H<sub>2</sub>O profile and the effect would depend on the gradient in Fe<sup>3+</sup>/Fe<sub>total</sub>. This flux of hydrogen would be against the flux of water. In most of our experiments the hydrous glasses were more

oxidized (higher  $\text{Fe}^{3+}/\text{Fe}_{\text{total}}$ ) than the dry ones. Because of the gradient in ferric and ferrous iron, molecular hydrogen may be released in the dry part, migrate into the hydrous part and react back to form  $\text{H}_2\text{O}$  and ferrous iron. This process would homogenize the ferric/ferrous ratio and transport  $\text{H}_2\text{O}$  from the dry to the hydrous side. It was estimated that  $\text{H}_2\text{O}_t$  would increase only by 0.2 or 0.3 wt.% in the hydrous half when the initial  $\text{Fe}^{3+}/\text{Fe}_{\text{total}}$  is reduced to the same value as in the anhydrous half. Therefore, molecular hydrogen transport covers a minor role in most of the experiments. However, if starting glasses were pre-equilibrated at similar conditions (i.e. f  $\text{H}_2$ ) there would be a little driving force for the hydrogen flux during diffusion experiments.

It was observed an increase in bulk water content ranging from 0.15 to 0.50 for some samples (P2, P4, P5, T1, T4, T5) as shown in Table 13 a-b of chapter 2.7.1.3, but most hydrous glasses show a lower bulk water content after the experiments ranging from 0.20 to 0.8. Only in two cases, P1 and T8, respectively a decrease of 1.31 wt% and an increase of 0.98 wt% were registered.

A decrease in water content of the hydrous part could have two causes:

- a water loss, e.g. the diffusion profile has reached the end of the sample (as in Behrens & Nowak, 1997);
- a changed in the absorption coefficients, as illustrated in the low temperature studies on dacite of Ni et al. (2008).

### ***2.8.2 Modelling $\text{H}_2\text{O}$ diffusion***

Three methods were applied to fit concentration of  $\text{H}_2\text{O}_t$  vs. distance profile to extract diffusion coefficients. On first instance, the profiles were fitted assuming a constant diffusivity. In second instance, a modified Boltzmann-Matano method was used. Finally, a functional relationship between diffusivity and water content was assumed.

### 2.8.2.1 Error function fit

Assuming a constant diffusivity  $D$ , the solution of Fick's second law for diffusion between two semi-infinite media with an initial concentration step at the interface is (Crank, 1975):

$$\frac{C - C_{\min}}{C_{\max} - C_{\min}} = 1 - \operatorname{erf}\left(\frac{x}{\sqrt{4Dt}}\right) \quad [66]$$

where  $C$  is the concentration at the distance  $x$ ,  $C_{\min}$  is the initial concentration in the dry half,  $C_{\max}$  is the initial concentration in the hydrous half, and  $t$  is the time.

None of the phonolitic samples are well reproduced by this fitting; the trachytic samples were not fitted with this method.

### 2.8.2.2 Modified Boltzmann-Matano method

To analyze the relationship between  $D_{\text{H}_2\text{O}_t}$  and  $C_{\text{H}_2\text{O}_t}$ , the  $\text{H}_2\text{O}_t$  profiles were evaluated using the Boltzmann-Matano method modified by Sauer and Freise (1962):

$$D(x) = \frac{1}{-2t(\partial C / \partial x)_x} \left[ (1 - C_x) \int_x^{+\infty} C dx + C_x \int_{-\infty}^x (1 - C) dx \right] \quad [67]$$

where  $C$  is the normalized concentration of  $\text{H}_2\text{O}_t$ :

$$C = \frac{C - C_{\min}}{C_{\max} - C_{\min}} \quad [68]$$

The approach of Sauer and Freise (1962) has two advantages compared to the original method of Boltzmann (1894) and Matano (1933): (1) the position of the Matano interface does not need to be found and (2) the precision is usually higher (Nowak and Behrens, 1997). To calculate the diffusion coefficients by the Sauer and Freise (1962) approach, profiles were fitted by seventh-order polynomials. Two profiles for phonolite compositions fitted by the Sauer and Freise method are shown in Fig. 40.

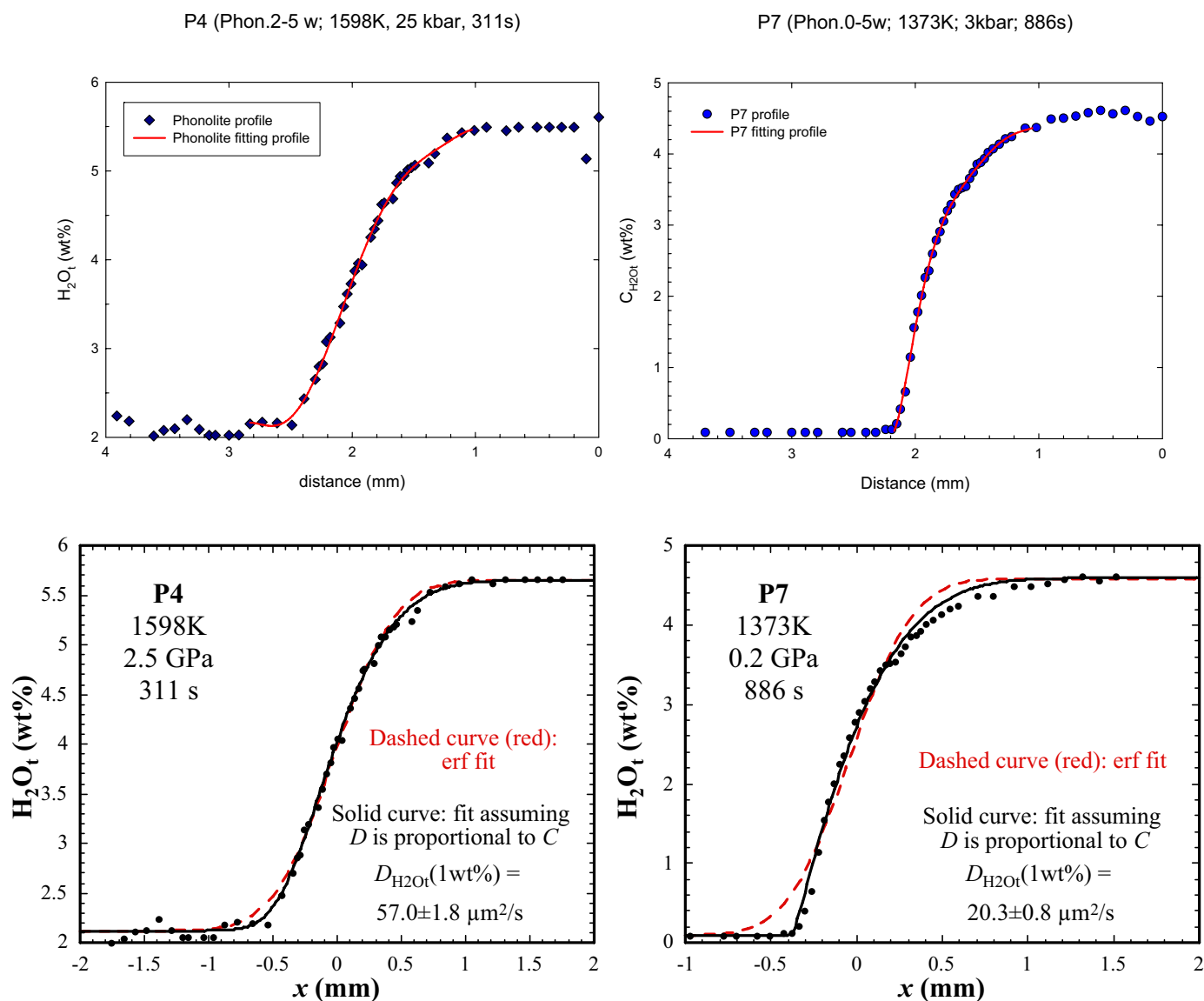


**Fig.40:** Total water concentration profile of samples P4 (left) and P7 (right). On top: red curves are seventh-order polynomial fitting used in the modified Boltzmann-Matano method. On bottom: red dashed curves are error function fit assuming constant diffusivity. The solid curves were fit assuming water diffusivity being proportional to  $C_{H_2O_t}$ . (For the error function fit and the numerical fitting we thanks Prof. Y. Zhang)

For trachyte compositions example is shown in Fig.41.

The obtained diffusion coefficients as function of total water are reported for some phonolitic glasses at 1598 K in Fig. 42. Here the samples P1, P2, P3, P4 and P5 are compared.

For the sample P3, the whole measured range is shown. The black triangles refer to the water range in which the Sauer and Freise (1962) approach yield reliable diffusivities. Outside of this range, systematic errors due to polynomial fitting and to the scatter of the data produce very large errors in diffusivity and even the compositional trends for the diffusivity might be obscured (Fig.42, dotted triangles shown for the sample P3).

T1 (Trach. 0-5 w, 1598K, 25 kbar, 311s)

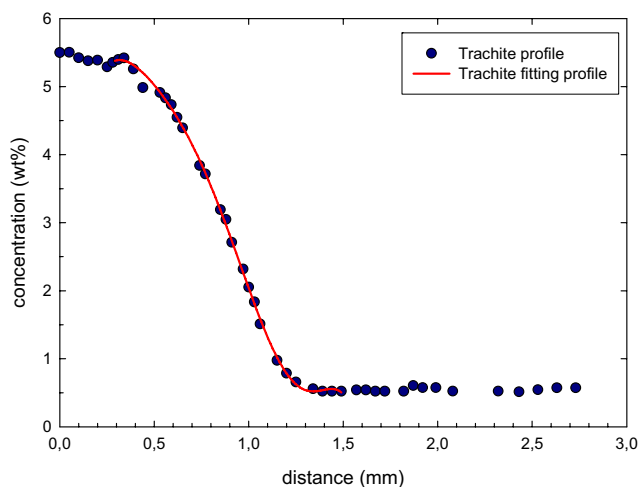


**Fig.41:** Total water concentration profile of sample T1. Red curves are seventh-order polynomial fitting used in the modified Boltzmann-Matano method.

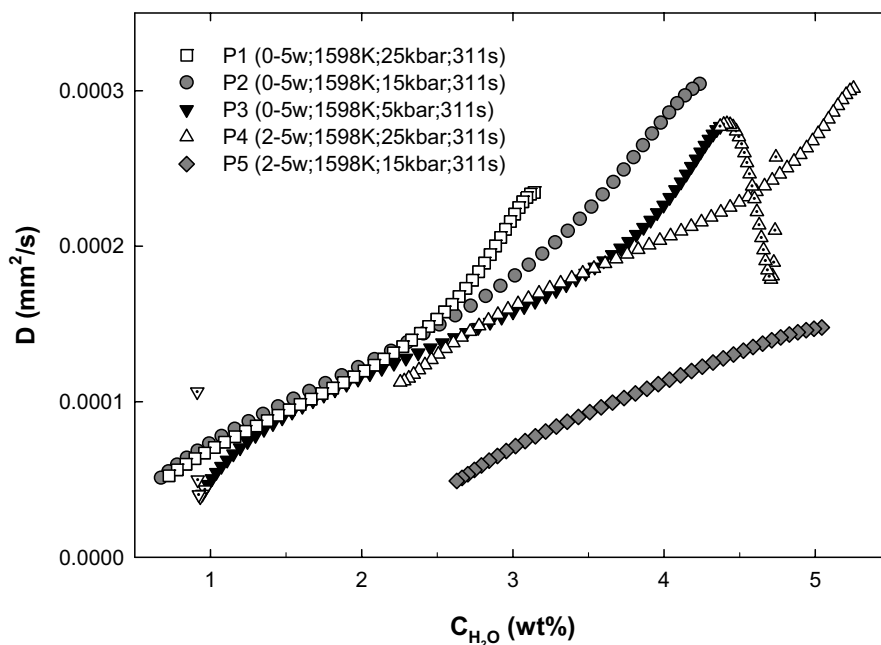


**Fig.42:** Comparison  $D_{H_2O_t}$  vs  $C_{H_2O_t}$  for phonolitic samples at different pressure: white symbols – 25 kbar; grey symbols – 15 kbar; black symbols – 5 kbar. For the sample P3, dotted triangles show the not reliable values. The experiments were performed in the PCA at  $T = 1598$  K and  $t = 311$  s).

The values of  $D_{H_2O_t}$  at 1, and 3.5 wt%  $H_2O_t$  ( $\mu m^2/s$ ) calculated by Boltzmann-Matano modified method are listed for both phonolitic and trachytic composition in Table 13 a-b. Samples P1 and P4 are in good agreement, while the sample P5 shows too low values and a not good profile (Appendix), hence it was not considered in further evaluations. For phonolitic melts was estimated that the water diffusivity is proportional to the total water content for  $C_{H_2O_t} < 3wt\%$ . A pressure effect is not evident in the range 5 – 25 kbar. At 1598 K, similar  $D_{H_2O_t}$  values were obtained in the range 1.3 – 2.3 wt% of  $H_2O_t$  at 5 and 25 kbar (Fig.42).

### ***2.8.2.3 Numerical fitting***

To verify the dependence of  $D_{H_2O_t}$  on  $C_{H_2O_t}$ , the  $H_2O_t$  profiles were numerically fitted using functional relationships between diffusivity and total water concentration.

The profiles in phonolitic melts are well reproduced assuming

$$D_{H_2O_t} = C_{H_2O_t} \cdot D_{H_2O}^{1wt\%} \quad [69]$$

where  $D_{H_2O}^{1wt\%}$  is the bulk water diffusivity for 1 wt%  $H_2O_t$  and  $C_{H_2O_t}$  is in weight percent. The relationship originates from glass science literature (e.g., Doremus, 1973) and was also applied to rhyolitic, dacitic and andesitic glasses using water speciation to model the bulk water diffusivity (Zhang et al., 1991; Behrens et al., 2004).

Most profiles were well fitted by assuming  $D_{H_2O_t}$  proportional to  $C_{H_2O_t}$ . Only the sample P7, reported in Fig.40, presented some misfit indicating that  $D_{H_2O_t}$  increases more rapidly with  $H_2O_t$  content than the proportionality assumption.

The values of  $D_{H_2O_t}$  at 1 wt%  $H_2O_t$  ( $\mu m^2/s$ ) calculated by numerical fitting are listed aside the ones calculated by Boltzmann-Matano modified method in Table 13 a-b for comparison. For most samples, the values are in good agreement showing discrepancies lower than 11% relative and therefore within the experimental error (20%). Only for the samples P2 and P3 values of  $D_{H_2O_t}$  at 1 wt%  $H_2O_t$  circa 30% relative higher were calculated by the modified Boltzmann-Matano method.

The numerical fitting was not used in the interpretation of trachytic data.

### 2.8.3 $P$ - $T$ - $C_{H_2O_t}$ dependence on bulk water diffusivity

The temperature and pressure dependence of diffusion can be described by the Arrhenius relationship:

$$D = D_0 e^{\left(\frac{-E_a + V_a P}{RT}\right)} \quad [70]$$

where  $D_0$  is a pre-exponential factor,  $E_a$  is the activation energy and  $V_a$  is the apparent activation volume. On a base-10 logarithmic scale this relationship translates to:

$$\log D = a + \frac{b}{T} + \frac{cP}{T} \quad [71]$$

with parameters  $a$ ,  $b$  and  $c$  being related to  $D_0$ ,  $E_a$ , and  $V_a$ , respectively.

#### 2.8.3.1 Modelling of Phonolite

It was already shown that the pressure effect of water diffusivities in phonolitic melts was too small to be resolved.

Two sets of experiments with the same temperature and pressure but different  $H_2O_t$  range were used to test the reliability of the experiments and of the models:  $D_{H_2O_t}^{1 \text{ wt}\%}$  should be the same in each set.

For the samples P6 and P10 at 2 kbar and 1473 K,  $D_{H_2O_t}^{1 \text{ wt}\%}$  is 43  $\mu\text{m}^2/\text{s}$  for P6 (this value coming from the numerical fitting is in good agreement with the value of 42  $\mu\text{m}^2/\text{s}$  calculated by the modified Boltzmann-Matano method) and 59  $\mu\text{m}^2/\text{s}$  for P10. The greater value for P10 (where the average  $H_2O_t$  content is higher) means that  $D$  increases more rapidly than the proportionality relation (Fig. 13). However, the difference (about 30%) is small and is close to the value of the experimental error, estimated around 20% after Behrens et al., 2004.

For the samples P1 and P4 at 25kbar and 1598 K,  $D_{H_2O_t}^{1 \text{ wt}\%}$  is 71,2  $\mu\text{m}^2/\text{s}$  for P1 (69  $\mu\text{m}^2/\text{s}$  by Boltzmann-Matano modified method) and 57  $\mu\text{m}^2/\text{s}$  for P4. The lower value for P4 (where the average  $H_2O_t$  content is higher) means that  $D$  increases more slowly than

the proportionality relation (see also Fig.42). However, the difference (about 20%) is small and is likely within experimental error.

Summarizing, the obtained data indicate that at lower temperature  $D_{\text{H}_2\text{O}_t}$  increases more rapidly than the proportionality assumption and at higher temperature  $D_{\text{H}_2\text{O}_t}$  increases more slowly.

To better interpret the data, experiments at lower temperatures would be needed. Several try were done at 773 and 873 K for different duration in PCA and IHPV but all of them were unsuccessful due to important crystallization.

Results of the modified Boltzmann-Matano method are displayed for temperatures from 1373 to 1673 K and pressure ranging from 2 – 5 kbar in Fig.43.

In the  $\text{H}_2\text{O}_t$  range of 0.5 to 3 wt% and in the temperature range of 1373 to 1673 K,  $D_{\text{H}_2\text{O}_t}$  ( $\text{m}^2/\text{s}$ ) can be calculated as a function of  $T$  (K) and  $C_{\text{H}_2\text{O}_t}$  (wt%) as:

$$\log D_{\text{H}_2\text{O}_t} = -7.11 - 2.07 \log C_{\text{H}_2\text{O}_t} - \frac{(4827 - 4620 \log C_{\text{H}_2\text{O}_t})}{T} \quad [72]$$

The experimental data are reproduced by this relationship with a standard error of 0.07 log units.

This equation, derived by the fitting with the Boltzmann-Matano method, shows that  $D_{\text{H}_2\text{O}_t}$  is proportional to  $C_{\text{H}_2\text{O}_t}$  and therefore is in good agreement with the numerical fitting.

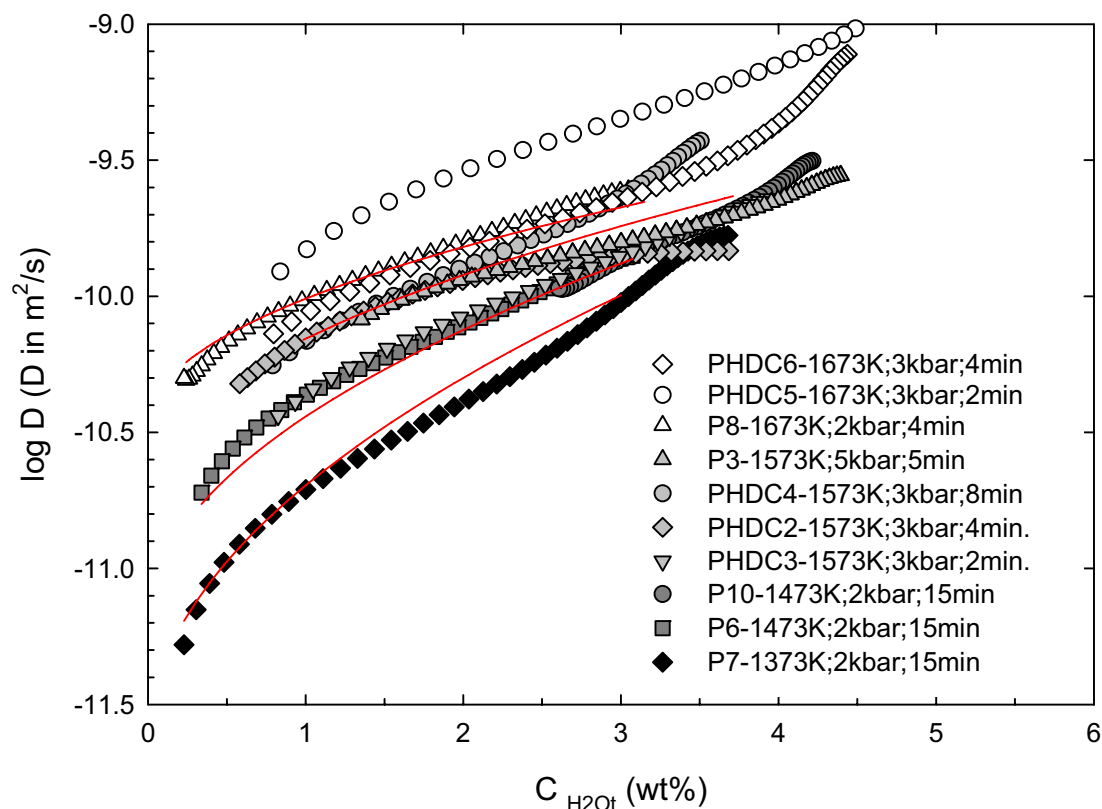


**Fig.43:** Plot of  $\log D_{H_2O_t}$  vs  $C_{H_2O_t}$  for phonolitic samples at different temperature based on Boltzmann-Matano fitting: white symbols – 1673 K; grey symbols – 1573 K; dark-grey symbols – 1473 K; black symbols – 1373 K. The linear regression used in modeling the diffusion trends are marked in red.

### 2.8.3.2 Trachyte

In trachyte samples with water content below 2wt% micro-crystallization of oxides occurred, that makes the water determination by NIR and MIR spectroscopy impossible. Anyway, small oxide crystals were present also in the hydrous samples. Therefore, almost all the experiments including dry and 1wt%  $H_2O_t$  were failed. The successful experiments are listed in Table 13-b. The diffusion profiles successfully fitted by Boltzmann-Matano method are reported in Fig. 44.

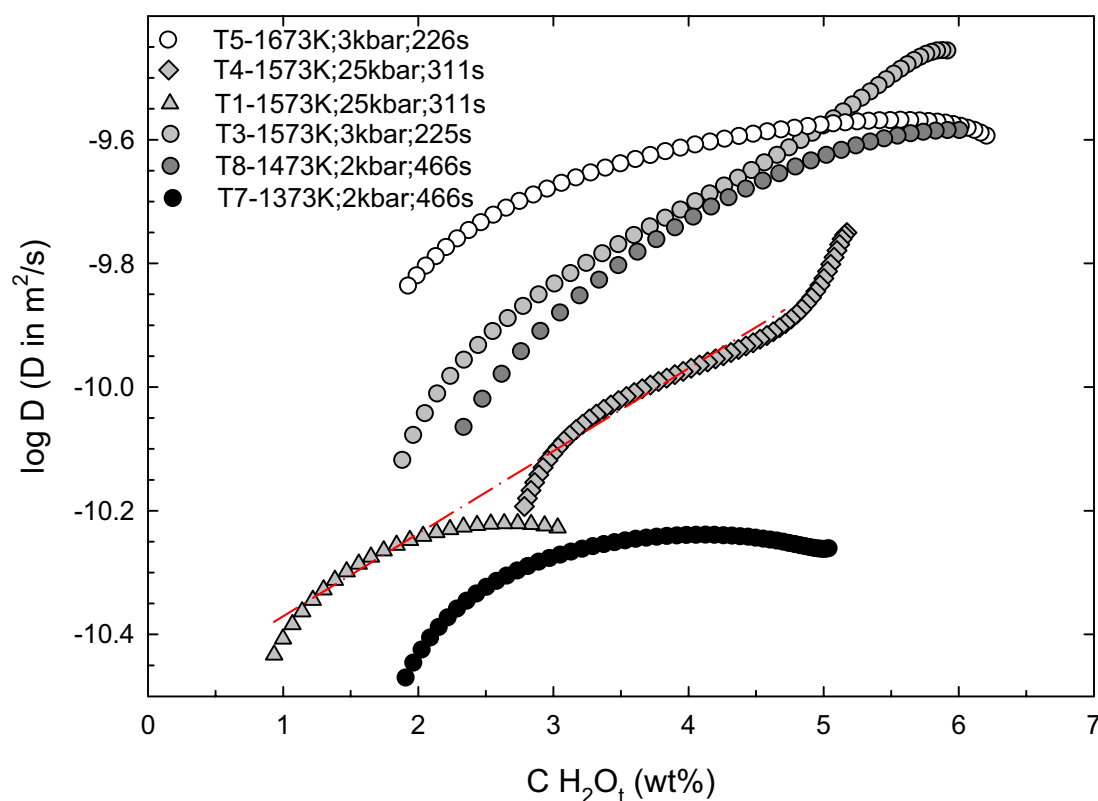


**Fig.44:** Plot of  $\log D_{H_2O_t}$  vs  $C_{H_2O_t}$  for trachytic samples at different temperature: white symbols – 1673 K; grey symbols – 1573 K; dark-grey symbols – 1473 K; black symbols – 1373 K. The pressure is ranging from 25 kbar - 2 kbar. The plots were fitted by modified Boltzmann-Matano method.

For trachyte composition smaller diffusivities at higher pressures were registered, indicating a negative pressure effect.. That is, the water diffusion in the samples T1 and T4, performed in the PCA at 25 kbar and 1573 K, is 0.2 log units lower than the sample T3, performed in the IHPV at 3 kbar and 1573 K.

The temperature dependence of water diffusivity cannot be well defined, being the  $D_{H_2O_t}$  in the sample T7 (1373 K) just 0.6-0.7 log units lower than the  $D_{H_2O_t}$  in the sample T5 (1673 K).

Three sets of experiments with the same temperature and pressure but different  $H_2O_t$  range were used to test the reliability of the experiments (T1-T4; T2-T8; T6-T7 see Table13-b). The fitting by the modified Boltzmann-Matano method of the samples T2 and T6 presented a roughly constant diffusion value, but the profiles did not present a good shape in particular in the low water content plateaux. The fitting of the samples

T1 and T4 show the same trend as indicated by the dash-dot line in Fig. 44. Therefore, extrapolating the diffusion value for the sample T4 at low water content, the same value of the sample T1 will be obtained.

It was not possible in the case of trachytic composition to derive an equation that correlates  $D_{H_2O_t}$  with water content. Anyway, several tries were done and considering  $D_{H_2O_t}$  proportional to  $C_{H_2O_t}$  as for phonolite, for temperature from 1373 – 1673 K, in the water range 2-5 wt%, the following relationship was suggested:

$$\log D_{H_2O_t} = -5.92 - 0.63 \log C_{H_2O_t} - \frac{(7389 - 1704 \log C_{H_2O_t})}{T} \quad [73]$$

The experimental data are reproduced by this relationship with a standard error of 0.09 log units (Fig.45).

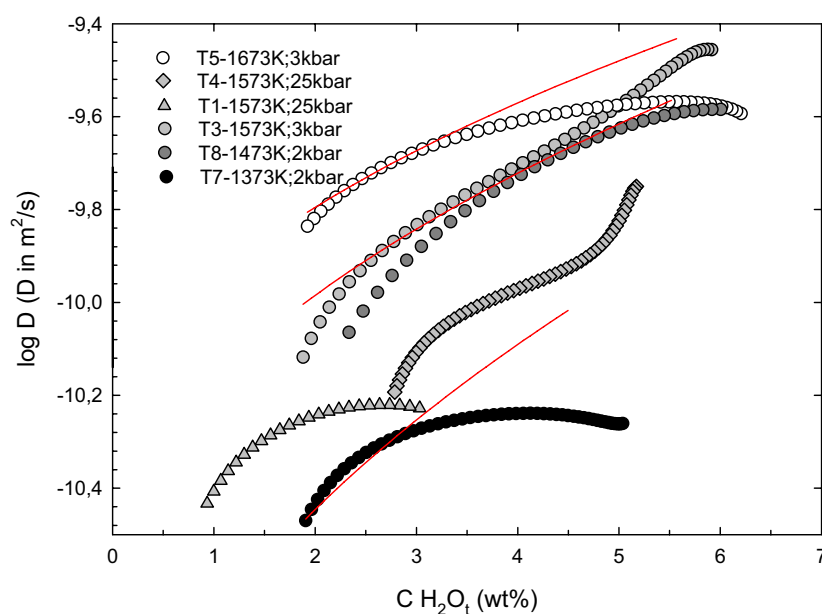


**Fig.45:** Plot of  $\log D_{H_2O_t}$  vs  $C_{H_2O_t}$  for trachytic samples at different temperature based on Boltzmann-Matano fitting: white symbols – 1673 K; grey symbols – 1573 K; dark-grey symbols – 1473 K; black symbols – 1373 K. The linear regression used in modeling the diffusion trends are marked in red.

### ***2.8.4 Water diffusion in Natural Melts***

In Fig.46 are plotted for comparison data for bulk water diffusivity in different natural melts.

For andesitic and basaltic melts diffusion data are available over a wide range of conditions. For both compositions at high temperatures (1608-1858 K; 5-15 kbar for andesite and 1573-1773 K; 10 kbar for basalt) was ruled out that  $D_{\text{H}_2\text{O}_t}$  is roughly proportional to  $C_{\text{H}_2\text{O}_t}$  (Behrens et al., 2004), in particular for basalts this applies to low water content ( $\approx 0.04\text{-}0.4$  wt%  $\text{H}_2\text{O}_t$ ) (Zhang & Stolper, 1991). At low temperatures (673-948 K and 1 bar) (Okumura & Nakashima, 2006) the total water diffusivities in basalt were determined by assuming the linear-dependent diffusivity on total water contents and that in andesite was obtained by assuming the constant diffusivity.

Also for rhyolitic and dacitic compositions diffusion data are available over a wide range of conditions: 673–1473 K, 10–8 kbar, and 0.1–7.7 wt%  $\text{H}_2\text{O}_t$  for rhyolite (Zhang & Behrens, 2000; Behrens & Zhang, 2001); 773-913 K at  $P < 2$  kbar and 1493-1798 K at  $5 < P < 15$  kbar for Dacite (Behrens et al., 2004; Liu et al., 2004). In these melts  $\text{H}_2\text{O}$  diffusion was modelled by assuming  $\text{H}_2\text{O}_m$  is the only diffusing species and  $D_{\text{H}_2\text{O}_m}$  depends exponentially on  $C_{\text{H}_2\text{O}_t}$ .

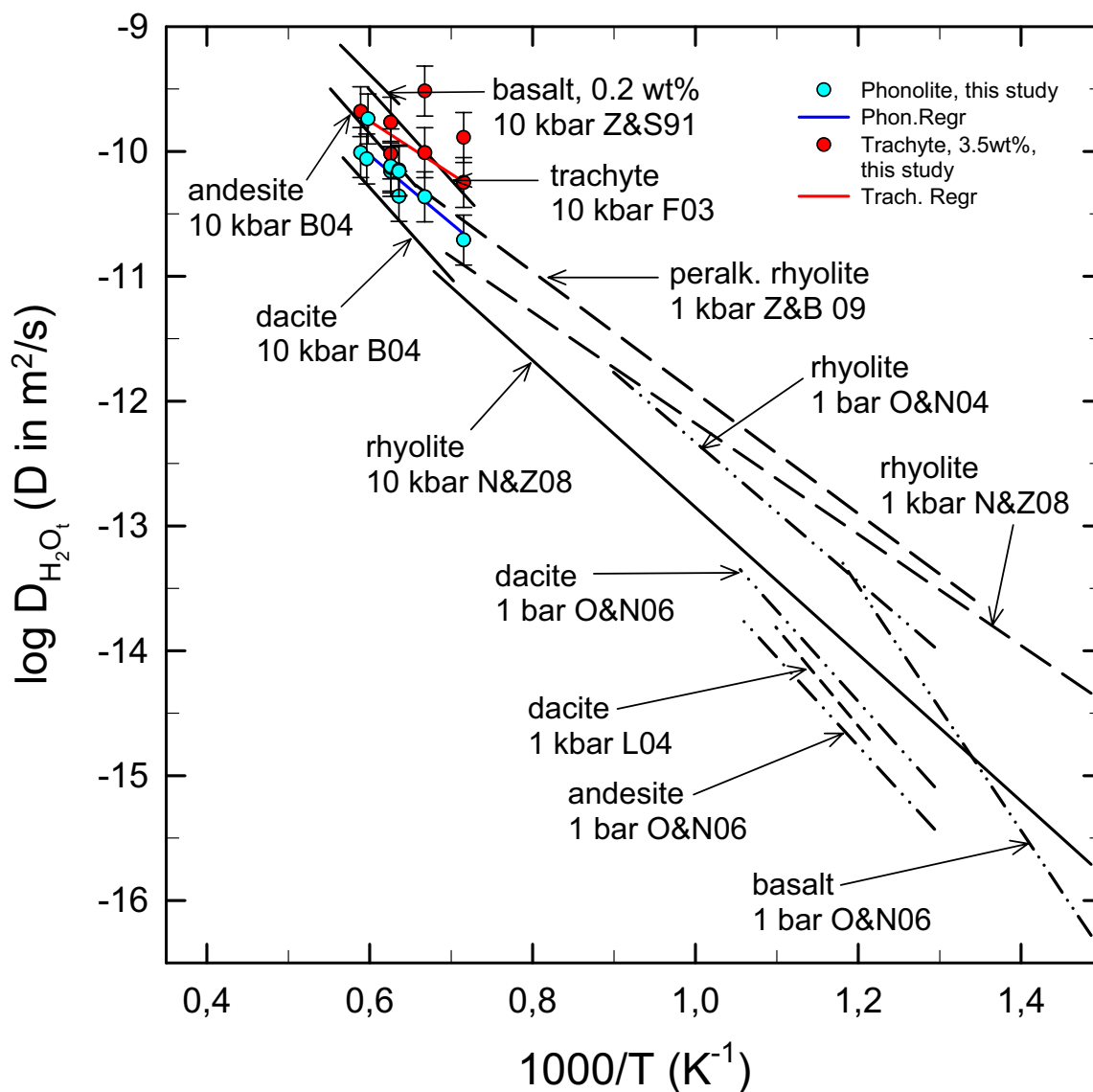


**Fig.46:** Compilation of data for bulk water diffusivity in natural melts. Diffusion data are for 1 wt%  $H_2O_t$  except for basalt (0.2 wt%  $H_2O_t$ ) and trachyte (3.5 wt%  $H_2O_t$ ). Diffusivity in phonolitic melts is based on fits of the profiles assuming  $D_{H_2O_t}$  being proportional to  $C_{H_2O_t}$ . Diffusivity in phonolitic and trachytic melt was obtained by a modified Boltzmann-Matano analysis. Data sources: basalt (Zhang and Stolper, 1991); rhyolite (Zhang and Behrens, 2000; Ni & Zhang, 2008); dacite at low  $T$  (Liu et al., 2004); trachyte (Freda et al., 2003); andesite and dacite (Behrens et al., 2004); dacite, andesite and basalt at low  $T$  (Okomura and Nakashima, 2006); peralkaline rhyolite (Zhang and Behrens, in press); other data (this work).

Considering the new results from this study, for phonolitic melts only high-temperature diffusion data are available. At high temperatures (1373–1673 K), 5–25 kbar, and  $H_2O_t$  of 0.5 to 3.5 wt%,  $D_{H_2O_t}$  was estimated roughly proportional to  $C_{H_2O_t}$ . The diffusion values obtained for the studied phonolite are lower than the diffusivity values measured for trachyte by Freda et al. (2003). One diffusivity datum (PHDC 5) is off the trend, circa 0.4 log units higher, and were not used in the fitting. Extrapolated value of  $\log D_{H_2O_t} = -12.64$  at 873 K for phonolite was calculated by eq. [5]. It is in the range of the peralkaline rhyolite but it has to be considered just as an indicative value. The diffusion data for trachytic composition were also reported in the plot. They refer to a water content of 3.5 wt%. Two diffusivity data (T2 and T6) are off the trend, circa 0.5–0.6 log units higher, and therefore were not considered in the fit. In the case of trachyte, it was not possible to derive an equation that correlate  $D_{H_2O_t}$  with  $C_{H_2O_t}$ .

Diffusion data for  $C_{H_2O_t}$  of 3.5 wt%  $H_2O_t$  for Phonolite and Trachyte in the temperature range 1373 – 1673 K, at pressure of 2–3 kbar show not reliable differences.

Summarising, for phonolite and trachyte a water diffusivity was determined lower than in trachyte of Freda et al. (2003) but faster than in rhyolite of Zhang et al. (2000) and Ni and Zhang (2008). In particular, the  $D_{H_2O_t}$  for phonolite at high temperature show values very close to that of the peralkaline rhyolite.

### ***2.8.5 Moving species***

There are several model to explain the complicated dependence of  $D_{H_2O_t}$  on  $C_{H_2O_t}$  and bulk composition of silicate melts:

- A model proposed by Behrens et al. (2004) inferred that molecular  $H_2O$  diffusivity increases with increasing  $C_{H_2O_t}$  for rhyolitic and dacitic melts, and decreases slightly with increasing  $C_{H_2O_t}$  for andesitic and basaltic melts. This explanation offers consistency in modelling  $H_2O$  diffusivity but it is against intuition that the addition of  $H_2O$  may decrease the diffusivity of hydrous species.

- Another possibility is contribution from “free” OH<sup>-</sup> groups (OH<sup>-</sup> groups not bonded to tetrahedral Si or Al) formed as follows:



Recent <sup>1</sup>H MAS NMR measurements support the presence of such species in alkaline earth silicate glasses (Xue and Kanzaki, 2004).

A rapid motion of protons in depolymerised glasses can be inferred from impedance measurements on hydrous barium disilicate glasses (Behrens et al., 2002) and from this study.

Another possible explanation is that contributions of OH groups bonded to tetrahedral cations ( $D_{\text{OH}}$ ) cannot be neglected in modeling the water diffusion profile for depolymerized melts at high temperatures.

In this work, values of OH diffusion were estimated for phonolitic melts using the viscosity data measured on trachyte by Misiti et al. (2006) and the Eyring relationship:

$$D = \frac{k \cdot T}{\lambda \cdot \eta} \quad [75]$$

where  $D$  is the diffusion coefficient,  $k$  is the Boltzmann constant,  $T$  is the temperature,  $\lambda$  is the jump distance and  $\eta$  is the viscosity.

Assuming an effective jump distance of 3 Å (Behrens et al., 2004), and considering  $\log \eta = 2.96$  for a trachyte sample containing 0.88 wt% of H<sub>2</sub>O<sub>t</sub> at 1573 K (Misiti et al., 2006) the estimated  $D_{\text{OH}}$  is 0.08 μm<sup>2</sup>/s. This value is less than the measured bulk water diffusivities of this study by circa 3 orders of magnitude. Therefore, confronting our data and elaborations of viscosity data, it is possible to suppose that the molecular water plays a major role in the diffusion processes.

## Conclusions

This work provides new information on the mechanisms of transport of hydrous species in silicate glasses and melts at low and high temperatures. On one side, electrical conductivity was studied at low temperature (up to 693 K) and ambient pressure on dry and hydrous silicate glasses with compositions along the join Diopside-Anorthite using Impedance Spectroscopy. On the other side, water diffusion was examined at high temperature (1373-1673 K) and different pressure (2-25 kbar) on phonolitic and trachytic melts by diffusion couple experiments.

Evidence for electrical conductivity in hydrous  $An_{100}$ ,  $An_{50}-Di_{50}$  and  $Di_{100}$  glasses, with bulk water content up to 3 wt%, were given by Impedance Spectroscopy. IR spectra showed that both OH groups and  $H_2O$  molecules were present in the glasses and that the abundance of strongly hydrogen bonded hydrous species is much lower in the studied glasses than in the barium silicate glass analysed by Behrens et al. (2002). The measured dc conductivity is higher by at least one order of magnitude in hydrous glasses than in dry glasses. The measurable conductivity shown by the anhydrous glasses was attributed to minor amounts of dissolved  $Na_2O$ . It is known that dissolved water reduces the mobility of alkali cations in glasses and, hence, we infer that the dc conductivity observed in the hydrous samples is mainly due to the charge carriers produced by hydration of the glasses. At similar water content, the depolymerised  $Di_{100}$  hydrous glass shows conductivity values circa 2 log units higher than the more polymerised  $An_{50}Di_{50}$  and the fully polymerised  $An_{100}$  glasses. This finding supports that the concentration of non-bridging oxygen is crucial for proton conduction in silicate glasses. It was suggested, according with previous studies, that the mobile charge carriers are either protons or OH groups which are not bond to tetrahedral cations. In the temperature range of 539-685 K, the diffusivity derived from the conductivity data for the samples  $Di_{100}$  with 1.22 wt%  $H_2O_t$  and  $An_{50}Di_{50}$  with 2.77 wt%  $H_2O_t$  is about one order magnitude faster than the diffusion data for hydrous species in silicate glasses. Furthermore, the values of proton diffusion for  $BaSi_2O_5$  with

2.75 wt% of  $H_2O_t$  at 1 atm (Behrens et al., 2002) are in good agreement with the values extrapolated to temperature around 500 K for the  $An_{50}Di_{50}$  with 2.77 wt%  $H_2O_t$  at 1 atm.

An investigation on  $H_2O$  diffusion in phonolitic and trachitic melts containing up to 6wt%  $H_2O_t$  at temperature ranging from 1373 - 1673 K and pressure ranging from 2 – 25 kbar has been carried out with the diffusion couple technique. For both compositions, in the low temperature range (773-873K), diffusion couple experiments failed due to large crystallization.

For phonolitic composition, good diffusion data were obtained in the temperature range of 1373-1673 K, pressure range from 2-25 kbar and  $C_{H_2O_t}$  from 1-4 wt%. For trachytic composition, although there were some analytical and experimental problems including abundant micro-crystallisation of the anhydrous samples and uncertainties in the calibration of the IR technique in the MIR range, diffusion data were obtained for  $t$  ranging from 1373 – 1673, pressure from 2-25 kbar and  $C_{H_2O_t} > 2$ wt%. Diffusion profiles for both compositions were fitted using a modified Boltzmann-Matano method. For phonolitic samples, the results obtained by this fitting were compared with those calculated with the error function fit and the numerical fitting. Diffusion data obtained by the modified Boltzmann-Matano method are in good agreement with the one evaluated by the numerical fitting, assuming  $D$  being proportional to the water content, while the error function fit gave no good results.

For phonolite, a new equation that correlates  $D_{H_2O_t}$  with water content was obtained by modelling the profiles assuming  $D_{H_2O_t}$  proportional to  $C_{H_2O}$ . A pressure effect on water diffusivity could not be resolved for phonolitic melt in the range 2 to 25 kbar, while for trachyte composition smaller diffusivities at higher pressures were registered, indicating a negative pressure effect (a maximum variation circa  $< 0.2$  log units for a pressure increase by 20 kbar). Diffusion data for  $C_{H_2O_t}$  of 3.5 wt%  $H_2O_t$  for

Phonolite and Trachyte in the temperature range 1373 – 1673 K, at pressure of 2-3 kbar show not reliable differences.

Comparing the new results for phonolite and trachyte given in this study with the water diffusivity in different natural melts, a water diffusivity lower than in trachyte of Freda et al. (2003) but faster than in rhyolite of Zhang & Behrens (2000) and Ni and Zhang (2008) was determined. In particular, the  $D_{\text{H}_2\text{O}_t}$  for phonolite at high temperature shows values very close to that of the peralkaline rhyolite (Zhang & Behrens, in press).

Using viscosity data measured on trachyte by Misiti et al. (2006),  $D_{\text{OH}}$  values were estimated circa 3 log units lower than the measured values of bulk water diffusivity in this study. Therefore, it was inferred that the molecular water plays a major role in the high temperature diffusion processes.

## References

- Abe Y., Shimakawa H., Hench L. L.** (1982) "Protonic conduction in alkaline-earth metaphosphate glasses containing water" *J. Noncryst. Solids* 51, p. 357-365.
- Abe Y., Hosono H., Ohta Y., Hench L. L.** (1988) "Protonic conduction in oxide glasses: simple relations between electrical conductivity, activation energy, and the O-H bonding state" *Phys. Rev. B* 38, p. 10166-10169.
- Abe Y., Hosono H., Lee W. H., Kasuga T.** (1993) "Electrical conduction due to protons and alkali-metal ions in oxide glasses" *Phys. Rev. B* 48, p. 15621-15625.
- Barclay J., Carroll M. R., Houghton B. F., and Wilson C. J. N.** (1996) "Pre-eruptive volatile content and degassing history of an evolving peralkaline volcano" *J. of Volc. and Geoth. Research* 74, p. 75-87.
- Bartholomew R. F., Butler B. L., Hoover H.L., Wu C. K.** (1980) "Infrared spectra of a water containing glass" *J. Am. Ceram. Soc.* 63, p. 481-485.
- Bartholomew R. F. and Schreurs J.W.H.** (1980). "Wide-line NMR study of protons in hydrosilicate glasses of different water content." *J. Non-cryst. Solids* 38-39, p. 679-684.
- Behrens H., Johannes W., and Schmalzried H.** (1990) "On the mechanism of cation diffusion processes internary feldspar" *Phys. Chem. Mineral.* 17, 62-78.
- Behrens H.** (1995) "Determination of water solubilities in high-viscosity melts: an experimental study on NaAlSi<sub>3</sub>O<sub>8</sub> and KAlSi<sub>3</sub>O<sub>8</sub> melts" *Eur. J. Mineral.*, 7, p. 905-920.
- Behrens H., Romano C., Nowak M., Holtz F. and Dingwell D.B.** (1996) "Near infrared spectroscopic determination of water species in glasses of the system MAlSi<sub>3</sub>O<sub>8</sub> (M=Li, Na, K): an interlaboratory study" *Chem. Geol.* 128, p. 41-63.
- Behrens H. and Nowak M.** (1997) "The mechanism of water diffusion in polymerized silicate melts." *Contrib. Mineral. Petrol.*, 126, p. 377-385.
- Behrens H., Meyer M., Holtz F., Benne D. and Nowak M.** (2001) "The effect of alkali ionic radius, temperature and pressure on the solubility of water in MAlSi<sub>3</sub>O<sub>8</sub> melts (M = Li, Na, K, Rb)" *Chem. Geol.* 174, p. 275-289.

- Behrens H., Kappes R., Heitjans P.** (2002) „Proton conduction in glass – an impedance and infrared spectroscopic study on hydrous BaSi<sub>2</sub>O<sub>5</sub> glass” *J. Noncryst. Solids* 306, p. 271-281
- Behrens H., Stuke A.** (2003) “Quantification of H<sub>2</sub>O contents in silicate glasses using IR spectroscopy - a calibration based on hydrous glasses analyzed by Karl-Fischer titration.” *Glass Sci. Techn.* 76, p. 176-189
- Behrens H., Zhang Y., and Xu Z.** (2004) „H<sub>2</sub>O diffusion in dacitic and andesitic melts“ *Geochim. Cosmochim. Acta* 68, p. 5139-5150.
- Behrens H. & Hahn M.** (2009) “Trace element diffusion and viscous flow in potassium-rich trachytic and phonolitic melts” *Chem. Geol.* 259, 63-77.
- Benne D., Behrens H.** (2003) “Water solubility in haplobasaltic melts” *Eur. J. Mineral.* 15, p. 803-814.
- Berndt J., Liebske C, Holtz F., Freise M., Nowak M., Ziegenbein D., Hurkuck W., Koepke J.** (1992) „A combined rapid-quench and H<sub>2</sub>-membrane setup for internally heated pressure vessels: description and application for water solubility in basaltic melts” *American Mineral.*, 87, p. 1717-1726.
- Binnewies M., Jäckel M., Willner H. and Rayner-Canham G.** (2004) “Allgemeine und Anorganische Chemie“ *Spektrum Akademische Verlag, Berlin*, 818 p..
- Boltzmann L.** (1894) “Integration der Diffusionsgleichung bei variablen Diffusionskoeffizienten.” *Ann. Phys.* 53, p. 959-964.
- Bunde A. and Maass P.** (1993) “Transport anomalies in glasses” *Physica A* 200, p. 80.
- Bunde A., Ingram M. D. and Maass P.** (1994) “The dynamic structure model for ion transport in glass” *J. Non-Cryst. Solids* 172-174, p. 1222-1236.
- Cahn J. W. and Charles R. W.** (1965) “The initial stages of phase separation in glasses” *Phys. Chem. Glasses* 6, p. 181.
- Christe K. O., Schack C. J. and Wilson R. D.** (1975) “Novel onium salts: Synthesis and characterization of OH<sub>4</sub>SbF<sub>6</sub> and OH<sub>4</sub>AsF<sub>6</sub>.” *Inorg. Chem.*, 14, p. 2224-2230.

- Cooper R. F., Fanselow J. B. and Poker D. B.** (1996) "The mechanism of oxidation of a basaltic glass: chemical diffusion of network-modifying cations." *Geochim. Cosmochim. Acta* 60, pp. 3253–3265.
- Crank J.** (1975) "The Mathematics of Diffusion." *Clarendon Press, Oxford, UK.*
- Day D.E.** (1976) "Mixed alkali glasses- Their properties and uses" *J. Non-Cryst. Solids* 21, p. 343-372.
- Delaney J. R. and Karsten J. L.** (1981) "Ion microprobe studies of water in silicate melts: concentration-dependent diffusion in obsidian" *Earth Planet. Sci. Lett.* 52, p. 191-202.
- Dietzel A. H.** (1983) "On the so called mixed alkali effect" *Phys. Chem. Glasses* 24, p. 172-180.
- Di Matteo V., Carroll M. R., Behrens H., Vetere F., Brooker R. A.** (2004) "Water solubility in trachytic melts" *Chem. Geol.* 213, p. 187-196.
- Dingwell D. B. and Webb S. L.** (1990) "Relaxation in silicate melts." *Eur. J. Min.* 4, p. 427-449.
- Dingwell D. B., Romano C. and Hess K. U.** (1996) "The effect of water on the viscosity of a haplogranitic melt under P-T-X conditions relevant to silicic volcanism." *Contrib. Mineral. Petrol.*, 124, p. 19-28.
- Doremus R. H.** (1960) "The role of gas diffusion in glass refining" *J. Amer. Ceram. Soc.* 12, p. 655-661.
- Doremus R. H.** (1969) "Diffusion of water in fused silica" *J.W. Mitchell, R.C. DeVries, R.W. Roberts and P. Cannon (Eds.) "Reactivity of solids", p. 667-673.*
- Doremus R. H.** (1973) "Glass Science." *John Wiley, New York.*
- Doremus R. H.** (1995) "Diffusion of water in silica glass" *J. Mater Res.* 10; p. 2379-2389.
- Doremus R. H.** (2000) "Diffusion of water in rhyolite glass: diffusion-reaction model" *J. Noncryst. Solids* 261, p. 101-107
- El-Damrawi G.** (2001) "Mixed mobile ion effect in some tellurite and phosphotellurite glasses" *Eur. J. Glass Sc. Techn.* 42-1, p. 56-60.
- Fleet M.E. and Muthupari S.** (1999) "Coordination of boron in alkali borosilicate glasses using XANES" *J. Non-cryst. Solids* 255, p.233-241.

- Freda C., Baker D. R., Romano C., and Scarlato P.** (2003) "Water diffusion in natural potassic melts" *Geol. Soc. London Spec. Publ.* 213, p. 53-62.
- Friedman, I., and Long, W.** (1976) "Hydratation rate of obsidian" *Science* 191, p. 347-352.
- Frischat G.H.** (1975) "Ionic diffusion in oxide glasses" *Diffusion and defect Monograph* 3/4, *Trans. Tech. Publications, Aedermannsdorf, Switzerland*, 182 p..
- Fulda M.**, (1927) "Electrical conductivity of glasses" *Sprechsaal* 60, p. 769-772.
- Funke K., Cramer C., Roling B.** (2000) „Dynamics of mobile ions in glass – What do conductivity spectra tell us?" *Glastech. Ber. Glass Sci. Technol.* 73, p. 244-254.
- Gaillard F., Scaillet B. and Pichavant M.** (2002) "Kinetics of iron oxidation-reduction in hydrous silicic melts." *American Mineralogist*, 87, p. 829–837.
- Gaillard F., Pichavant M., Mackwell S., Champallier R., Scaillet B. and McCammon C.** (2003) "Chemical transfer during redox exchanges between H<sub>2</sub> and Fe-bearing silicate melts." *Am. Mineral.* 88 (2-3) p. 308-315.
- Geotti-Bianchini F., Geibler H. and Kramer F.** (1999) "Recommended procedure for the IR spectroscopic determination of water in soda-lime-silica glass. Report of the International Commission on Glass (ICG) Technical committee 14 "Gases in Glass". *Glastech. Ber. Glass Sci. Technol.* 72, p. 103- 1 11.
- Goldschmidt V. M.** (1937) "The principles of distribution of chemical elements in minerals and rocks" *J. Chem. Soc. London* 655, p. 655-673.
- Haider Z. and Roberts G. J.** (1970) "The diffusion of water into simple silicate and aluminosilicate glasses at temperatures near the transformation range." *Glass. Technol.*, 6, p. 158-163.
- Heide G., Müller B., Kloess G., Moseler D. and Frischat G. H.** (2003) "Structural classification of natural non-crystalline silicates." *J. Non-Cryst. Solids* 323, p. 68-71.
- Helmich M. & Rauch F.** (1993) "On the mechanism of diffusion of water in silica glass." *Glastech. Ber.*, 66, p. 195–200.
- Henderson G. S. and Wang H. M.** (2002) "Germanium coordination and the germinate anomaly" *Eur. J. Mineralogy* 14-4, p.733-744.

- Hendrichson J. R. and Bray P. J.** (1972) "A theory for the mixed alkali effect in glasses, Part I" *Phys. Chem Glasses* 13, p. 43.
- Holloway J. R.** (1971) "Internally heated pressure vessels." In *G.C. Ulmer Ed., Research techniques for high temperature and pressure*, p. 217-258. Springer Verlag, New York.
- Holloway J. R. and Wood B. J.** (1988) "Simulating the Earth, Experimental Geochemistry" 196 p. Unwin Hyman Inc., London.
- Holloway J. R., Dixon J. E., and Pawley A. R.** (1992) "An internally heated, rapid quench, high-pressure vessel" *American Mineral.*, 77, p. 643-646.
- Hunt G. R. & Salisbury J. W.** (1970) "Visible and near-infrared spectra of minerals and rocks I. Silicate minerals." *Mod. Geol.*, 1, p. 283-300.
- Hunt G. R., Salisbury J. W. and Lenhoff C. J.** (1971) "Visible and near-infrared spectra of minerals and rocks, III. Oxides and hydroxides." *Mod. Geol.*, 2, p. 195-205.
- Ildelfonse P. H., Cabaret D., Saintavit P. H., Calas G., Flank A. M. and Lagarde P.** (1998) "Aluminum X-ray absorption Near Edge Structure in model compounds and Earth's surface minerals" *Phys. Chem. Minerals* 25, p. 112-121.
- Ingram M. D.** (1987) "Ionic conductivity in glass" *Phys. Chem. Glasses* 28, p. 215-234.
- Isard J. O.** (1969) "the mixed alkali effect in glass" *J. Non-Cryst. Solids* 1, p. 235-261.
- Jakobsson S.** (1997) "Solubility of water and carbon dioxide in an icelandite at 1400°C and 10 kbar" *Contr. Mineral. Petrol.* 127, p. 129-135.
- Jambon, A.,** (1979) "Diffusion of water in a granitic melt: an experimental study" *Carnegie Inst. Washington, Year Book*, p. 352-355.
- Jambon, A.,** (1983) "Diffusion dans les silicates fondues: un bilan des connaissances actuelles" *Bull. Mineral.* 106, p. 229-246.
- Jambon, A., Zhang, Y., and Stolper, E. M.** (1992) "Experimental dehydration of natural obsidian and estimation of  $D_{H_2O}$  at low water contents" *Geochim. Cosmochim. Acta* 56, p. 2931-2935.

- Karsten J. L., Holloway J. R., and Delaney J. R. (1982) "Ion microprobe studies of water in silicate melts: temperature-dependent water diffusion in obsidian" *Earth Planet. Sci. Lett.* 59, p. 420-428.
- Kohn S. C., Dupree R. and Smith M. E. (1989) "A multinuclear magnetic resonance study of the structure of hydrous albite glasses." *Geochim. Cosmochim. Acta* 53, pp. 2925-2935.
- Kohn S. C., Dupree R. and Mortuza M. G. (1992) "The interaction between water and aluminosilicate magmas." *Chem. Geol.* 96, pp. 399-409.
- Kohn S. C., Smith M. E., Dirken P. J., van Eck E. R. H., Kentgens A. P. M. and Dupree R. (1998) "Sodium environments in dry and hydrous albite glasses: Improved  $^{23}\text{Na}$  solid state NMR data and their implications for water dissolution mechanisms." *Geochim. Cosmochim. Acta* 62, pp. 79-87.
- Lapham K. E., Holloway J. R. and Delaney J.R. (1984) "Diffusion of  $\text{H}_2\text{O}$  and  $\text{D}_2\text{O}$  in obsidian at elevated temperatures and pressures" *J. Non-Cryst. Solids* 67, p. 179-191.
- Lengyel B. and Boksay Z. (1963) *J. Phys. Chem. (Leipzig)* 223, p. 49.
- Leschik M., Heide G., Frischat G. H., Behrens H., Wiedenbeck M., Wagner N., Heide K., Geißler H., and Reinholz U. (2004) „Determination of  $\text{H}_2\text{O}$  and  $\text{D}_2\text{O}$  contents in rhyolitic glasses using KFT, NRA, EGA, IR spectroscopy, and SIMS." *Phys. Chem. Glasses* 45, p. 238-251.
- Liebske C., Behrens H., Holtz F., Lange R. A. (2003) "The influence of pressure and composition on the viscosity of andesitic melts" *Geochim. Cosmochim. Acta* 67, p. 473-485.
- Litovitz T. A. (1960) "Liquid relaxation phenomena and the glass state." *J. Non-Cryst. Solids* edited by V. N. Frechette, p.252-268, John Wiley.
- Liu Y. and Zhang Y. (2000) "Bubble growth in rhyolitic melt" *Earth Planet. Sci. Lett.* 181, p. 251-264.
- Liu Y., Zhang Y. and Behrens H. (2004) " $\text{H}_2\text{O}$  diffusion in dacitic melts." *Chem. Geol.* 209, pp. 327-340.

**Macdonald J.R.** (1996) "Impedance spectroscopy emphasizing solid materials and systems" *John Wiley, New York*, p. 346.

**Mandeville C. W., Webster J. D., Rutherford J. M., Taylor B. E., Timbal<sup>3</sup> A. and Faure K.** (2002) "Determination of molar absorptivities for infrared absorption bands of H<sub>2</sub>O in andesitic glasses" *Am. Mineral.* 87-7, p. 813-821.

**Martel C., Dingwell D. B., Spieler O., Pichavant M., and Wilke M.** (2000) "Fragmentation of foamed silicic melts: an experimental study" *Earth Planet. Sci. Lett.* 178, p. 47-58.

**Matano C.** (1932–1933) "The relation between the diffusion coefficients and concentrations of solid metals (the nickel-copper system)." *Jpn. J. Phys.* 8, p. 109–113.

**Maxwell J. C.** (1867) "On the dynamical theory of gases." *Phil. Trans. Roy. Soc., A157*, p. 49-88.

**Mazurin O.V.**, (1965) "Structure of Glass" *vol.4, Consultants Bureau, New York*.

**McVay G. L., Knotek M. L., Johnson R. L., Baughman R. J. and Fagan R. J.** (1976) "The effect of water on ionic conductivity and diffusion in Na<sub>2</sub>O·SiO<sub>2</sub> glasses" *Tech. Rept. No. 76, Sandia Laboratories*, p. 3-27.

**Mc Millan P. F. and Remmele R. L.** (1986) "Hydroxyl sites in SiO<sub>2</sub> glass: a note on Infrared and Raman spectra" *Am. Mineral.* 71, p. 772-778.

**Milnes G. C. and Isard J. O.** (1962) "The mechanism of electrical conductivity in lead-silicate glasses and its dependence on water content" *Phys. Chem. Glasses* 3, p. 157-162.

**Misiti V., Freda C., Taddeucci J., Romano C., Scarlato P., Longo A., Papale P. and Poe B.T.** (2006) "The effect of H<sub>2</sub>O on the viscosity of K-trachytic melts at magmatic temperatures." *Chem. Geol.* 235, p. 124–137.

**Mysen B. O., Virgo D., Harrison W. J. and Scarfe C. M.** (1980) "Solubility mechanisms of H<sub>2</sub>O in silicate melts at high pressures and temperatures: A Raman spectroscopic study." *Am. Mineral.* 65, pp. 900–914.

**Mysen B.O., Virgo D. and Seifert F. A.** (1985) "Relationship between properties and structure of aluminosilicate melts" *American Mineral.* 70, p. 88-105.

- Mysen B.O. and Virgo D.** (1986) "Volatiles in silicate melts at high pressure and temperature: interaction between OH groups and Si<sup>4+</sup>, Al<sup>3+</sup>, Ca<sup>2+</sup>, Na<sup>+</sup> and H<sup>+</sup>." *Chem. Geol.* 57, p. 303-331.
- Mysen B. O.** (1988) "Structure and properties of silicate melts" *Elsevier Amsterdam*, p. 354.
- Moulson A. J. and Roberts J. P.** (1961) "Water in silica glass." *Trans. Faraday Soc.* 57, p. 1208-1216.
- Murugan G. S. & Varma K. B. R.** (2002) "Lithium borate–strontium bismuth tantalate glass nanocomposite: a novel material for nonlinear optic and ferroelectric applications." *Mater. Chem.*, 12, p.1426 – 1436.
- Nakamoto K., Margoshes M. and Rundle R.E.** (1955) "Stretching frequencies as a function of distance in hydrogen bonds." *J. Am. Chem. Soc.*, 77, 6480–6488.
- Navon O., Chekhmir A., and Lyakhovsky V.** (1998) "Bubble growth in highly viscous melts: theory, experiments and autoexplosivity of dome lavas" *Earth Planet. Sci. Lett.* 160, p. 763-776.
- Ni H. & Zhang Y.** (2008) "H<sub>2</sub>O diffusion models in rhyolitic melt with new high pressure data." *Chem. Geol.* 250, 1-4, p. 68-78.
- Nogami M. & Abe Y.** (1996) "Evidence of water-cooperative proton conduction in silica glasses" *Phys. Rev. B* 55, 18, p. 108-112.
- Nogami M., Nagao R. and Wong C.** (1998) "Proton conduction in porous silica glasses with high water content." *J. Phys. Chem. B*, 102 (30), p. 5772–5775.
- Nowak M. and Behrens H.** (1997) "An experimental investigation on diffusion of water in haplogranitic melts" *Contrib. Mineral. Petrol.* 126, p. 365-376.
- Ohlhorst S., Behrens H. and Holtz F.** (2001) "Compositional dependence of molar absorptivities of near-infrared OH<sup>-</sup> and H<sub>2</sub>O bands in rhyolitic to basaltic glasses" *Chem. Geol.* 174, p. 5-20.
- Okumura S. & Nakashima S.** (2004) "Water diffusivity in rhyolitic glasses as determined by in situ IR spectrometry." *Phys. Chem. Miner.* 31, p. 183–189.

- Okumura S. & Nakashima S.** (2006) "Water diffusion in basaltic to dacitic glasses." *Chem. Geol.* 227, 1-2, p.70-82.
- Owen A. E. and Douglas R. W.** (1959) "The electrical properties of vitreous silica," *J. Soc. Glass Technol.*, vol. 43, p. 159-178.
- Papale P.** (1999) "Strain-induced magma fragmentation in explosive eruptions." *Nature* 397, p. 425-428.
- Pearson A. D., Pasteur G. A. and Northover W. R.** (1979) "Determination of the absorptivity of OH in a sodium borosilicate glass." *J. Mat. Sci.* 14, p. 869-872.
- Proussevitch A. A. and Sahagian D.L.** (1998) "Dynamics and energetics of bubble growth in magmas: Analytical formulation and numerical modeling." *J. Geophys. Res.*, 103(B8), p. 18223-18251.
- Ravaine D.** (1980) "Glasses and solid electrolytes" *J. Non-Cryst. Solids* 38-39, p. 353-358.
- Ricci G.** (2000) "Il distretto vulcanico dei Campi Flegrei: petrologia e geochimica dei depositi di breccia e dei prodotti piroclastici associati" *Ph.D. Thesis, University of Catania, Italy*
- Richet P., Whittington A., Holtz F., Behrens H., Ohlhorst S. and Wilke M.** (2000) "Water and the density of silicate glasses." *Contrib. Mineral. Petrol.* 138, p. 337-347.
- Roberts G. J. and Roberts J. P.** (1966) "An oxygen tracer investigation of the diffusion of water in silica glass" *Phys. Chem. Glasses*, 7, p. 82-89.
- Roux J. and Lefèvre A.** (1992) "A fast quench device for internally heated pressure vessel" *Eur. J. Mineral.* 4, p. 279-281.
- Sasek L. and Meissnerova H.** (1981) "Electrical conductivity of silicate glasses melts" *Kilikaty* 25, p. 21-34.
- Sato R. K., Kirkpatrick R. J. and Brow R. K.** (1992) "Structure of Li, Na metaphosphate glasses by <sup>31</sup>P and <sup>23</sup>Na MAS-NMR correlated with the mixed alkali effect" *J. Non-Cryst. Solids*
- Sauer F. and Freise V.** (1962) "Diffusion in binären Gemischen mit Volumenänderung." *Z. Elektrochem. Angew. Phys. Chem.* 66, p. 353-363.

- Schëffer H. A., Mecha J. and Steinmann J.** (1979) "Mobility of Sodium ions in silica glass of different OH content" *J. Amer. Ceram. Soc.* 7-8, p. 343-346.
- Scherer G. W.** (1984) "Use of the Adam-Gibbs equation in the analysis of structural relaxation." *J. Amer. Cer. Soc.* 67, p. 504-511.
- Scholze H.** (1959) "Der Einbau des Wassers in Glaser. I. Der Einflu6 des im Glas gelosten Wassers auf das Ultrarot-Spektrum und die quantitative ultrarotspektroskopische Bestimmung des Wassers in Glasern." *Glastechn. Ber.* 32, p. 81-88.
- Scholze H.** (1960) "Distinguishing between H<sub>2</sub>O molecules and OH groups in glasses and minerals" *Naturwissenschaften* 47, p. 226.
- Scholze, H.** (1966) "Gases and water in glass." *The Glass Industry*, October, 1966. Part one, 546-551; part two, 622-628; part three, 670-675.
- Scholze H. and Kreidl N.J.** (1986) "Technological aspect of viscosity." *In: Glass Science and Technology. Eds. Uhlmann D. R. and Kreidl N. J. Academic Press London*, p. 233-273.
- Scholze H.** (1991) "Glass – Nature, Structure and Properties" *Springer Verlag*, 364 p..
- Schuessler J.A., Botcharnikov R.E., Behrens H., Misiti V. and Freda C.** (2008) "Oxidation state of iron in hydrous phono-tephritic melts." *Am. Mineral.* 93, p. 1493–1504.
- Shaw H. R.** (1974) "Diffusion of H<sub>2</sub>O in granitic liquids: I. Experimental data; II. Mass transfer in magma chambers" In: Hoffmann, A.W., Giletti, B.J., Yoder, H.S., Yund, R.A. (Eds), *Geochemical Transport and Kinetics. Carnegie Inst. Washington Publ., Washington, DC*, p. 139-170.
- Shelby J.E.** (1997) "Introduction to glass science and technology" *The Royal Society of Chemistry, Cambridge, England*, 255 p.
- Shelby J. E.** (2005) "Introduction to Glass Science and Technology." *2th edition, Royal Society of Chemistry*, p. 291.
- Silver L. A., Ihinger P. D. and Stolper E.** (1990) " The influence of bulk composition on the speciation of water in silicate glasses" *Contrib. Mineral. Petrol.* 104, p. 142-162.

- Stanton T.R., Tyburczy J.A., Holloway J.R. and Petuskey W.T. (1990) "Electromigration of water in silicate glass: Resolution of the valence charge of the diffusing species." *EOS Transactions AGU*, 71, 652.
- Stevens J. M. (1957) "Handbuch der physik" ed. S. Flugge, Springer-Verlag, Berlin, vol. 20, p. 372.
- Stevenson R. J., Dingwell D. B., Webb S. L. and Bagdassarov N.S. (1995) "The equivalence of enthalpy and shear stress relaxation in rhyolitic obsidians and quantification of the liquid-glass transition in volcanic processes." *J. Volcanol. Geotherm. Res.* 68, p. 297-306.
- Stolper E. (1982) "The speciation of water in silicate melts" *Geochim. Cosmochim. Acta* 46, p. 2609-2620.
- Stuke A., Behrens H., Schmidt B.C. and Dupree R. (2006) "H<sub>2</sub>O speciation in float glass and soda lime silica glass." *Chem. Geol.* 229, p. 64-77.
- Tomozawa M. (1985) "Concentration dependence of the diffusion coefficient of water in SiO<sub>2</sub> glass." *J. Am. Ceram. Soc.*, 68: p. 251-252.
- Wang L., Zhang Y. and Essene E. J. (1996) "Diffusion of the hydrous component in pyrope." *Amer. Mineral.* 81, p. 706-718.
- Wasserburg G. J. (1988) "Diffusion of water in silicate melts" *J. Geol.* 96; p. 363-367.
- Watson E. B. (1994) "Diffusion in volatile-bearing magmas." *Rev. Mineral.* 30, p. 371-411.
- Webb S. L. and Dingwell D. B. (1990) "Non-Newtonian viscosities of geologic melts at high stresses: experimental results for rhyolite, andesite, basalt and nephelinite." *J. Geophys. Res.* 95 (B10), p. 15695-15701.
- Williams J. P., Su Y.-S., Strzegowski W. R., Butler B. L., Hoover H. L. and Altemose V.O. (1976) "Direct determination of water in glass." *Ceramic Bull* 55, p. 524-527.
- Williams Q. and Jeanloz R. (1988) "Spectroscopic evidence for pressure-induced coordination changes in silicate glasses and melts" *Science* 239, p.902-905.

- Wilson L., Sparks R. S. J. and Walker G. P. L. (1980) "Explosive volcanic eruption-IV. The control of magma properties and conduit geometry on eruption column behavior." *Geophys. J. Roy. Astro. Soc.* **63**, p. 117-148.
- Withers A. C. and Behrens H. (1999) "Temperature-induced changes in the NIR spectra of hydrous albitic and rhyolitic glasses between 300 and 100K" *Phys. Chem. Minerals* **27**, p. 119-132.
- Woods A. W. (1995) "The dynamics of explosive volcanic eruptions" *Rev. Geophys.* **33**, p. 495-530.
- Wu C. K. (1980) "Nature of incorporated water in hydrated silicate glasses." *J. Am. Ceram. Soc.* **63**, p. 453-457.
- Xue X. and Kanzaki M. (2001) "An ab initio calculation of the  $^{17}\text{O}$  and  $^1\text{H}$  NMR parameters for various OH groups: Implications to the speciation and dynamics of dissolved water in silicate glasses." *J. Phys. Chem. B* **105**, p. 3422-3434.
- Xue X. and Kanzaki M. (2004) "Dissolution mechanisms of water in depolymerized silicate melts: Constraints from  $^1\text{H}$  and  $^{29}\text{Si}$  NMR spectroscopy and ab initio calculations." *Geoch. et Cosmoch. Acta*, **68(24)**, p. 5027-5057.
- Yamashita S., Kitamura T. and Kusakabe M. (1997) "Infrared spectroscopy of hydrous glasses of arc magma compositions" *Geochem. J.* **31**, p. 169-174.
- Zachariasen W. H. (1932) "The atomic arrangement in glass" *J. Am. Chem. Soc.* **54** (10), p. 3841-3851.
- Zarzycki J. (1990) "Glasses and the vitreous state" *Cambridge University Press*, 505 p..
- Zhang Y., Stolper E. M., and Wasserburg G. J. (1991) "Diffusion of water in rhyolitic glasses" *Geochim. Cosmochim. Acta* **55**, p. 441-456.
- Zhang Y. and Stolper. E. M. (1991) "Water diffusion in a basaltic melt" *Nature* **351**, p. 306-309.
- Zhang Y., Stolper E. M., and Ihinger P. D. (1995) "Kinetics of the reaction  $\text{H}_2\text{O} + \text{O} = 2\text{OH}$  in rhyolitic and albitic glasses: Preliminary results" *American Mineral.* **80**, p. 593-612.
- Zhang Y. (1996) "Dynamics of  $\text{CO}_2$ -driven lake eruptions" *Nature* **379**, 57-59.

Zhang Y., Belcher R., Ihinger P. D., Wang L., Xu Z. and Newman S. – a (1997) “New calibration of infrared measurement of dissolved water in rhyolitic glasses“ *Geochim. Cosmochim. Acta* 61, p. 3089-3100.

Zhang Y., Sturtevant B. and Stolper E. M.- b (1997) “Dynamics of gas-driven eruptions: experimental simulations using CO<sub>2</sub>–H<sub>2</sub>O- polymer system” *J. Geophys. Res.* 102, p. 3077-3096.

Zhang Y. (1999) “A criterion for the fragmentation of bubbly magma based on brittle failure theory” *Nature* 402, p. 648-650.

Zhang Y. and Behrens H. (2000) “H<sub>2</sub>O diffusion in rhyolitic melts and glasses” *Chem. Geol.* 169, p. 243-262.

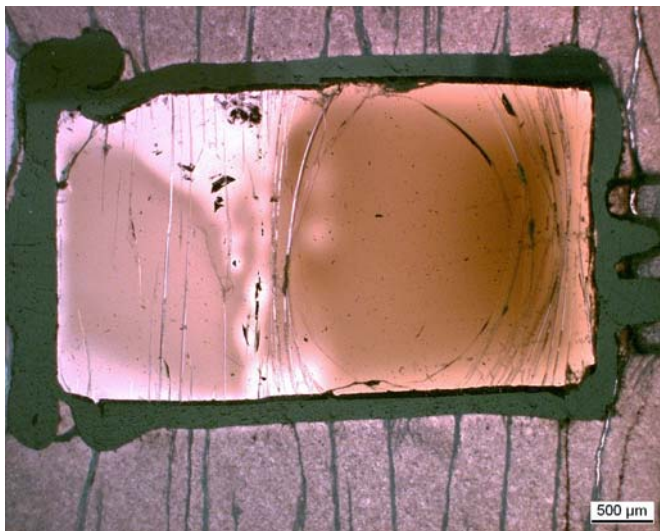
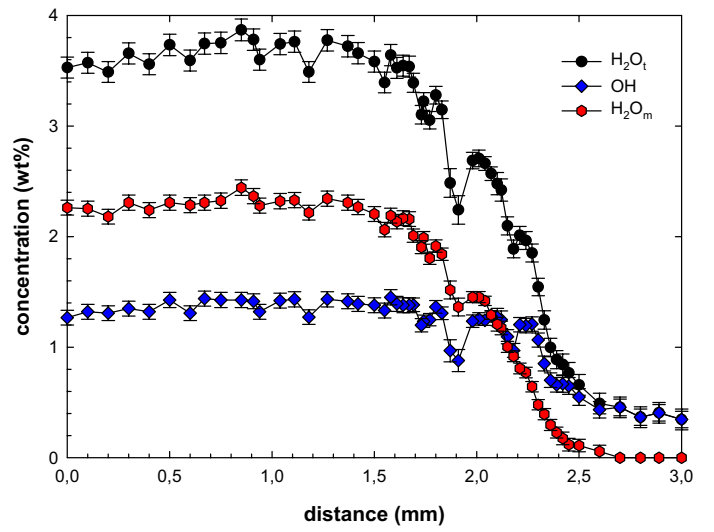
Zhang Y. (2008) “Geochemical Kinetics” *Princeton University Press*, 656 p.

## Appendix

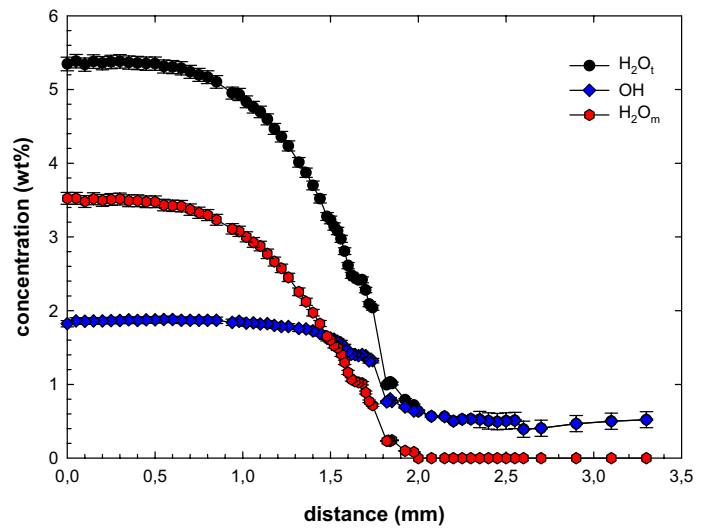
Micro-photographs of successful diffusion couple experiments are here illustrated with the respective measured diffusion profiles.



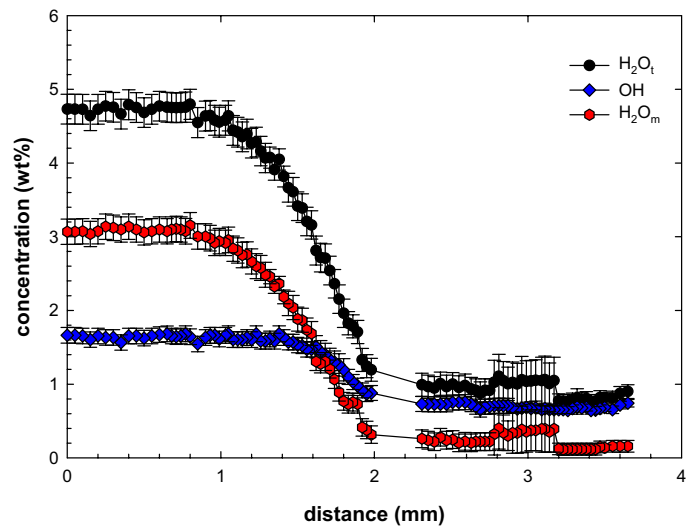
P1 (Phon.0-5w; 1598 K; 25 kbar; 311s)

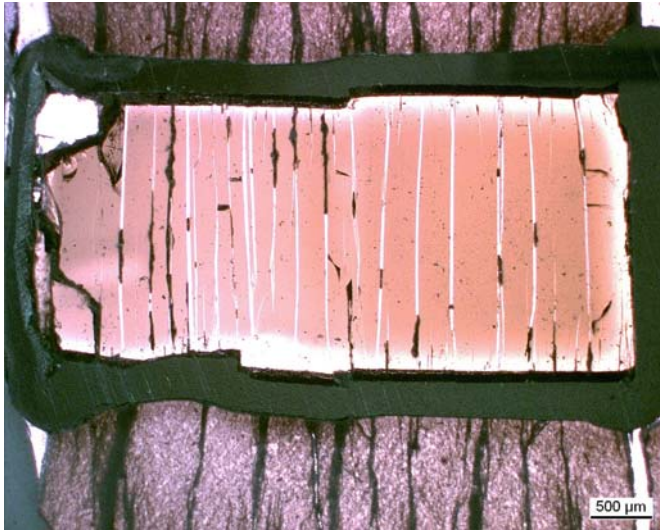


P2 (Phon.0-5 w; 1598 K; 15 kbar; 311s)

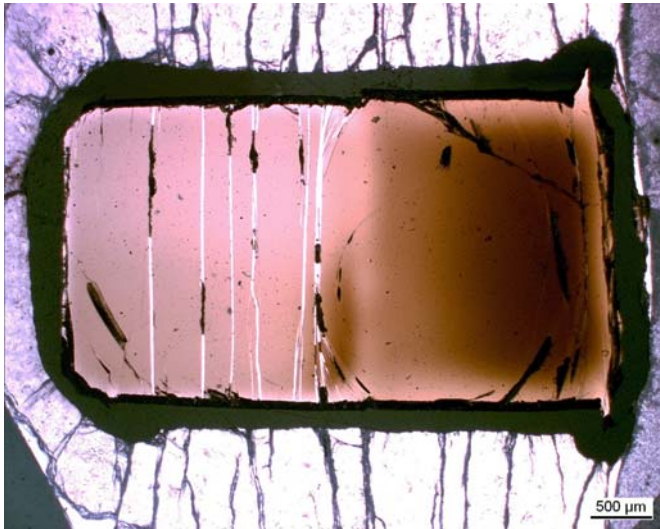
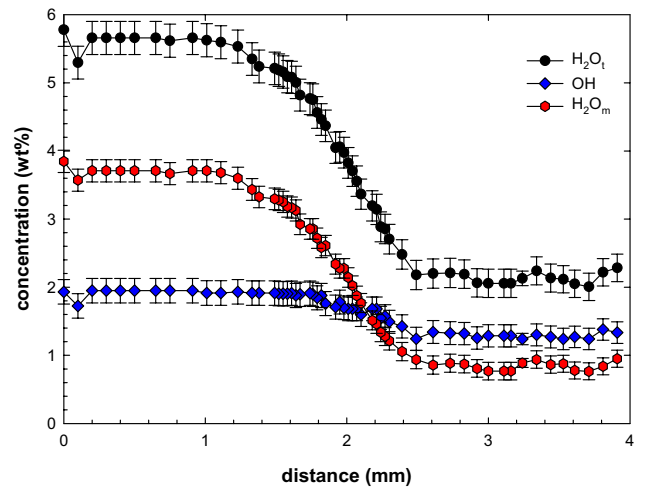


P3 (Phon.0-5 w; 1598 K; 5 kbar; 311s)

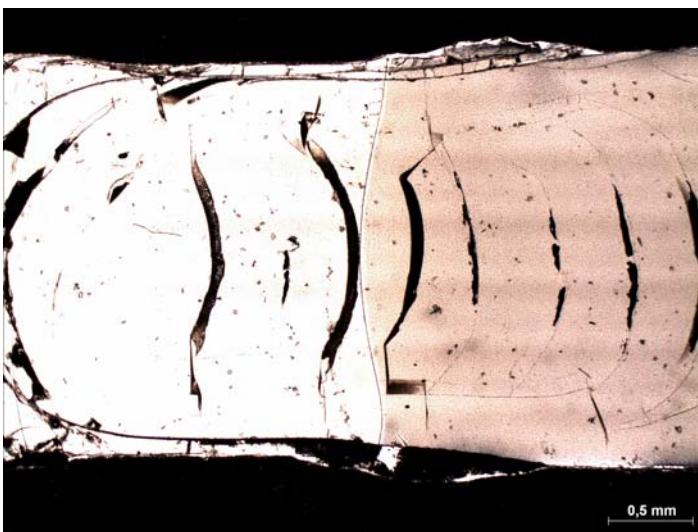
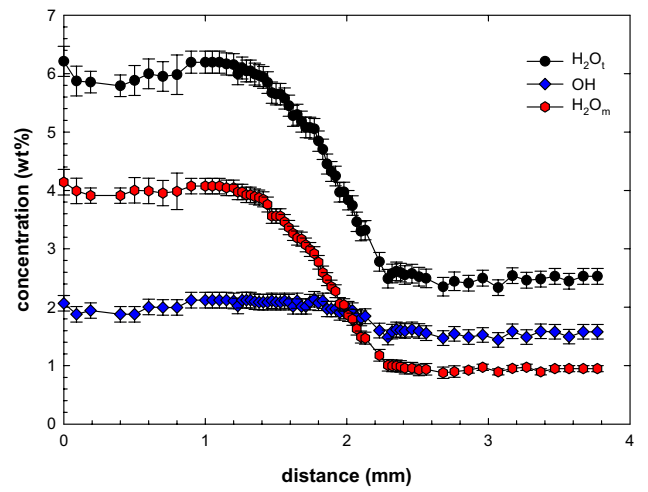




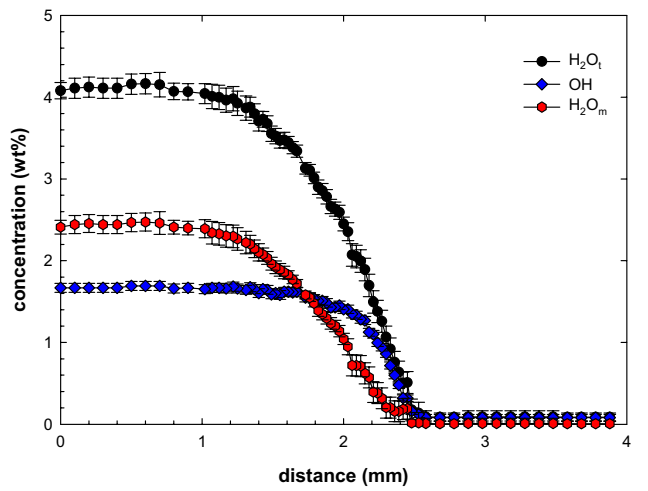
P4 (Phon.2-5 w; 1598 K; 25 kbar; 311s)



P5 (Phon.2-5 w; 1598 K; 15 kbar; 311s)

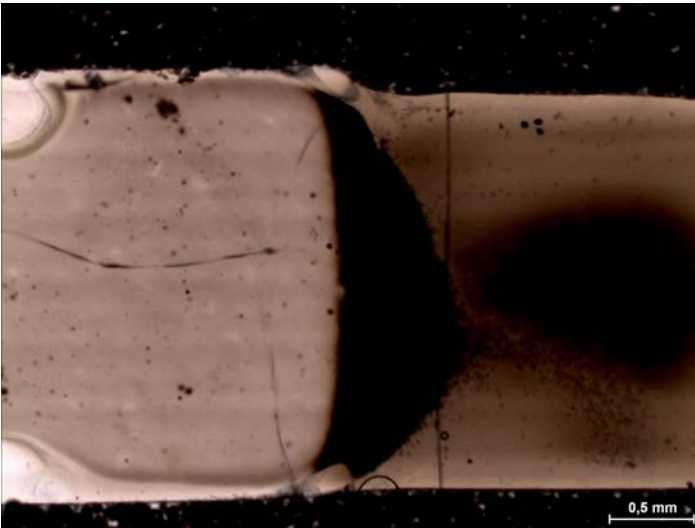
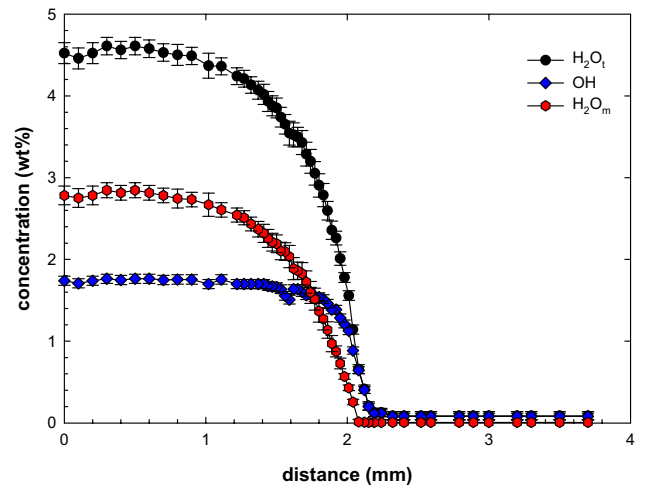


P6 (Phon.0-5 w; 1473 K; 2 kbar; 886s)

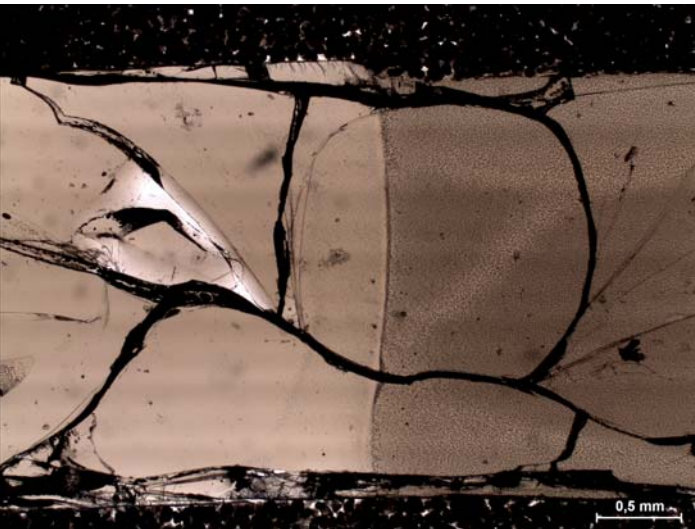
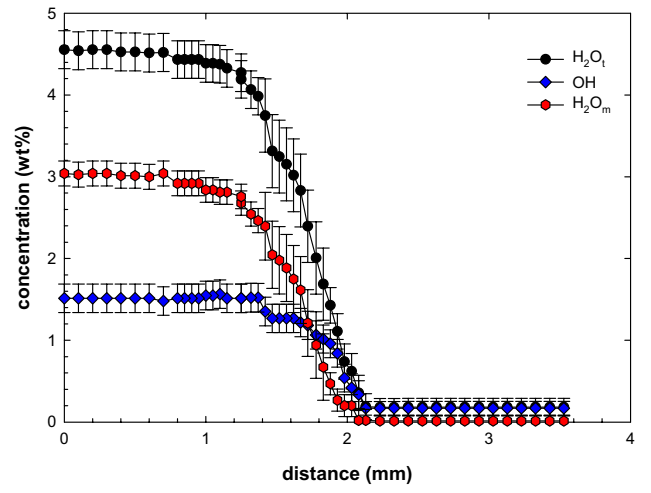




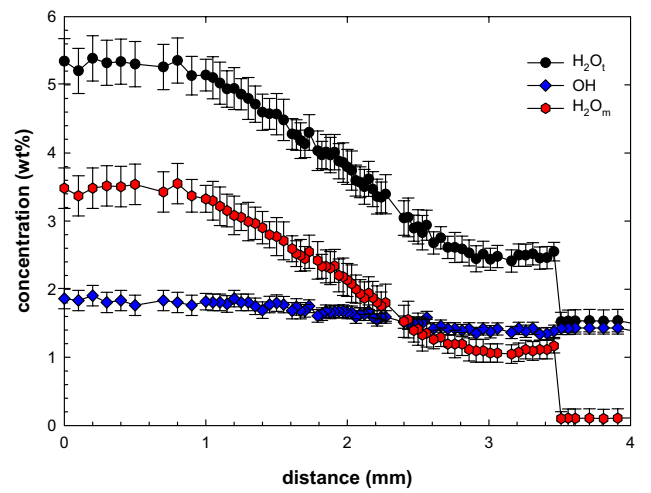
P7 (Phon.0-5 w; 1373 K; 2 kbar; 886s)

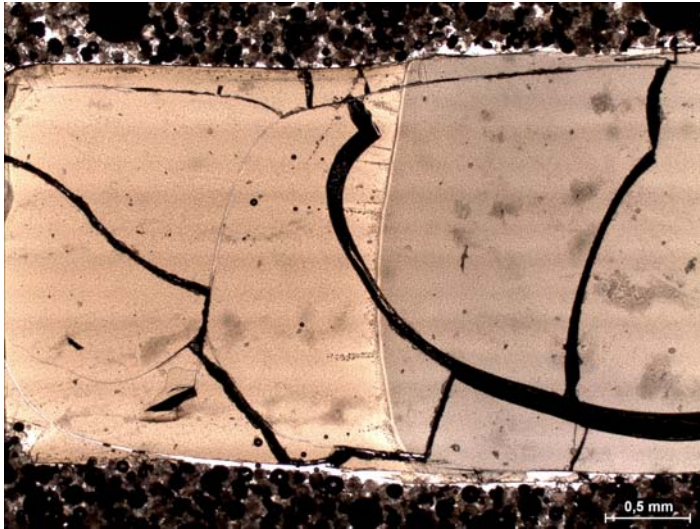


P8 (Phon.0-5 w; 1673 K; 2 kbar; 225s)

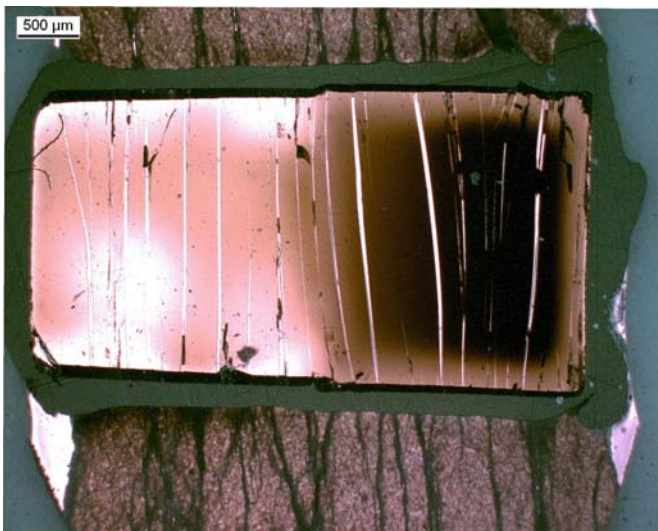
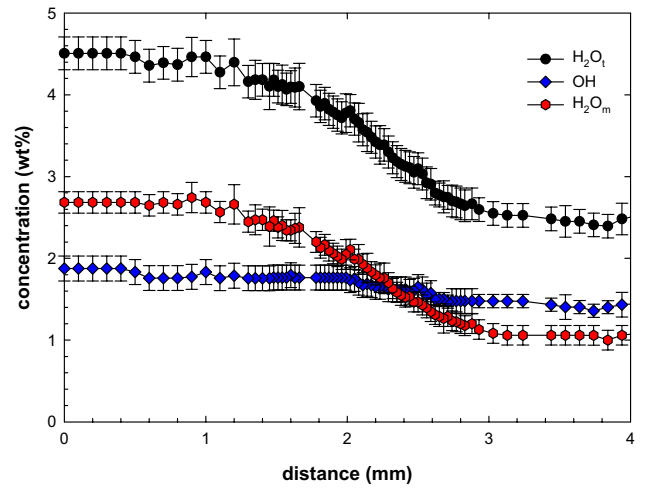


P9 (Phon.2-5 w; 1373 K; 2 kbar; 1186s)

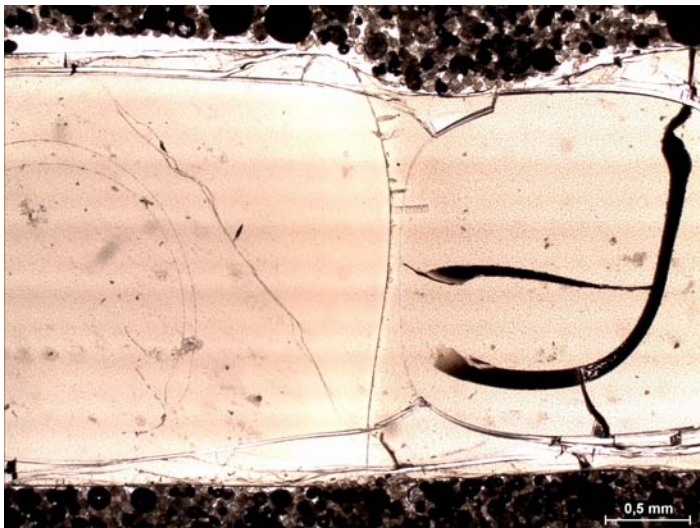
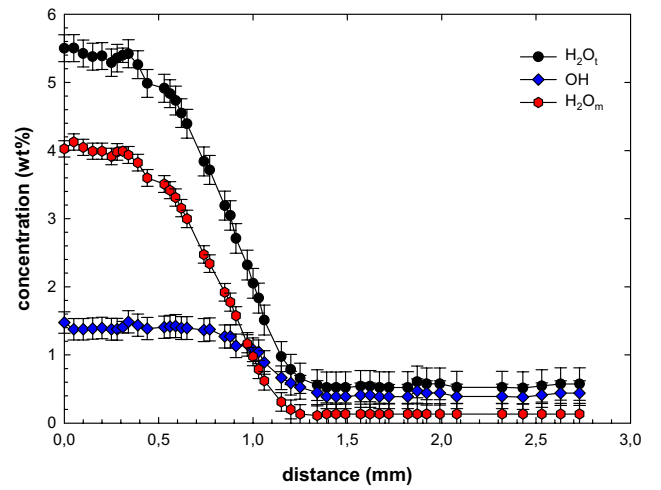




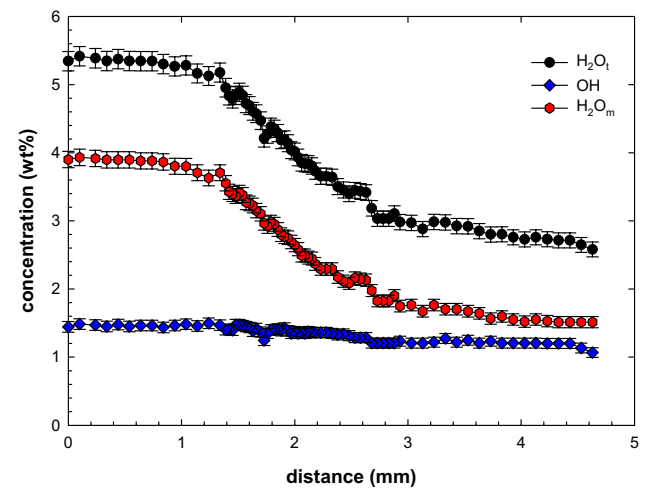
P10 (Phon.2-5 w; 1473 K; 2 kbar; 886s)

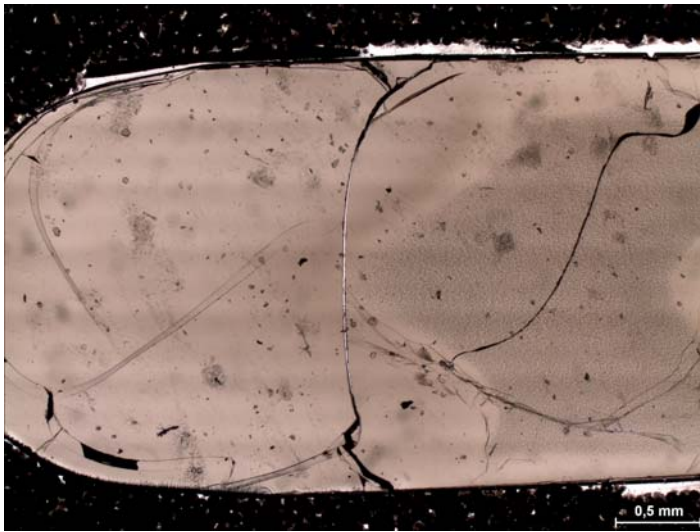


T1 (Trach.0-5 w; 1598 K; 25 kbar; 311s)

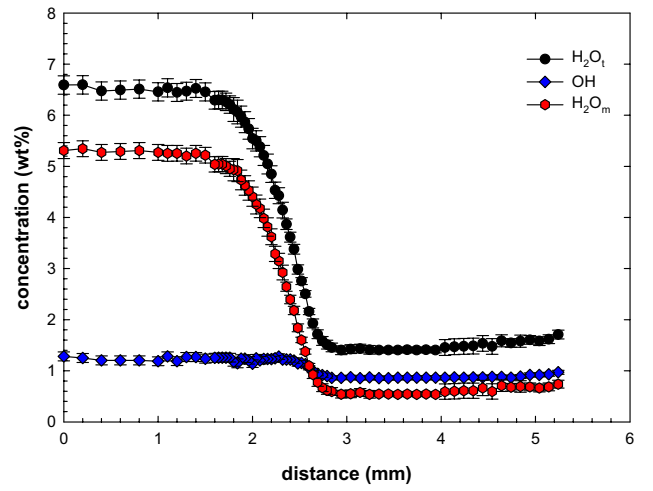


T2 (Trach.2-5 w; 1473 K; 2 kbar; 886s)

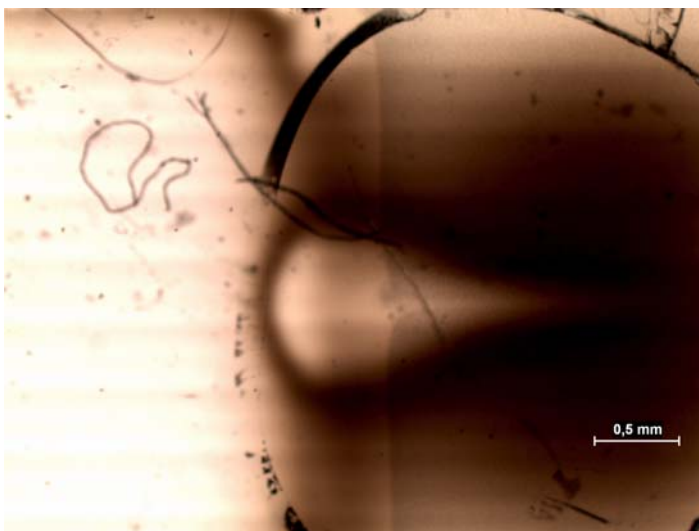
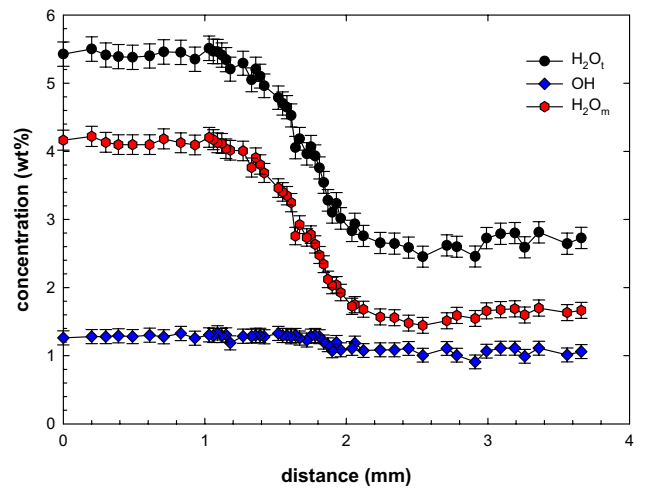




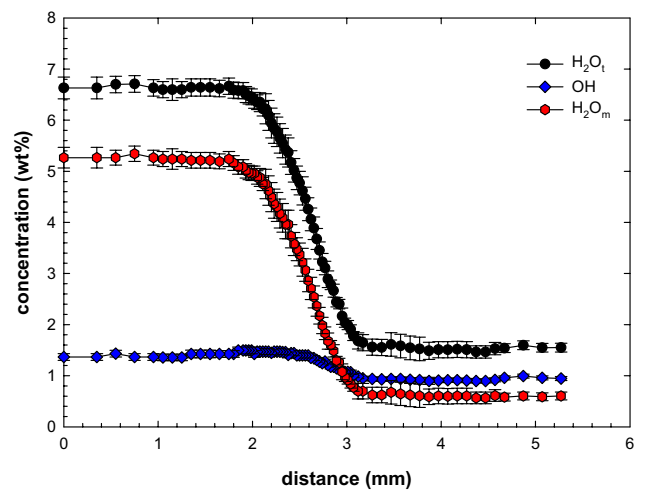
T3 (Trach.1-6 w; 1573 K; 3 kbar; 226s)



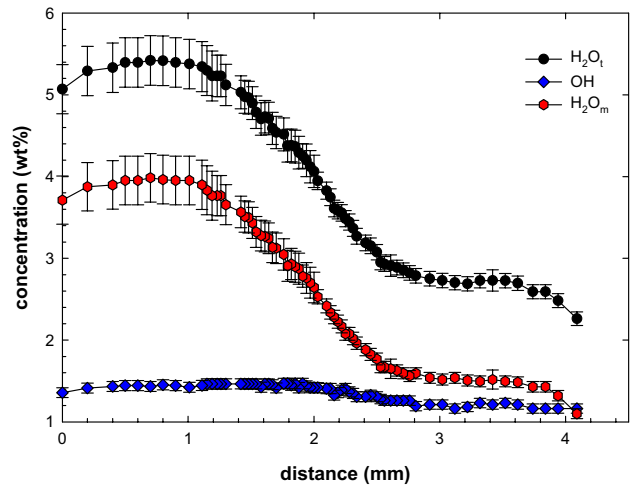
T4 (Trach.2-5 w; 1573 K; 25 kbar; 311s)



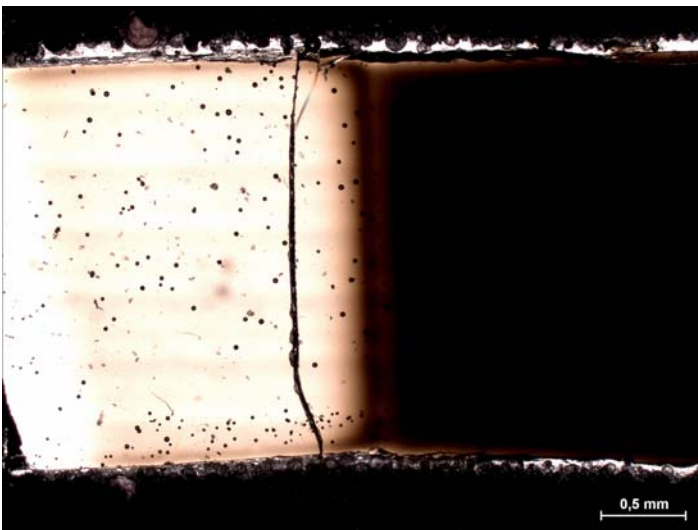
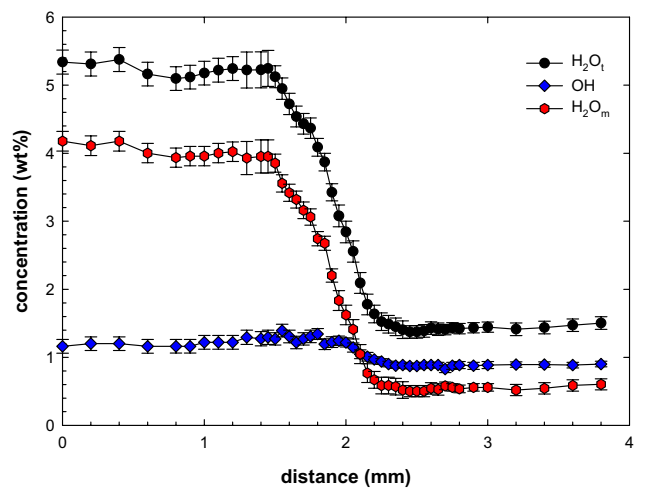
T5 (Trach.1-6 w; 1673 K; 3 kbar; 226s)



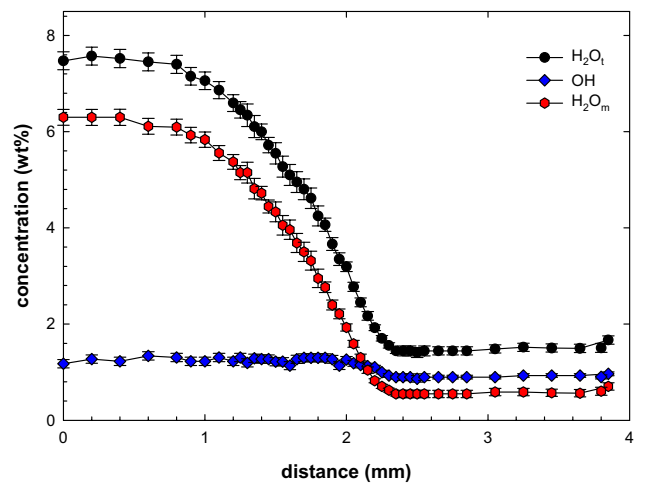
T6 (Trach.1-6 w; 1373 K; 2 kbar; 886s)



T7 (Trach.1-5 w; 1373 K; 2 kbar; 466s)



T8 (Trach.1-6 w; 1473 K; 2 kbar; 466s)



# CURRICULUM VITAE Sara Fanara

---

## Personal Information

Date of birth: 30<sup>th</sup> August 1978 in Rome (Italy)  
Present Address: Richard Wagner str.1, 30177 Hannover (Germany)  
Permanent Address: Via Arnaldo Cervesato N°21 D/19, 00159 Rome (Italy)  
Telefon: +39 06 4392506; +39 3384939408  
+49 0511 7625280; +49 176 29621440  
Nationality: Italian  
  
E-mail address: [s.fanara@mineralogie.uni-hannover.de](mailto:s.fanara@mineralogie.uni-hannover.de)  
[sara.fanara@libero.it](mailto:sara.fanara@libero.it)

## Education

---

- Since 5/2005** Ph.D. Scholarship (three years) “*G.C. Lichtenberg-Stipendium*”, at Leibniz Universität Hannover, Institut für Mineralogie.  
Topic: “Water diffusion and proton conduction in silicate glasses and melts”.  
Supervisor: Prof. H. Behrens.
- 1997-2004** “Diploma di Laurea” in Earth Science (Five Years Degree) University of Rome “La Sapienza”.  
Thesis Title: “*Studio geo-vulcanologico dei centri eruttivi del settore compreso fra l’Isola Bisentina e Marta, Monti Vulsini Meridionali, (VT)*”.  
Supervisor: Prof. M.D.Palladino.
- 13-12-2004** Final mark: 110/110 *cum laude*.
- 07-1997** “Maturità Classica” (High School Degree), High School “Gaio Lucilio” (Rome).  
Final mark: 48/60.

## Professional Experiences

---

- 2000/2004** Scholarship (four years) at “Museo di Mineralogia della Sapienza di Roma”  
Gave guided tours of the Museum.

## Foreign Languages

---

English: good knowledge of English  
German: basic knowledge. German course (A1+A2) at “Fachsprachenzentrum” of Univesrität Hannover

## Publications

---

- S. Fanara, H. Behrens, R. Kappes.** “Ionic Conductivity of hydrous silicate glasses”. *Advances in Science and Technology Vol. 46 (2006) pp 89-92.*

## Communications

---

1. **Fanara S., Behrens H., Kappes R.** "*Ionic conductivity of hydrous silicate melts*". Poster Contribution, CIMTEC 2006 International Conference, (Acireale CT, Italy, June, 2006).
2. **Fanara S., Behrens H., Zhang Y.** "*Water diffusion in Trachyte and Phonolite melts*". Poster Contribution, Goldschmidt Conference 2007, (Köln, Germany, August, 2007).
3. **Fanara S., Behrens H.** "*Proton conduction and water diffusion in silicate glasses and melts*". Poster Contribution, Silicate Melt Workshop 2007, (La Petite Pierre, Strasbourg, France, Oktober, 2007).

## Partecipation to Symposia, Schools and Workshops

---

4. Meeting in Altenau, Harz Mountain, Germany, March 21-22, 2006. Oral contribution. Title: "*Proton conduction and water diffusion in silicate glasses and melts*".
5. DMG Meeting, Universität Hannover, September, 2006. Poster contribution. Title: "*Ionic conductivity of hydrous silicate glasses*".
6. Universität Hannover, January 24, 2007. Oral contribution. Title: "*Proton conduction and water diffusion in silicate glasses and melts*".